

Electronic Thesis and Dissertation Repository

12-2-2021 9:50 AM

Staudinger Reactions on Azide Functionalized Au₂₅ Nanoclusters as a Route to Linked Frameworks

Sung Kyun Lim, *The University of Western Ontario*

Supervisor: Workentin, Mark S., *The University of Western Ontario*

Co-Supervisor: Corrigan, John F., *The University of Western Ontario*

A thesis submitted in partial fulfillment of the requirements for the Master of Science degree in Chemistry

© Sung Kyun Lim 2021

Follow this and additional works at: <https://ir.lib.uwo.ca/etd>

Recommended Citation

Lim, Sung Kyun, "Staudinger Reactions on Azide Functionalized Au₂₅ Nanoclusters as a Route to Linked Frameworks" (2021). *Electronic Thesis and Dissertation Repository*. 8297.
<https://ir.lib.uwo.ca/etd/8297>

This Dissertation/Thesis is brought to you for free and open access by Scholarship@Western. It has been accepted for inclusion in Electronic Thesis and Dissertation Repository by an authorized administrator of Scholarship@Western. For more information, please contact wlsadmin@uwo.ca.

Abstract

Azide-functionalized $[\text{Au}_{25}(\text{SR})_{18}]$ gold nanoclusters $[\text{Au}_{25}(\text{SCH}_2\text{CH}_2\text{C}_6\text{H}_4\text{-N}_3)_{18}]^-$ are able to undergo post-assembly surface modification via click reaction chemistry. In this study, we report the reaction of the azide cluster, $(\text{Oct}_4\text{N})[\text{Au}_{25}(\text{SCH}_2\text{CH}_2\text{-}i{p}\text{-C}_6\text{H}_4\text{N}_3)_{18}]$ (AuNC-azide) with triarylphosphine bidentates. The $-\text{N}_3$ groups on AuNC-azide undergo Staudinger reactions with PPh_3 , yielding surface $-\text{C}_6\text{H}_4\text{N}=\text{PPh}_3$ at room temperature under inert atmosphere: this reaction favours the formation of $-\text{C}_6\text{H}_4\text{N}=\text{PPh}_3$ over surface displacement of the thiolate ligands when using up to 14 equivalents of PPh_3 . However, when a greater number of equivalents of triphenylphosphine are used, surface displacement of thiolate ligands also occurred in competition with the Staudinger reaction. Reactions of AuNC-azide with the bidentate phosphine ligand $4,4'\text{-Ph}_2\text{PC}_6\text{H}_4\text{-C}_6\text{H}_4\text{PPh}_2$ leads to covalent linking of the gold clusters via intermolecular $-\text{C}_6\text{H}_4\text{-N}=\text{PPh}_2\text{C}_6\text{H}_4\text{-C}_6\text{H}_4\text{Ph}_2\text{P}=\text{N-C}_6\text{H}_4-$ bridges to form networks of clusters.

Keywords

Gold, nanocluster, Staudinger, click chemistry, surface modification

Summary for Lay Audience

Gold nanoclusters are atomically precise nanomaterials that have been widely used for their unique optical and chemical properties. They comprise of an internal metallic framework surrounded by an external layer of protecting ligands. However, because most gold clusters reported so far bear ligands that have no reactive functional group, the use of the clusters for application has been somewhat limited because of the need to synthesize cluster with ligands that has reactive functional groups. Recently, gold nanoclusters with a ligand bearing a reactive handle, known as the azide, has been developed. The advantage of this newly developed gold nanocluster is that the surface ligands can now undergo reactions with the azide, which undergoes rapid, efficient chemistry with appropriate reaction partners through a “click reaction”. The azide nanocluster thus serves as a template material to access a wide variety of new nanocluster to change the properties of the nanocluster and tune their properties for potential applications. This thesis includes one of the many click type reactions that can occur on the azide group of the ligands on the cluster, also known as the Staudinger reaction. The reaction will form networks of the nanometer sized clusters.

Co-Authorship Statement

The work described in this thesis contains contribution from the author, under supervision of Dr. John F. Corrigan and Dr. Mark S. Workentin.

Chapter 1 was written by the author and edited by Dr. Corrigan and Dr. Workentin.

Chapter 2 describes the Staudinger reaction on model compounds and on AuNC-azide clusters. The crystal structure analysis was done by Dr. John F. Corrigan. TEM images were taken by Natalie Hamada from Canadian Centre for Electron Microscopy. All other experiments were performed by the author. The chapter was written by the author and edited by Dr. Corrigan and Dr. Workentin

Chapter 3 was written by the author and edited by Dr. Corrigan and Dr. Workentin.

Acknowledgments

First and foremost, I would like to thank my supervisors John Corrigan and Mark Workentin. Thank you for all the guidance I have received throughout my graduate study and help me grow as a chemist.

Special thanks go to my friends and lab mates (Nils, Mansha, Jeffrey, Richard, Jay, Wilson, Praveen, Raj, Justin, Kyle, Christian and Johanna) for all the fun I had in the lab and being patient with me drawing Diels-Alder everywhere and listening to my ridiculous ideas.

I'd also like to give thanks to my friends and families for all their support throughout my graduate studies.

Table of Contents

Abstract.....	ii
Summary for Lay Audience.....	iii
Co-Authorship Statement.....	iv
Acknowledgments.....	v
Table of Contents.....	vi
List of Figures.....	viii
List of Schemes.....	x
List of Appendices.....	xi
List of abbreviation.....	xii
Chapter 1.....	1
1 Introduction.....	1
1.1 Gold nanomaterials.....	1
1.2 Synthesis of Gold nanoclusters.....	2
1.3 Structure and stability of the nanoclusters.....	2
1.4 Ligands in Gold nanocluster chemistry.....	4
1.5 Properties of Gold nanoclusters.....	7
1.6 Click chemistry.....	9
1.7 Click chemistry on gold nanoclusters.....	10
1.8 Scope of thesis.....	13
1.9 References.....	13
Chapter 2.....	22
2 Staudinger Reactions on Azide Functionalized Au ₂₅ Nanoclusters as a Route to Linked Frameworks.....	22
2.1 Introduction.....	22

2.2 Experimental	26
2.2.1 General Considerations and Characterization Methods.....	26
2.2.2 Preparation and Characterization of Compounds	27
2.3 Results and Discussion.....	30
2.4 Conclusion	47
2.5 Reference.....	47
Chapter 3.....	55
3 Conclusion and Outlook.....	55
3.1 Summary and conclusion	55
3.2 Future Work	56
3.3 Reference.....	57
Appendices.....	58
Appendix 1 Permission to Reuse Copy Right Material	58
Appendix 2 Supporting information for Chapter 2	60
Curriculum Vitae	79

List of Figures

Figure 1.1 Au ₁₃ centred icosahedron core along with 6 staple motifs to compose [Au ₂₅ (SR) ₁₈] ⁻ . ¹⁶ Yellow = gold; red = sulfur. Organic ligands omitted for clarity.	3
Figure 1.2 [Au ₂₅ (SR) ₁₈] ⁻ , [Au ₁₁ (PPh ₃) ₇ Cl ₃] and [Au ₁₃ (NHC) ₉ Cl ₃] ²⁺ . Yellow = gold, red = sulfur, green = chlorine, orange=phosphorus, grey=carbon. Organic layers omitted for clarity. ^{19,22,33}	4
Figure 1.3 Synthesis of various azide-functionalized gold nanoclusters using LEIST method. Figure reproduced with permission from ref [45].....	6
Figure 1.4 Continuous energy band for bulk gold (left). Discrete energy level and general emission method for gold nanoclusters (right). ⁴⁹ Blue arrow = absorption, orange arrow = internal conversion, green arrow = vibrational relaxation, red arrow = fluorescence, purple arrow = intersystem crossing, black arrow = phosphorescence.....	7
Figure 1.5 Proposed emission profile after formation of gold nanocluster network via addition of zinc to glutathione protected AuNC. ⁴⁹	9
Figure 2.1 Molecular structure of [(CH ₃ -(CH ₂) ₇) ₄ N][Au ₂₅ (SCH ₂ CH ₂ -p-C ₆ H ₄ -N ₃)] Yellow = gold, red = sulfur, black = carbon (cluster), light blue = carbon (counterion), green = nitrogen. Figure reproduced with permission from ref. [36]	23
Figure 2.2 a) ³¹ P{ ¹ H} NMR spectra of the bidentate phosphine <i>dppb</i> (green) and the thioether Staudinger adduct (2) (red). b) ATR-IR spectrum of the thioether (1) (black) and the Staudinger adduct (2) (red).	32
Figure 2.3 Molecular structure of the gold(I) thiolate coordination complex in the crystal. Thermal ellipsoids drawn at the 50 % probability level. Hydrogen atoms omitted for clarity. [(IPr)Au(SCH ₂ CH ₂ -p-C ₆ H ₄ -N ₃)] (3) in the crystal. Selected angles (deg): N3-N4-N5=173.1(3), C1-Au1-S1=177.52(6), N2-C1-N1=104.2(2). Selected bond lengths (Å): C1-Au1=2.003(2) Au1-S1=2.2869(6).	34

Figure 2.4 a) IR spectrum of the gold complex (3) (black) and reaction sample of gold complex (3) and <i>dppb</i> (red) b) $^{31}\text{P}\{^1\text{H}\}$ NMR spectra of the thioether Staudinger adduct (2) (green) and the reaction sample of the gold complex (3) and <i>dppb</i> (red).....	35
Figure 2.5 UV-Vis absorption spectra of AuNC-azide with different amounts of PPh ₃ stirred at room temperature (above) and at 0°C (below).	38
Figure 2.6 a) $^{31}\text{P}\{^1\text{H}\}$ NMR spectrum of the mixture between AuNC-azide and 3 equivalents of PPh ₃ (green) and 10 equivalents of PPh ₃ (red) b) ATR-IR spectrum of AuNC-azide (black) and the reaction of AuNC-azide and 10 equivalents of PPh ₃ (red).....	39
Figure 2.7 UV-Vis absorption spectra of [AuNC-azide] ⁻ with different amounts of <i>dppb</i> , varying from 0 to 9 equivalents.	40
Figure 2.8 a) $^{31}\text{P}\{^1\text{H}\}$ NMR spectrum of the mixture between [AuNC-azide] ⁻ and 10 equivalents of PPh ₃ (green) and the mixture between [AuNC-azide] ⁻ and 3 equivalents of <i>dppb</i> (red). b) ATR-IR spectra of [AuNC-azide] ⁻ (black) and the mixture between [AuNC-azide] ⁻ and 3 equivalents of <i>dppb</i> . (red).....	41
Figure 2.9 Diffuse reflectance UV-Vis absorption spectra of AuNC-azide (black) and precipitates formed between AuNC-azide and 3 equivalents of <i>dppb</i> (red).....	43
Figure 2.10 ATR-IR spectra of AuNC-azide (black) and the precipitates formed from the mixture between AuNC-azide and 3 equivalents of <i>dppb</i> (red).	44
Figure 2.11 Negative ESI-MS of [Au ₂₅ (SCH ₂ CH ₂ C ₆ H ₄ N ₃) ₁₆ (SCH ₂ CH ₂ C ₆ H ₄ NH ₂) ₂] ⁻ (left) and [Au ₂₅ (SCH ₂ CH ₂ C ₆ H ₄ N ₃) ₁₇ (SCH ₂ CH ₂ C ₆ H ₄ NH ₂)] ⁻ (right).	45
Figure 2.12 TEM image of [AuNC-azide] ⁻ with 3 equivalents of <i>dppb</i> . Top left: the 4 dark spots within the red circle have a diameter of ~1.2 nm, with the distance between them being ~3 nm. Dark spot within yellow circle also has a diameter of ~1.2 nm but has no additional dark spot within 3 nm. Top right: the 3 dark spots within the red circles have a diameter of ~1.2 nm, with the distance between them being ~3 nm. Bottom: the 4 dark spots within the red circles have a diameter of ~1.2 nm, with the distance between them being ~3 nm.	46

List of Schemes

Scheme 1.1 Staudinger reaction between azide and phosphines to form iminophosphorane and hydrolysis to amine and phosphine oxide.	10
Scheme 1.2 Strain-promoted azide-alkyne click reaction between [AuNC-azide] ⁻ and 1-cycloocten-5-yne. ⁴⁴	12
Scheme 1.3 Assemblies of AuNCs via Staudinger between AuNC-azide and phosphine linker.	13
Scheme 2.1 Strain-promoted azide-alkyne click reaction between AuNC-azide and 1-cycloocten-5-yne.....	24
Scheme 2.2 Staudinger reaction between an azide moiety and phosphines to form iminophosphorane. Addition of water to hydrolyze the adduct to amine and phosphine oxide (top). ⁴⁰ The addition of a phosphine linker to couple Staudinger adduct (bottom).	25
Scheme 2.3 Assemblies of AuNCs via Staudinger between AuNC-azide and diphosphine linker (top).	26
Scheme 2.4 Reaction between two equivalents of CH ₃ SCH ₂ CH ₂ - <i>p</i> -C ₆ H ₄ -N ₃ and <i>dppb</i>	31
Scheme 2.5 Reaction between [(IPr)Au(SCH ₂ CH ₂ - <i>p</i> -C ₆ H ₄ -N ₃)] and <i>dppb</i> to form [{(IPr)Au(SCH ₂ CH ₂ C ₆ H ₄ N)} ₂ PPh ₂ C ₆ H ₄ -C ₆ H ₄ PPh ₂] and side product.....	34
Scheme 2.6 Transformation of the cluster [Au ₂₅ (SCH ₂ CH ₂ Ph) ₁₈] ⁻ to [Au ₁₃ (PPh ₃) ₇ (SCH ₂ CH ₂ Ph) ₃] ²⁺ via addition of PPh ₃	36
Scheme 2.7 Possible reaction pathways between [AuNC-azide] ⁻ and PPh ₃	37
Scheme 2.8 Formation of Au ₂₅ network using AuNC-azide and <i>dppb</i>	40
Scheme 3.1 General scheme of Staudinger-Bertozzi ligation on [AuNC-azide] ⁻	57

List of Appendices

Appendices.....	58
Appendix 1 Permission to Reuse Copy Right Material	58
Appendix 2 Supporting information for Chapter 2	60

List of abbreviation

°C	Degree Celcius
δ	Chemical shift
ϵ	Molar absorptivity
λ	Wavelength
AuNC	Gold nanocluster
BSA	Bovine Serum Albumin
cm ⁻¹	Wavenumber
CQD	Colloidal quantum dots
dppb	4,4'-Ph ₂ P-C ₆ H ₄ -C ₆ H ₄ -PPh ₂
ESI-MS	Electrospray Ionization Mass Spectrometry
HOMO	Highest occupied molecular orbital
IPr	bis-1,3-(2,6-diisopropylphenyl) imidazole-2-ylidene
IR	Infrared
LEIST	ligand-exchanged-induced size/structure transformation
LUMO	Lowest unoccupied molecular orbital
MBT	methylbenzenethiolates
mg	milligram
MHz	Megahertz
mL	milliliter
mmol	millimol
nm	nanometer
NHC	N-Heterocyclic carbene
NMR	Nuclear Magnetic Resonance
PEG5	Pentaethaneglycol
PET	Phenylethanethiolate
Ph	Phenyl; C ₆ H ₅
PL-QY	Photoluminescence Quantum Yield
ppm	part per million
SPAAC	Strain-Promoted Azide Alkyne Click
SPANC	Strain-Promoted Alkyne Nitrene Click
TBBT	4- <i>tert</i> -butylbenzethiol
TEM	Transmission Electron Microscopy

THF	Tetrahydrofuran
TOAB	Tetraoctylammonium bromide
UV-Vis	Ultraviolet-Visible

Chapter 1

1 Introduction

1.1 Gold nanomaterials

Colloidal gold has been used around the world for thousands of years.^{1,2} However, it was not until the mid-1800s where the study of the gold nanomaterials began by Faraday.³ The study of gold nanomaterials and their properties has been done extensively over the last few decades due to their applications in such areas as optical imaging⁴, catalysis⁵ and sensing.⁶ The most popular synthetic method to access gold nanomaterials involved reducing tetrachloroauric acid (HAuCl_4) salt in the presence of a protecting organic ligand such as citrates, phosphines and more recently thiolates.² By changing the synthetic conditions, it is possible to synthesize many different types of gold nanomaterials such as nanoparticles⁷ and nanoclusters.⁸ While the shapes and sizes of the gold nanoparticles can be easily characterized via TEM images⁹, it is difficult to analyze their chemical characteristics. The synthesis of nanoparticles often leads to polydispersity, meaning that they are synthesized with a wide size distribution in which the amount of gold atoms and protecting ligands are different, as well as the morphology.^{10,11} Because of the polydispersity, it is often difficult to analyze the chemical properties of gold nanoparticles using typical analysis tools, such as NMR spectroscopy.¹² However, nanoclusters can resolve the problems mentioned above. A nanocluster by definition, is an atomically precise nanomaterial with the diameter of metallic core being less than 2 nm. This means that each cluster can be represented with a definite chemical formula and possesses a precise size and structure. Gold nanoclusters are less than 2 nm because greater sized nanoclusters show plasmonic behaviour, which is a characteristic of nanoparticles.¹³ The study of nanoclusters is important because it helps understand how the metal nanomaterials and ligands are arranged and how the ligands are bonded to the surface. By doing so, it is possible to correlate material properties (optical, catalytic, etc.) with size and shape.¹² In this section, we will take a look at the synthesis and unique properties gold nanoclusters have.

1.2 Synthesis of Gold nanoclusters

The synthesis of gold nanoparticles is typically done via Brust-Schiffrin two-phase method, where HAuCl_4 salt in an aqueous solution is first transferred to an organic layer with the addition of a phase-transfer reagent such as tetraoctylammonium bromide (TOAB). HAuCl_4 is first reduced from Au (III) to Au (I) in the presence of a thiol such as dodecanethiol ($\text{C}_{12}\text{H}_{25}\text{SH}$), then to Au(0) via sodium borohydride (NaBH_4).¹⁴ The Brust-Schiffrin method has had significant impact on synthetic strategies for gold nanoclusters, as the modification of the method and change in the ligand to $\text{SC}_2\text{H}_4\text{C}_6\text{H}_5$ (phenylethylthiolate; PET) eventually lead to the synthesis of $[\text{Au}_{25}(\text{PET})_{18}]^-$.^{15,16} Despite the success in making the Au_{25} cluster, the synthesis also produced clusters with different sizes, leading to low yields.¹⁵ To resolve this limitation, modifications to the Brust-Schiffrin strategy, such as lowering temperature and stirring speed while adding the thiol, can increase the synthetic yield of the cluster via kinetic control. The kinetically controlled synthesis of $[\text{Au}_{25}(\text{PET})_{18}]^-$ has shown that the control of the intermediate $[\text{Au}(\text{I})\text{-SR}]_x$ aggregate is important to successfully synthesize the clusters with high yield. If the size distribution of the aggregate is too large, it can lead to the synthesis of different sized clusters, lowering the yield and making the isolation of the clusters difficult.¹⁷

Another synthetic method for making gold nanoclusters is ligand-exchanged-induced size/structure transformation process, also known as LEIST. With the addition of different ligands, it is possible to rearrange a parent gold nanocluster into another cluster with a different size and monodisperse arrangement.¹⁸ For example, by adding thiolate to $[\text{Au}_{11}(\text{PPh}_3)_7\text{Cl}_3]$, it is possible to rearrange the clusters into $[\text{Au}_{25}(\text{SR})_{18}]^-$, due to the stronger interaction between gold and thiolate compared to gold and phosphine.¹⁹ However, there have also been rare cases where the phosphine displaces the thiolate-protected clusters, such as $[\text{Au}_{25}(\text{SR})_{18}]^-$, to form phosphine-stabilized clusters with different size and monodisperse arrangement.²⁰

1.3 Structure and stability of the nanoclusters

To understand the stability and bonding between the ligands and the cluster, determining the overall structure is critical. The first reported structures of thiolate protected gold

nanoclusters were $[\text{Au}_{102}(\text{SR})_{44}]$ by Kornberg in 2007²¹ and $[\text{Au}_{25}(\text{SR})_{18}]^-$ by Jin in 2008.^{16,22} While many different kernels can be observed within the gold nanoclusters, a centred icosahedron is the most widely observed core structure.¹² Many of the clusters are protected by surface “staple motifs” of $\text{Au}_x(\text{SR})_{x+1}$ as well.²³ For example, $[\text{Au}_{25}(\text{SR})_{18}]^-$ includes an Au_{13} centred icosahedral core, along with 6 staple motifs, with each staple motif consisting of three thiolates and two gold arranged as $(-\text{SR}-\text{Au}-\text{SR}-\text{Au}-\text{SR}-)$ (**Figure 1.1**).²² In each staple motif for $[\text{Au}_{25}(\text{SR})_{18}]^-$, Au (I) is bonded to two SR, with the S-Au-S unit being approximately linear, while the sulfur centre of Au-S-Au within the staple motif has a bond angle of $\sim 100^\circ$.¹⁶ Within $[\text{Au}_{25}(\text{SR})_{18}]^-$, there are two different bonding modes for sulfur: one is the sulfur binding between the kernel and the motif while the other is the sulfur linking the gold atoms within the motif. The sulfur binding to the kernel has much more stable bond compared to the one bonding two golds within the motif.²⁴

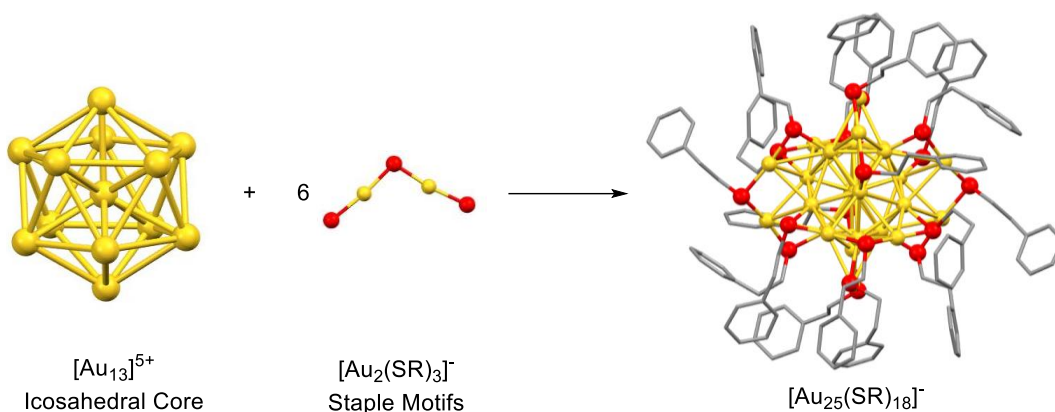


Figure 1.1 Au_{13} centred icosahedron core along with 6 staple motifs to compose $[\text{Au}_{25}(\text{SR})_{18}]^-$.¹⁶ Yellow = gold; red = sulfur. Organic ligands omitted for clarity.

While it is possible to synthesize different sized clusters, there are unique sets of gold nanoclusters with ‘magic numbers’. The magic numbered clusters, such as $[\text{Au}_{25}(\text{SR})_{18}]^-$, are more stable compared to others.²⁵ The magic numbered clusters fill the orbitals in a superatom electron configuration. In superatom theory, the entire cluster will have a delocalized electronic structure, instead of having each individual atoms in the cluster having their own electronic structure. The theory helps predict the stability and chemical nature of the clusters. The valence electronic structure of an entire cluster would be

arranged in the order $|1S^2|1P^6|1D^{10}|2S^2|1F^{14}|2P^6|...$ ²⁶ The order of the electronic structure comes from what is known as the Jellium model which arranges the electronic structure under the assumption that the clusters are spherical. The electronic structures and orbitals in this case are different from the ones in atomic theory, so it is possible to possess orbitals such as 1P and 1D. As the clusters deviate away from spherical shape, the electronic structure starts to deviate from the above model. The stability of the magic numbered clusters come from filling the valence electron shell.²⁷ For example, $[Au_{25}(SR)_{18}]^-$ possesses 8 valence electrons delocalized throughout the cluster and has electronic structure of $1S^2|1P^6$, completely closing the shell and making it more stable compared to other gold nanoclusters without closed electron shell configuration.²⁸ Au_{25} is one of a few gold clusters that can have different charges, -1, 0 and +1. The Au_{25} cluster with 0 and +1 charge have $1S^2|1P^5$ and $1S^2|1P^4$ electron configurations, respectively. The 0 and +1 states are found to have lower thermal stability, mainly because they consist of open shell electron configurations.²⁹

1.4 Ligands in Gold nanocluster chemistry

Gold nanoclusters (AuNCs) are typically protected by various types of organic ligands, including but not limited to thiolates³⁰, phosphines¹⁹, carbenes³¹ and alkynyl groups.³² For example, depending on various synthetic methods, AuNCs such as $[Au_{11}(PPh_3)_7Cl_3]$, $[Au_{25}(SR)_{18}]^-$ (SR = thiolate) and $[Au_{13}(NHC)_9Cl_3]^{2+}$ (NHC = N-heterocyclic carbene) have been previously synthesized (**Figure 1.2**).^{19,22,33}

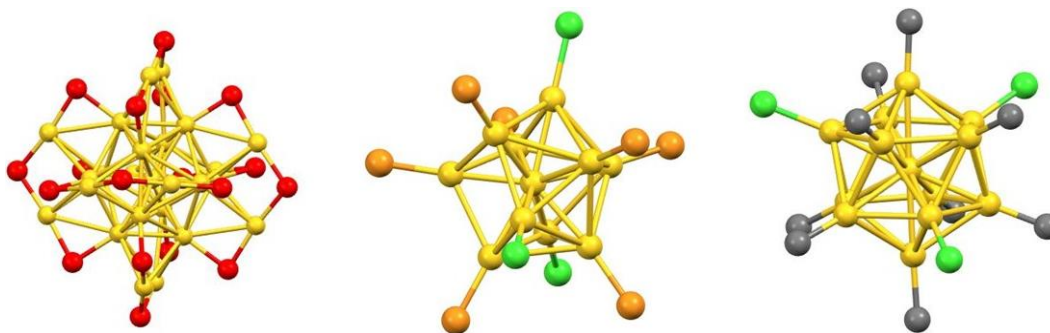


Figure 1.2 $[Au_{25}(SR)_{18}]^-$, $[Au_{11}(PPh_3)_7Cl_3]$ and $[Au_{13}(NHC)_9Cl_3]^{2+}$. Yellow = gold, red = sulfur, green = chlorine, orange=phosphorus, grey=carbon. Organic layers omitted for clarity.^{19,22,33}

Thiolate protected gold nanoclusters have shown several important roles that ligands play in terms of cluster size and structure. First, depending on the steric interactions of the α -carbon (carbon adjacent to the sulfur), it is possible to rearrange the cluster frameworks. For example, with the addition of 4-*tert*-butylbenzenethiol (TBBT), $[\text{Au}_{38}(\text{PET})_{24}]$ can be transformed to $[\text{Au}_{36}(\text{TBBT})_{24}]$.³⁴ Second, the structure of isomeric ligands can change the cluster size as well. For example, Chen's group has shown that by using isomeric ligands such as *o*/*m*/*p*-methylbenzenethiolates (*o*/*m*/*p*-MBT), the cluster size will be different ($[\text{Au}_{40}(\text{SR})_{24}]$, $[\text{Au}_{104}(\text{SR})_{41}]$, $[\text{Au}_{130}(\text{SR})_{50}]$, respectively), despite using similar synthetic methods.³⁵ Lastly, the para position of the phenyl group has an effect on the cluster size as well. For example, *p*-MBT and *p*-TBBT ligands yield $[\text{Au}_{130}(\text{p-MBT})_{50}]$ and $[\text{Au}_{133}(\text{p-TBBT})_{52}]$, respectively.³⁶ The factors above show that subtle changes to ligands can have significant impact on the cluster size and shapes.¹²

While the ligands mentioned above had significant impact in terms of investigating nanocluster synthesis, they all possess thiolates without any reactive functional groups. The advantage of synthesizing clusters with ligands that bear a reactive functional group is that these nanoclusters can undergo further reactions to tune their properties through reaction with substrates possessing the complementary reactive group, without changing the size of the core.³⁷ To date there are few nanoclusters reported that have thiolate ligands that incorporate functional groups such as glutathione³⁸, amine³⁹ and bovine serum albumin (BSA)⁴⁰. In order to synthesize clusters with such ligands, there are some conventional approaches that have been developed. The first is to directly synthesize the clusters with thiolate ligands that bear functional groups, such as glutathione³⁸. However, the controlled synthesis of a functional cluster is difficult due to how sensitive the cluster synthesis is with different ligands, particularly when the ligand possesses chemically sensitive functionalities. Another method to incorporate new ligands without developing new synthesis methods is to perform what is known as a place exchange reaction. A place exchange reaction is one where a newly introduced ligand can replace a ligand bound onto a parent nanocluster.⁴¹ For example, the Murray group has shown that by adding excess pentaethaneglycol thiol (PEG5-SH) at ambient conditions to parent $[\text{Au}_{25}(\text{PET})_{18}]$, it is possible to displace some of the PET ligands to produce $[\text{Au}_{25}(\text{PET})_{18-x}(\text{PEG5-S})_x]$

.⁴² However, with place exchange reactions it is not always possible to replace all the ligands on the cluster and because of this, all the clusters would effectively have different number of new ligands and different ligand arrangement from one another.⁴³ Recently, the Workentin and Corrigan group found a method to develop a reactive azide-modified AuNC via reduction of H₂AuCl₄ salt with NaBH₄ in the presence of an azide functionalized thiol. The AuNC consists of thiolate ligand that bears azide functional group [Au₂₅(SCH₂CH₂C₆H₄N₃)₁₈]⁻.⁴⁴ Most recently, by using LEIST method, Zhang's group developed different azide functionalized AuNCs: [Au₂₅(PPh₃)₁₀(SPhN₃)₅Cl₂] from [Au₁₁(PPh₃)₇Cl₃], [Au₂₈(SPhN₃)₂₀] from both [Au₂₃(S-*c*-C₆H₁₁)₁₆] and [Au₂₅(PET)₁₈] clusters and [Au₃₆(SPhN₃)₂₄] from both [Au₃₀(S-*t*-C₄H₉)₁₈], and [Au₃₈(SC₂H₄Ph)₂₄], as shown in **figure 1.3**.⁴⁵

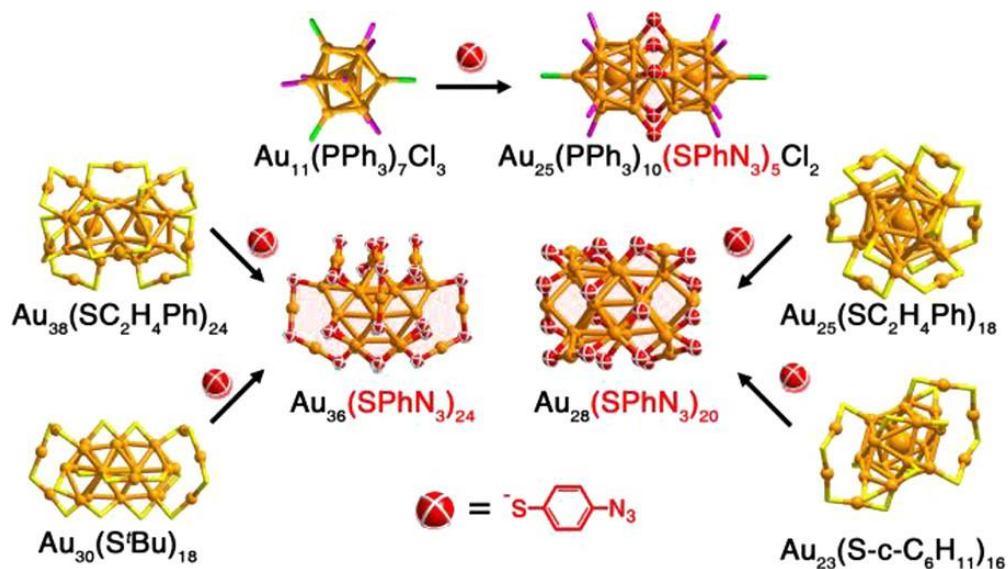


Figure 1.3 Synthesis of various azide-functionalized gold nanoclusters using LEIST method. Figure reproduced with permission from ref [45].

The cluster [Au₂₅(PPh₃)₁₀(SPhN₃)₅Cl₂] has a bi-icosahedral shape, which is different from the typical [Au₂₅(SR)₁₈]⁻ cluster structure shown above. All of the transformations show that the energy required for rearrangement is low and strongly dependent on the new surface ligands. While the transformations of the clusters listed above have been shown previously via introduction of non-functional thiolate ligands,^{19,34,46–48} the transformation of the cluster via an azide-functionalized ligand is new. The development of such new

methodologies for the synthesis of azide-functionalized nanocluster is important because the surface azide moieties can undergo different reactions with substrates possessing different complementary reactive partners. This can lead to change in surface properties, also known as post-assembly surface modification, meaning that the surface properties of the material can change after the synthesis of a fixed framework AuNC.⁴⁵

1.5 Properties of Gold nanoclusters

In contrast to bulk gold which has continuous energy bands, AuNCs have discrete molecular-like energy levels. This means that the energy level of the AuNC is quantized and can absorb only distinct energy (**Figure 1.3**).

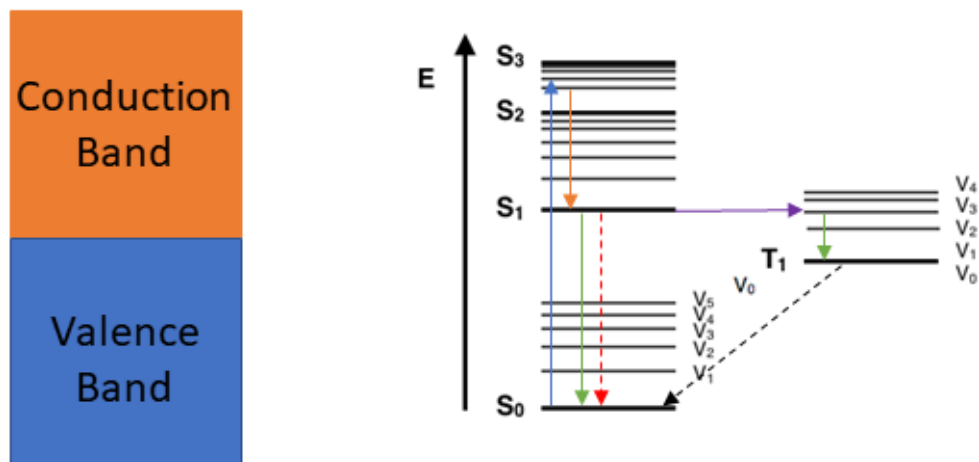


Figure 1.4 Continuous energy band for bulk gold (left). Discrete energy level and general emission method for gold nanoclusters (right).⁴⁹ Blue arrow = absorption, orange arrow = internal conversion, green arrow = vibrational relaxation, red arrow = fluorescence, purple arrow = intersystem crossing, black arrow = phosphorescence.

Depending on the cluster size and shape, the absorption properties may vary.¹⁰ However, the exact energy levels of the clusters were not well known until 2008, after the crystal structure of $[\text{Au}_{25}(\text{PET})_{18}]^-$ was analyzed.²² The cluster $[\text{Au}_{25}(\text{PET})_{18}]^-$ has a set of resolved peaks in the visible absorption spectrum at 680 nm, 440 nm and 400 nm.⁵⁰ It has been found that the peak at 680 nm arises from a transition from the highest occupied molecular orbital (HOMO) to lowest unoccupied molecular orbital (LUMO). The HOMO

and LUMO orbital contribution comes mainly from the Au₁₃ icosahedral core, which implies that the transition is mainly from the electronic structure of the central Au₁₃.²² Other thiolate protected gold clusters such as glutathione protected Au₂₅ consistently have peaks at the 3 wavelengths listed above.⁵¹ The selenium analogue [Au₂₅(SeCH₂CH₂C₆H₅)₁₈]⁻ has a peak at 683 nm, a slight bathochromic shift compared to [Au₂₅(PET)₁₈]⁻, which implies that the anchoring atom of the ligands can affect the energy levels of the HOMO and LUMO, which in turns affects the absorption profile.⁵²

Gold nanoclusters typically have poor photoluminescence quantum yields (PL-QYs) (~1 %).⁵³ However, there are many different factors that can influence the PL-QY and a few AuNCs have been reported with higher PL-QYs. One of the factors that influences the luminescent property is the ligand's ability to transfer the charge onto the metal core. Jin's group has shown that out of PET, -SC₁₂H₂₅ and -SC₆H₁₃ ligands, [Au₂₅(PET)₁₈]⁻ has the highest fluorescence intensity while [Au₂₅(SC₆H₁₃)₁₈]⁻ has the lowest. Out of the three ligands, -SC₆H₁₃ has the lowest electron donating capability, while PET has the stronger donating capability compared to the two. It has also been shown that the fluorescence intensity becomes greater as the positive charge on the cluster increases. This shows that by either increasing a ligand's ability to donate charges, or by increasing the cluster oxidation state, it is possible to increase the fluorescence intensity, due to better charge transfer from ligand to gold. By exchanging the glutathione ligands of Au₂₅ with peptides that include many electron-rich nitrogen and oxygen atoms, the Au₂₅ is able to exhibit greater fluorescence intensity.⁵⁴

A recent report from Yuan's group has shown that with the addition of zinc to a glutathione protected gold nanocluster, the carboxylate group of the glutathione ligands can coordinate onto zinc. By doing so, they found that the gold nanoclusters can form assemblies. It was found that while glutathione protected gold clusters have poor PL-QY (~1 %), the formation of the gold cluster network can improve the PL-QY up to 40 %. It was found that the formation of such assemblies results in significant suppression of non-radiative relaxation from restricting vibration and rotation, along with an increase in ligand-to-metal charge transfer, which in turn increases PL-QY and photoluminescent lifetime (**Figure 1.4**). Also, it was found that such assemblies do not suffer from self-

quenching.³⁷ The increase in PL-QY for the gold nanocluster network has potential to be used as light-emitting material just like colloidal quantum dots (CQDs), which are often used as a light-emitting materials in industry due to their photophysical properties, with tunable light absorption and efficient PL emission.⁵⁵ However, unlike AuNCs, CQDs often involve toxic heavy-metal elements and tend to suffer from self-quenching due to aggregation.^{56,57}

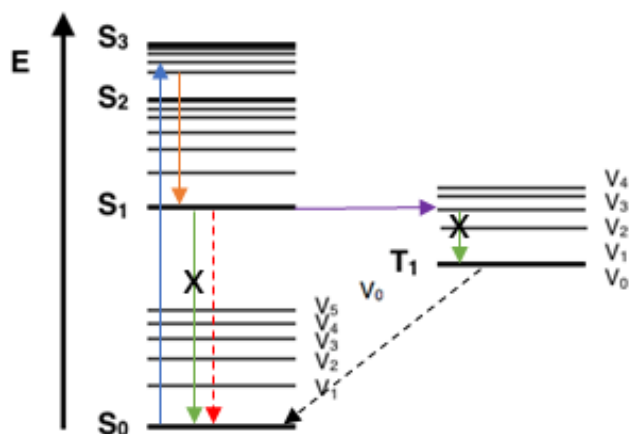
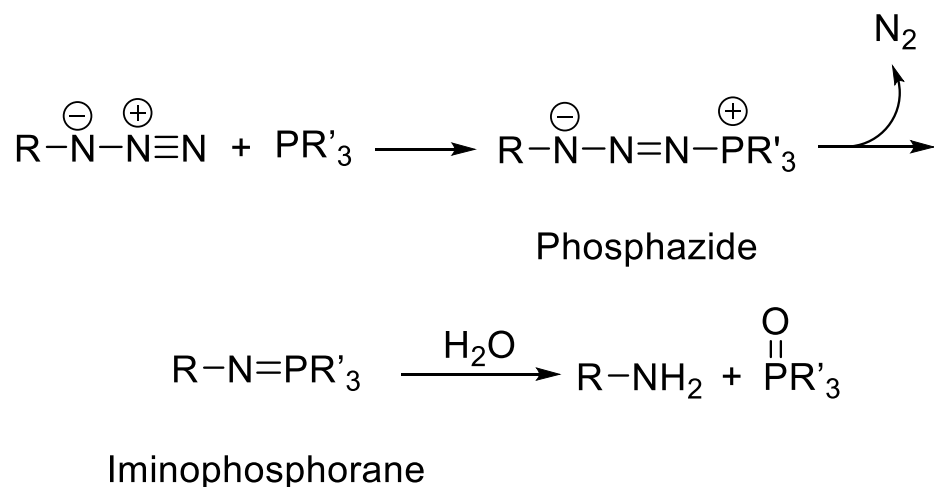


Figure 1.5 Proposed emission profile after formation of gold nanocluster network via addition of zinc to glutathione protected AuNC.⁴⁹

1.6 Click chemistry

In 2001, Sharpless coined the term ‘click chemistry’, which describes reactions that proceed with high yields, very fast reaction rates, are very easy to purify and produce only inoffensive or no by-products. Such reactions also need to proceed selectively with a particular functional group.⁵⁸ Ever since the click reaction criteria have been defined by Sharpless, they have been widely applied on materials, including gold nanoparticles.⁵⁹ The advantage of a click reaction is that it is possible to selectively react with materials after their synthesis, also known as post-assembly surface modification. By performing post-assembly modification it is thus possible to change the surface property of the materials.⁵⁹

While the most common click reaction is one between an azide and an alkyne to form triazole click adduct, there are many other click reactions including a reaction between alkyne and nitrene, also known as SPANC and Staudinger-Bertozzi ligation, which involves ortho-ester triphenylphosphine and azide to form amide.^{60,61} Another click reaction involving an azide as one of the reaction partners and one that is the focus of this thesis is the Staudinger reaction. Originally developed in early 1900s, the Staudinger reaction involves azide moieties and phosphines.⁶² The lone pair on phosphorus acts as a soft nucleophile and attacks the terminal nitrogen of the azide, which acts as a soft electrophile, to form a phosphazide intermediate. The intermediate undergoes rearrangement to form an iminophosphorane with the elimination of N₂ gas. In the absence of water, the reaction stops at the iminophosphorane. However, when water is present, it is possible to hydrolyze the iminophosphorane group into the corresponding primary amine and phosphine oxide. The Staudinger reaction has been used often to reduce azides to amines (**Scheme 1.1**).⁶³

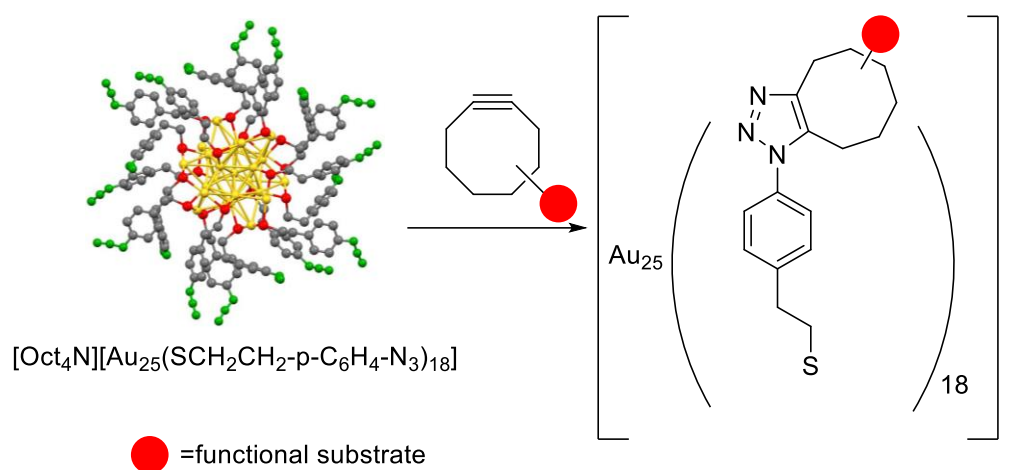


Scheme 1.1 Staudinger reaction between azide and phosphines to form iminophosphorane and hydrolysis to amine and phosphine oxide.

1.7 Click chemistry on gold nanoclusters

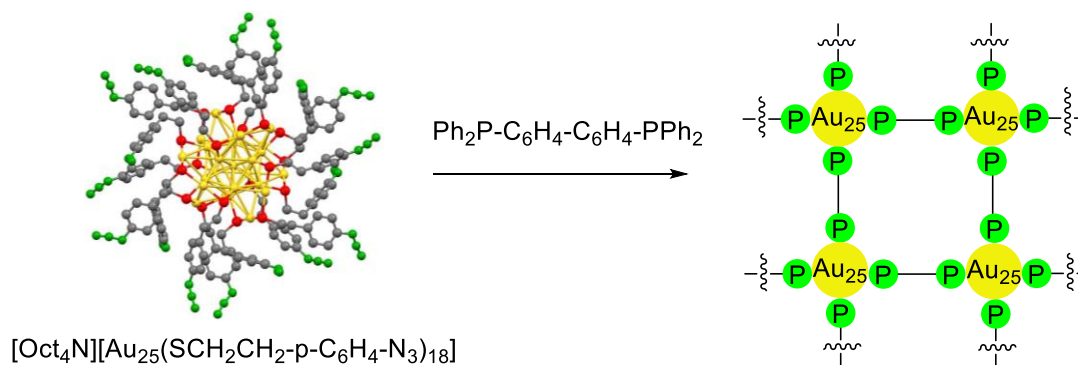
The Workentin group in the past has performed different types of click reactions, such as strain-promoted azide-alkyne click (SPAAC) reaction on gold nanoparticles.⁶⁴ While

many different click reactions have been performed on gold nanoparticles, the lack of ligands bearing functional groups that are able to undergo click reaction currently limits the study of click chemistry on gold nanocluster platforms. The lack of methods to couple compounds such as fluorophores or proteins limited the application driven studies on gold nanoclusters. However, the recently synthesized azide functionalized AuNC has opened the possibility of series of click reaction on gold nanoclusters, such as SPAAC. The Workentin and Corrigan groups, and later that of Zhang's group have demonstrated that click reaction such as SPAAC on gold nanocluster can be achieved on the azide-functionalized gold nanocluster with the addition of strained alkyne.^{44,45} However, the azide moiety is a reactive group that can undergo many different click reactions, such as SPAAC and the Staudinger-Bertozzi ligation, which in turn opens up the possibility for other post-assembly surface modifications of gold nanoclusters.^{65,66} The Workentin and Corrigan groups has shown that all 18 azide-functionalized thiolate ligands incorporated on the cluster $[\text{Au}_{25}(\text{S}-\text{CH}_2\text{CH}_2\text{C}_6\text{H}_4-\text{N}_3)_{18}]^-$, ($[\text{AuNC}-\text{azide}]^-$), are accessible for click reaction via SPAAC reaction with minimal side products (**Scheme 1.2**), showing that there is a possibility of giving the cluster multi-function, or the possibility of performing different click reactions on the same cluster. Also, due to the high ring strain on alkyne functional group, the SPAAC reaction on the cluster is done within 5 minutes. The SPAAC reaction has been used to demonstrate fast post-assembly surface modification with no side products. By incorporating different functional substrates onto the strained-alkyne, such as biomolecules onto the strained-alkyne, it is also possible to find easier approaches to add functionality to the nanocluster surface.⁴⁴



Scheme 1.2 Strain-promoted azide-alkyne click reaction between $[\text{AuNC-azide}]^-$ and 1-cycloocten-5-yne. ⁴⁴

The methodology for the synthesis of azide-functionalized cluster is still new, meaning that the study of other click reactions involving azide, such as the Staudinger reaction on the gold nanocluster is still lacking. With the addition of phosphines, it is possible to perform Staudinger reactions and stop the reaction under dry reaction conditions to form iminophosphorane on the gold nanoclusters with nitrogen gas being the only side product. By hydrolyzing it, it is also possible to form amine functionalized gold nanocluster, providing an additional level of control over the surface reactivity that doesn't exist when using the SPAAC reaction. Furthermore, with the addition of diphosphines, it is possible to form networks of clusters via formation of iminophosphoranes, which could potentially increase PL-QY (**Scheme 1.3**). The formation of network via formation of iminophosphorane should give couple advantages over Yuan's group's glutathione protected AuNC network. First, the only side product from the formation of iminophosphorane in a Staudinger reaction is nitrogen gas, meaning that the purification method is simpler compared to other non-click reactions. Second, by using different phosphine linkers (longer chain, different side group on the phosphine), there is a possibility that photophysical properties of the cluster can be changed easier compared to Yuan's group.



Scheme 1.3 Assemblies of AuNCs via Staudinger between AuNC-azide and phosphine linker.

1.8 Scope of thesis

This thesis explores the viability of the Staudinger reaction on the AuNC-azide clusters along with formation of the AuNC-networks via formation of iminophosphorane from Staudinger reaction between 4,4'-Ph₂P-C₆H₄-C₆H₄-PPh₂ (*dppb*) and AuNC-azide. The Staudinger reaction was performed on *p*-azido-phenylethane methyl thioether and [(IPr)Au(SCH₂CH₂C₆H₄N₃)] prior to formation of network with AuNC-azide to find suitable phosphine partner for the Staudinger reaction. It was also done so the data could be used to compare the data for the Staudinger reaction on AuNC-azide. Chapter 2 focuses on Staudinger reaction between *dppb* on model compounds and AuNC-azide, along with Staudinger reaction between triphenylphosphine and AuNC-azide. Chapter 3 summarizes the results from previous chapter and focuses on future outlooks for the project.

1.9 References

- (1) Daniel, M. C. M.; Astruc, D. Gold Nanoparticles: Assembly, Supramolecular Chemistry, Quantum-Size Related Properties and Applications toward Biology, Catalysis and Nanotechnology. *Chem. Rev.* **2004**, *104*, 293–346.
- (2) Sharma, V.; Park, K.; Srinivasarao, M. Colloidal Dispersion of Gold Nanorods: Historical Background, Optical Properties, Seed-Mediated Synthesis, Shape Separation and Self-Assembly. *Mater. Sci. Eng. R Reports* **2009**, *65*, 1–38.

- (3) Reddy, V. R. Gold Nanoparticles: Synthesis and Applications. *Synlett* **2006**, 1791–1792.
- (4) Raut, S. L.; Shumilov, D.; Chib, R.; Rich, R.; Gryczynski, Z.; Gryczynski, I. Two Photon Induced Luminescence of BSA Protected Gold Clusters. *Chem. Phys. Lett.* **2013**, 561–562, 74–76.
- (5) Nasaruddin, R. R.; Yao, Q.; Chen, T.; Hülsey, M. J.; Yan, N.; Xie, J. Hydride-Induced Ligand Dynamic and Structural Transformation of Gold Nanoclusters during a Catalytic Reaction. *Nanoscale* **2018**, 10, 23113–23121.
- (6) Xie, J.; Zheng, Y.; Ying, J. Y. Highly Selective and Ultrasensitive Detection of Hg²⁺ Based on Fluorescence Quenching of Au Nanoclusters by Hg²⁺-Au⁺ Interactions. *Chem. Commun.* **2010**, 46, 961–963.
- (7) Yeh, Y.-C.; Creran, B.; Rotello, V. M. Gold Nanoparticles: Preparation, Properties, and Applications in Bionanotechnology. *Nanoscale* **2012**, 4, 1871–1880.
- (8) Qian, H.; Zhu, M.; Wu, Z.; Jin, R. Quantum Sized Gold Nanoclusters with Atomic Precision. *Acc. Chem. Res.* **2012**, 45, 1470–1479.
- (9) Young, N. P.; van Huis, M. A.; Zandbergen, H. W.; Xu, H.; Kirkland, A. I. Transformations of Gold Nanoparticles Investigated Using Variable Temperature High-Resolution Transmission Electron Microscopy. *Ultramicroscopy* **2010**, 110, 506–516.
- (10) Jin, R. Atomically Precise Metal Nanoclusters: Stable Sizes and Optical Properties. *Nanoscale* **2015**, 7, 1549–1565.
- (11) Kurashige, W.; Niihori, Y.; Sharma, S.; Negishi, Y. Precise Synthesis, Functionalization and Application of Thiolate-Protected Gold Clusters. *Coord. Chem. Rev.* **2016**, 320–321, 238–250.
- (12) Jin, R.; Zeng, C.; Zhou, M.; Chen, Y. Atomically Precise Colloidal Metal

- Nanoclusters and Nanoparticles : Fundamentals and Opportunities. *Chem. Rev.* **2016**, *116*, 10346–10413.
- (13) Kang, X.; Chong, H.; Zhu, M. Au₂₅(SR)₁₈: The Captain of the Great Nanocluster Ship. *Nanoscale* **2018**, *10*, 10758–10834.
- (14) Brust, M.; Walker, M.; Bethell, D.; Schiffrin, D. J.; Whyman, R. Synthesis of Thiol-Derivatized Gold Nanoparticles in a Two-Phase Liquid-Liquid System. *J. Chem. Soc., Chem. Commun.* **1994**, *7*, 801–802.
- (15) Price, R. C.; Whetten, R. L. All-Aromatic, Nanometer-Scale, Gold-Cluster Thiolate Complexes. *J. Am. Chem. Soc.* **2005**, *127*, 13750–13751.
- (16) Heaven, M. W.; Dass, A.; White, P. S.; Holt, K. M.; Murray, R. W. Crystal Structure of the Gold Nanoparticle [N(C₈H₁₇)₄][Au₂₅(SCH₂CH₂Ph)₁₈]. *J. Am. Chem. Soc.* **2008**, *130*, 3754–3755.
- (17) Zhu, M.; Lanni, E.; Garg, N.; Bier, M. E.; Jin, R. Kinetically Controlled, High-Yield Synthesis of Au₂₅ Clusters. *J. Am. Chem. Soc.* **2008**, *130*, 1138–1139.
- (18) Zeng, C.; Chen, Y.; Das, A.; Jin, R. Transformation Chemistry of Gold Nanoclusters: From One Stable Size to Another. *J. Phys. Chem. Lett.* **2015**, *6*, 2976–2986.
- (19) McKenzie, L. C.; Zaikova, T. O.; Hutchison, J. E. Structurally Similar Triphenylphosphine-Stabilized Undecagolds, Au₁₁(PPh₃)₇Cl₃ and [Au₁₁(PPh₃)₈Cl₂]Cl, Exhibit Distinct Ligand Exchange Pathways with Glutathione. *J. Am. Chem. Soc.* **2014**, *136*, 13426–13435.
- (20) Li, M.; Tian, S.; Wu, Z.; Jin, R. Peeling the Core – Shell Au₂₅ Nanocluster by Reverse Ligand- Exchange. *Chem. Mater.* **2016**, *28*, 1022–1025.
- (21) Jadzinsky, P. D.; Calero, G.; Ackerson, C. J.; Bushnell, D. A.; Kornberg, R. D. Structure of a Thiol Monolayer-Protected Gold Nanoparticle at 1.1 Å Resolution. *Science* **2007**, *318*, 430–433.

- (22) Zhu, M.; Aikens, C. M.; Hollander, F. J.; Schatz, G. C.; Jin, R. Correlating the Crystal Structure of A Thiol-Protected Au₂₅ Cluster and Optical Properties. *J. Am. Chem. Soc.* **2008**, *130*, 5883–5885.
- (23) Jiang, D. E. The Expanding Universe of Thiolated Gold Nanoclusters and Beyond. *Nanoscale* **2013**, *5*, 7149–7160.
- (24) Wu, Z.; Jin, R. Stability of the Two Au-S Binding Modes in Au₂₅(SG)₁₈ Nanoclusters Probed by NMR and Optical Spectroscopy. *ACS Nano* **2009**, *3*, 2036–2042.
- (25) Kurashige, W.; Niihori, Y.; Sharma, S.; Negishi, Y. Recent Progress in the Functionalization Methods of Thiolate-Protected Gold Clusters. *J. Phys. Chem. Lett.* **2014**, *5*, 4134–4142.
- (26) Yoon, B.; Koskinen, P.; Huber, B.; Kostko, O.; Von Issendorff, B.; Häkkinen, H.; Moseler, M.; Landman, U. Size-Dependent Structural Evolution and Chemical Reactivity of Gold Clusters. *ChemPhysChem* **2007**, *8*, 157–161.
- (27) Tsukamoto, T.; Haruta, N.; Kambe, T.; Kuzume, A.; Yamamoto, K. Periodicity of Molecular Clusters Based on Symmetry-Adapted Orbital Model. *Nat. Commun.* **2019**, *10*, 1–8.
- (28) Akola, J.; Walter, M.; Whetten, R. L.; Häkkinen, H.; Gronbeck, H. On the Structure of Thiolate-Protected Au₂₅. *J. Am. Chem. Soc.* **2008**, *130*, 3756–3757.
- (29) Tofanelli, M. A.; Ackerson, C. J. Superatom Electron Configuration Predicts Thermal Stability of Au₂₅(SR)₁₈ Nanoclusters. *J. Am. Chem. Soc.* **2012**, *134* (41), 16937–16940.
- (30) Yao, Q.; Wu, Z.; Liu, Z.; Lin, Y.; Yuan, X.; Xie, J. Molecular Reactivity of Thiolate-Protected Noble Metal Nanoclusters: Synthesis, Self-Assembly, and Applications. *Chem. Sci.* **2021**, *12*, 99–127.
- (31) Shen, H.; Deng, G.; Kaappa, S.; Tan, T.; Han, Y.; Malola, S.; Lin, S.; Teo, B. K.;

- Hannu, H.; Zheng, N. Highly Robust but Surface-Active : An N-Heterocyclic Carbene-Stabilized Au₂₅ Nanocluster. *Angew. Chem. Int. Ed.* **2019**, *58*, 17731–17735.
- (32) Lei, Z.; Li, J. J.; Wan, X. K.; Zhang, W. H.; Wang, Q. M. Isolation and Total Structure Determination of an All-Alkynyl-Protected Gold Nanocluster Au₁₄₄. *Angew. Chem. Int. Ed.* **2018**, *57*, 8639–8643.
- (33) Narouz, M. R.; Takano, S.; Lummis, P. A.; Levchenko, T. I.; Nazemi, A.; Kaappa, S.; Malola, S.; Yousefalizadeh, G.; Calhoun, L. A.; Stampelcoskie, K. G.; Häkkinen, H.; Tsukuda, T.; Crudden, C. M. Robust, Highly Luminescent Au₁₃ Superatoms Protected by N-Heterocyclic Carbenes. *J. Am. Chem. Soc.* **2019**, *141*, 14997–15002.
- (34) Zeng, C.; Liu, C.; Pei, Y.; Jin, R.; Avenue, F.; States, U.; Chemistry, E. F.; Province, H. Thiol Ligand-Induced Transformation of Au₃₈(SC₂H₄Ph)₂₄ to Au₃₆(SPh-*t*-Bu)₂₄. *ACS Nano* **2013**, *7*, 6138–6145.
- (35) Chen, Y.; Zeng, C.; Kauffman, D. R.; Jin, R. Tuning the Magic Size of Atomically Precise Gold Nanoclusters via Isomeric Methylbenzenethiols. *Nano Lett.* **2015**, *15*, 3603–3609.
- (36) Chen, Y.; Zeng, C.; Liu, C.; Kirschbaum, K.; Gayathri, C.; Gil, R. R.; Rosi, N. L.; Jin, R. Crystal Structure of Barrel-Shaped Chiral Au₁₃₀(*p*-MBT)₅₀ Nanocluster. *J. Am. Chem. Soc.* **2015**, *137*, 10076–10079.
- (37) Huang, H. Y.; Cai, K. Bin; Talite, M. J.; Chou, W. C.; Chen, P. W.; Yuan, C. T. Coordination-Induced Emission Enhancement in Gold-Nanoclusters with Solid-State Quantum Yields up to 40% for Eco-Friendly, Low-Reabsorption Nano-Phosphors. *Sci. Rep.* **2019**, *9*, 1–11.
- (38) Negishi, Y.; Takasugi, Y.; Sato, S.; Yao, H.; Kimura, K.; Tsukuda, T. Magic-Numbered Au_n Clusters Protected by Glutathione Monolayers (N=18, 21, 25, 28, 32, 29): Isolation and Spectroscopic Characterization. *J. Am. Chem. Soc.* **2004**,

126, 6518–6519.

- (39) Lavenn, C.; Albrieux, F.; Bergeret, G.; Chiriach, R.; Delichère, P.; Tuel, A.; Demessence, A. Functionalized Gold Magic Clusters: Au₂₅(SPhNH₂)₁₇. *Nanoscale* **2012**, *4*, 7334–7337.
- (40) Xie, J.; Zheng, Y.; Ying, J. Y. Protein-Directed Synthesis of Highly Fluorescent Gold Nanoclusters. *J. Am. Chem. Soc.* **2009**, *131*, 888–889.
- (41) Hostetler, M. J.; Templeton, A. C.; Murray, R. W. Dynamics of Place-Exchange Reactions on Monolayer-Protected Gold Cluster Molecules. *Langmuir* **1999**, *15*, 3782–3789.
- (42) Tracy, J. B.; Crowe, M. C.; Parker, J. F.; Hampe, O.; Fields-zinna, C. A.; Dass, A.; Murray, R. W. Electrospray Ionization Mass Spectrometry of Uniform and Mixed Monolayer Nanoparticles: Au₂₅[S(CH₂)₂Ph]₁₈ and Au₂₅[S(CH₂)₂Ph]_{18-x}(SR)_x. *J. Am. Chem. Soc.* **2007**, *129*, 16209–16215.
- (43) Dass, A.; Stevenson, A.; Dubay, G. R.; Tracy, J. B.; Murray, R. W. Nanoparticle MALDI-TOF Mass Spectrometry without Fragmentation: Au₂₅(SCH₂CH₂Ph)₁₈ and Mixed Monolayer Au₂₅(SCH₂CH₂Ph)_{18-x}(L)_x. *J. Am. Chem. Soc.* **2008**, *130*, 5940–5946.
- (44) Gunawardene, P. N.; Corrigan, J. F.; Workentin, M. S. Golden Opportunity: A Clickable Azide-Functionalized [Au₂₅(SR)₁₈] – Nanocluster Platform for Interfacial Surface Modifications. *J. Am. Chem. Soc.* **2019**, *141*, 11781–11785.
- (45) Kang, X.; Ren, M.; Zhu, M.; Zhang, K. Azide-Functionalized Nanoclusters via a Ligand-Induced Rearrangement. *Chem. Mater.* **2020**, *32*, 6736–6743.
- (46) Zeng, C.; Li, T.; Das, A.; Rosi, N. L.; Jin, R. Chiral Structure of Thiolate-Protected 28-Gold-Atom Nanocluster Determined by X-Ray Crystallography. *J. Am. Chem. Soc.* **2013**, *135*, 10011–10013.
- (47) Higaki, T.; Liu, C.; Chen, Y.; Zhao, S.; Zeng, C.; Jin, R.; Wang, S.; Rosi, N. L.; Jin,

- R. Oxidation-Induced Transformation of Eight-Electron Gold Nanoclusters: $[\text{Au}_{23}(\text{SR})_{16}]^-$ to $[\text{Au}_{28}(\text{SR})_{20}]^0$. *J. Phys. Chem. Lett.* **2017**, *8*, 866–870.
- (48) Dass, A.; Jones, T. C.; Theivendran, S.; Sementa, L.; Fortunelli, A. Core Size Interconversions of $\text{Au}_{30}(\text{S-TBu})_{18}$ and $\text{Au}_{36}(\text{SPhX})_{24}$. *J. Phys. Chem. C* **2017**, *121*, 14914–14919.
- (49) McEwen, J. Jablonski diagram - Chemistry LibreTexts [https://chem.libretexts.org/Bookshelves/Physical_and_Theoretical_Chemistry_Textbook_Maps/Supplemental_Modules_\(Physical_and_Theoretical_Chemistry\)/Spectroscopy/Electronic_Spectroscopy/Jablonski_diagram](https://chem.libretexts.org/Bookshelves/Physical_and_Theoretical_Chemistry_Textbook_Maps/Supplemental_Modules_(Physical_and_Theoretical_Chemistry)/Spectroscopy/Electronic_Spectroscopy/Jablonski_diagram) (accessed Sep 24, 2021).
- (50) Patel, A.; On, M. C.; Choi, J. Optical Properties of Molecule-Like Au 25 Nanoparticles. *Int. J. Eng. Sci. Invent.* **2017**, *6*, 71–76.
- (51) Katla, S. K.; Zhang, J.; Castro, E.; Bernal, R. A.; Li, X. Atomically Precise $\text{Au}_{25}(\text{SG})_{18}$ Nanoclusters: Rapid Single-Step Synthesis and Application in Photothermal Therapy. *ACS Appl. Mater. Interfaces* **2018**, *10*, 75–82.
- (52) Song, Y.; Zhong, J.; Yang, S.; Wang, S.; Cao, T.; Zhang, J.; Li, P.; Hu, D.; Pei, Y.; Zhu, M. Crystal Structure of $\text{Au}_{25}(\text{SePh})_{18}$ Nanoclusters and Insights into Their Electronic, Optical and Catalytic Properties. *Nanoscale* **2014**, *6*, 13977–13985.
- (53) Herbert, P. J.; Ackerson, C. J.; Knappenberger, K. L. Size-Scalable Near-Infrared Photoluminescence in Gold Monolayer Protected Clusters. *J. Phys. Chem. Lett.* **2021**, *12*, 7531–7536.
- (54) Wu, Z.; Jin, R. On the Ligand's Role in the Fluorescence of Gold Nanoclusters. *Nano Lett.* **2010**, *25*, 2568–2573.
- (55) Bourzac, K. Quantum Dots Go on Display. *Nature* **2013**, *493*, 283.
- (56) Dupont, D.; Tessier, M. D.; Smet, P. F.; Hens, Z. Indium Phosphide-Based Quantum Dots with Shell-Enhanced Absorption for Luminescent Down-Conversion. *Adv. Mater.* **2017**, *29*, 1–6.

- (57) Wang, X.; Yan, X.; Li, W.; Sun, K. Doped Quantum Dots for White-Light-Emitting Diodes without Reabsorption of Multiphase Phosphors. *Adv. Mater.* **2012**, *24*, 2742–2747.
- (58) Kolb, H. C.; Finn, M. G.; Sharpless, K. B. Click Chemistry: Diverse Chemical Function from a Few Good Reactions. *Angew. Chem. Int. Ed.* **2001**, *40*, 2004–2021.
- (59) Poonthiyil, V.; Lindhorst, T. K.; Golovko, V. B.; Fairbanks, A. J. Recent Applications of Click Chemistry for the Functionalization of Gold Nanoparticles and Their Conversion to Glyco-Gold Nanoparticles. *Beilstein J. Org. Chem.* **2017**, *14*, 11–24.
- (60) Agard, N. J.; Baskin, J. M.; Prescher, J. A.; Lo, A.; Bertozzi, C. R. A Comparative Study of Bioorthogonal Reactions with Azides. *ACS Chem. Biol.* **2006**, *1*, 644–648.
- (61) MacKenzie, D. A.; Sherratt, A. R.; Chigrinova, M.; Cheung, L. L. W.; Pezacki, J. P. Strain-Promoted Cycloadditions Involving Nitrones and Alkynes-Rapid Tunable Reactions for Bioorthogonal Labeling. *Curr. Opin. Chem. Biol.* **2014**, *21*, 81–88.
- (62) Gololobov, Y. G.; Kasukhin, L. F. Recent Advances in the Staudinger Reaction. *Tetrahedron* **1992**, *48*, 1353–1406.
- (63) Leffler, J. E.; Temple, R. D. The Staudinger Reaction between Triarylphosphines and Azides. A Study of the Mechanism. *J. Am. Chem. Soc.* **1967**, *89*, 5235–5246.
- (64) Wang, X.; Gobbo, P.; Suchy, M.; Workentin, M. S.; Hudson, R. H. E. Peptide-Decorated Gold Nanoparticles via Strain-Promoted Azide-Alkyne Cycloaddition and Post Assembly Deprotection. *RSC Adv.* **2014**, *4*, 43087–43091.
- (65) Gobbo, P.; Luo, W.; Cho, S. J.; Wang, X.; Biesinger, M. C.; Hudson, R. H. E.; Workentin, M. S. Small Gold Nanoparticles for Interfacial Staudinger–Bertozzi Ligation. *Org. Biomol. Chem.* **2015**, *13*, 4605–4612.

- (66) Gobbo, P.; Novoa, S.; Biesinger, M. C.; Workentin, M. S. Interfacial Strain-Promoted Alkyne-Azide Cycloaddition (I-SPAAC) for the Synthesis of Nanomaterial Hybrids. *Chem. Commun.* **2013**, *49*, 3982–3984.

Chapter 2

2 Staudinger Reactions on Azide Functionalized Au₂₅ Nanoclusters as a Route to Linked Frameworks

2.1 Introduction

Nanoclusters are atomically precise materials which are smaller than 2 nm in diameter, and are monolayer-protected,¹⁻³ meaning that the core of the cluster is protected by a layer of surface ligands, such as thiolates.^{1,4,5} Gold nanoclusters (AuNCs) can also possess other types of surface ligands, such as alkynyls⁶⁻⁸, phosphines⁹⁻¹³ or N-heterocyclic carbenes¹⁴⁻¹⁷ and, depending on the cluster size and ligand selection, it is possible to tune the size and electronic properties of these metallic arrangements.^{2,18}

Out of all the AuNCs reported to date, the complex [Au₂₅(SR)₁₈]⁻ has been studied most extensively due in part to the fact that the synthetic yield for [Au₂₅(SR)₁₈]⁻ is high relative to other AuNCs.¹⁹ The synthetic yield of specific clusters is often low because in addition to the desired cluster, other cluster sizes consisting of different number of atoms also form under the reaction conditions employed.²⁰ The [Au₂₅(SR)₁₈]⁻ cluster consists of a central, centered Au₁₃ icosahedron core with 6 surface staple motifs, with each staple consisting of two gold and three μ_2 -thiolates.²¹⁻²³ The electronic structure of anionic [Au₂₅(SR)₁₈]⁻ is described with the “superatom” model and a closed-shell octet configuration in the Au₁₃ metal core.²¹ Au₂₅ is one of the few AuNC that exhibits the ability to be isolated with differing oxidation states, an overall charge of -1, 0 or +1.^{24,25} More generally, investigations of AuNCs for wide ranging applications include the areas of catalysis,^{26,27} nanomedicine²⁸⁻³⁰ and optical imaging,^{31,32} due to the different electronic, optical and chemical properties depending on the number of gold atoms, and the specific arrangement of the gold atoms within the cluster.¹ For example, a previous report has shown that bovine insulin can be incorporated onto BSA-protected AuNCs to control glucose levels in type 1 diabetes.³⁰

Despite numerous reports of the synthesis of AuNCs using non-functional thiolates, the synthesis of AuNCs using thiolate ligands with reactive groups has been more limited

with incorporation taking place via place exchange reactions. Although functional thiols will displace the non-functional thiolates on the clusters under appropriate conditions³³ it is not always possible to substitute all ligands and controlling the ultimate stoichiometry is difficult to achieve.³⁴ Such displacement reactions can also promote rearrangement of the core structure as demonstrated recently by Zhang's group with the preparation of -S-*p*-C₆H₄N₃ AuNCs.³⁵ Recently, we have found a method to directly prepare AuNCs with the azide-functionalized thiolate-ligand -S-CH₂CH₂-*p*-C₆H₄N₃ and the isolation of the nanocluster [(CH₃-(CH₂)₇)₄N][Au₂₅(SCH₂CH₂-*p*-C₆H₄N₃)₁₈], “[[(CH₃-(CH₂)₇)₄N][AuNC-azide]”⁻ [AuNC-azide]⁻ (**Figure 2.1**) has been shown to undergo subsequent surface modification and its properties can be manipulated via the -N₃ moieties all undergoing strain-promoted alkyne-azide click (SPAAC) reaction with complementary strained alkynes.³⁶

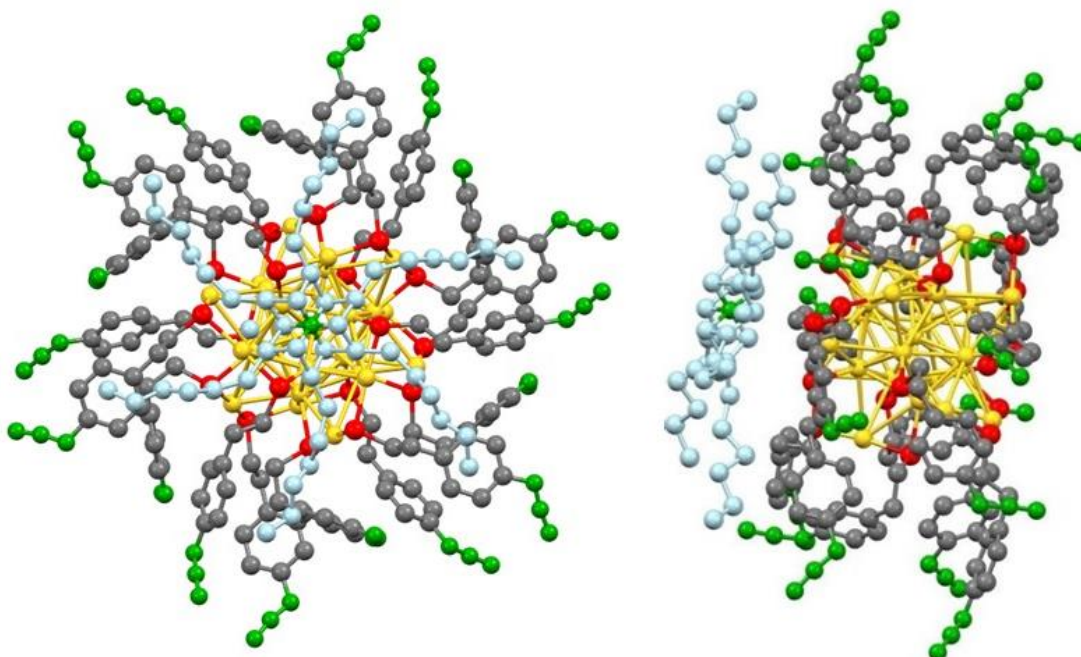
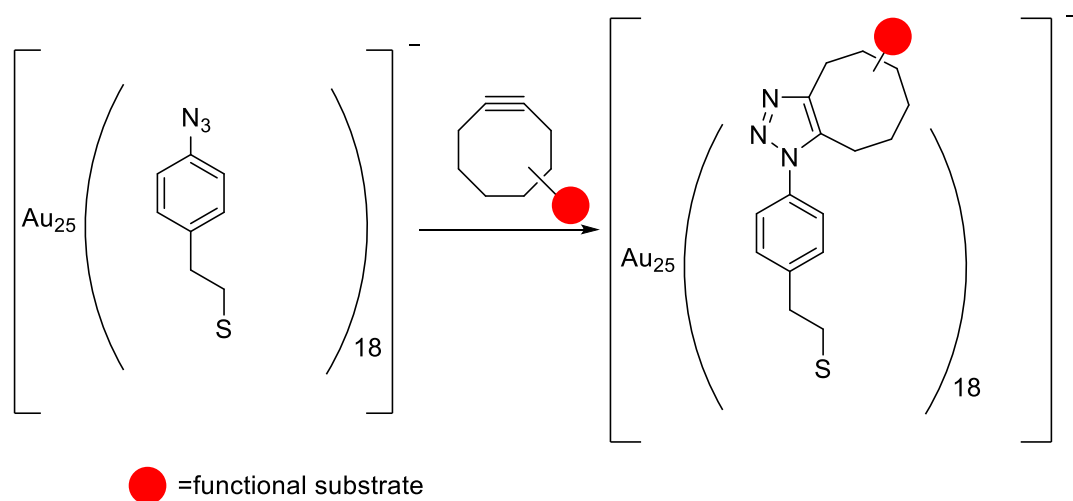


Figure 2.1 Molecular structure of [(CH₃-(CH₂)₇)₄N][Au₂₅(SCH₂CH₂-*p*-C₆H₄-N₃)₁₈] Yellow = gold, red = sulfur, black = carbon (cluster), light blue = carbon (counterion), green = nitrogen. Figure reproduced with permission from ref. [36]

Click reactions, by definition, are reactions with high yields, fast reaction rates and are easy to purify.³⁷ For example, post-assembly modifications can be done by having the an

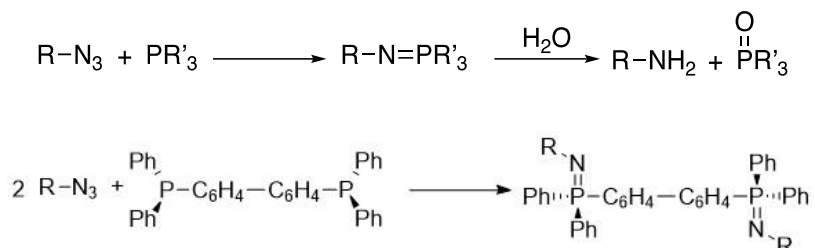
azide undergo SPAAC.^{38,39} By adding a specific functionality, such as a fluorophore onto the complementary reactive partner, it is possible to envisage more applications for clusters containing these surface groups (**Scheme 2.1**). Furthermore, because there are multiple azide-thiolate surface ligands, it is possible to imagine creating multi-functional nanocluster frameworks by treating reactive AuNC platforms with different substrates possessing the complementary click partner. The SPAAC reaction has been used to demonstrate the reactivity of AuNC-azide and to observe that all azides are accessible for reactivity at least with the model alkyne used in the study.³⁶



Scheme 2.1 Strain-promoted azide-alkyne click reaction between AuNC-azide and 1-cycloocten-5-yne.

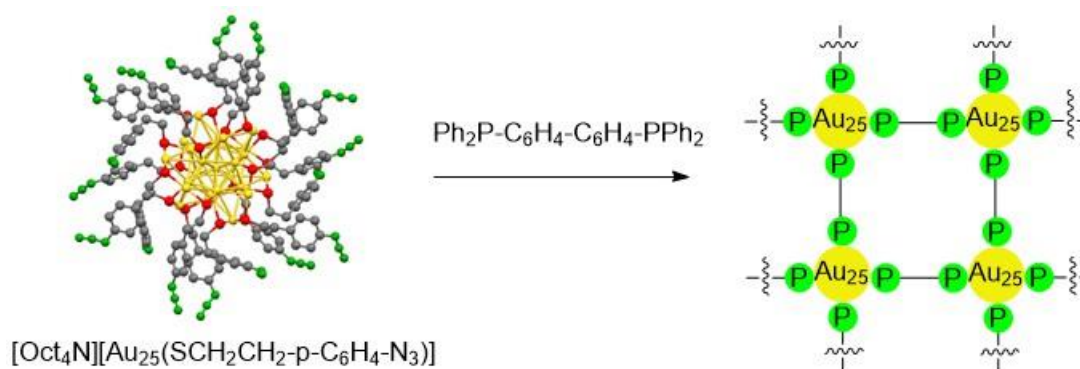
One potential use of these AuNC-azide frameworks is to build assemblies of AuNCs using phosphine linkers, taking advantage of another well-known click reaction, the Staudinger reaction. The Staudinger reaction is one where the phosphine reacts with the azide moiety to form an iminophosphorane, $R-N=PR'_3$ with the elimination of N_2 . With the addition of water, it is also possible to subsequently hydrolyze the iminophosphorane to an amine and phosphine oxide (**Scheme 2.2**, top).⁴⁰ By performing the Staudinger reaction with a rigid, bidentate phosphine such as 4,4'-Ph₂PC₆H₄-C₆H₄PPh₂ (**Scheme 2.2**, bottom) it would be possible to build networks of AuNCs via the generation of intermolecular iminophospharene linkages (scheme 3). Yuan's group has demonstrated that the formation of the cluster network can increase the photoluminescent quantum

yield.⁴¹ Likewise, the formation of the network via iminophosphorane could potentially increase the quantum yield of the cluster.



Scheme 2.2 Staudinger reaction between an azide moiety and phosphines to form iminophosphorane. Addition of water to hydrolyze the adduct to amine and phosphine oxide (top).⁴⁰ The addition of a phosphine linker to couple Staudinger adduct (bottom).

Herein we report the surface modification of [AuNC-azide]⁻ using the Staudinger reaction. To probe this, model reactions were first carried out using the thioether CH₃SCH₂CH₂-*p*-C₆H₄-N₃ (**1**) and the Au(I) coordination complex [(IPr)Au-SCH₂CH₂-*p*-C₆H₄-N₃] (IPr=1,3-diisopropyl-4,5-dimethylimidazol-2-ylidene) (**2**). The “linked” products from their reaction with the rigid bidentate phosphine 4,4'-Ph₂P-C₆H₄-C₆H₄-PPh₂ (*dppb*) were characterized as were the corresponding iminophosphorane complexes. Reactions of the cluster AuNC-azide with varying amounts of *dppb* (**Scheme 2.3**) also lead to surface iminophosphorane moieties and chemically linked Au₂₅ frameworks, although competition for surface thiolate displacement reactions by the phosphines was also observed. This represents a step forward in manipulating nanoscale AuNC architectures with atomically precise control towards tuning physical and chemical properties for potential applications.



Scheme 2.3 Assemblies of AuNCs via Staudinger between AuNC-azide and diphosphine linker (top).

2.2 Experimental

2.2.1 General Considerations and Characterization Methods

All reagents were purchased and used as received from Sigma-Aldrich. All common solvents were purchased from Caledon. All syntheses described were conducted under an atmosphere of high-purity dry nitrogen and all solvents used were dried over Na, Mg, P₂O₅ and CaH₂ by refluxing under N₂ prior to collecting by distillation before used. Deuterated chloroform was dried over P₂O₅ by refluxing under N₂ prior to collecting by distillation. Deuterated dichloromethane was used as received. 4,4'-Ph₂PC₆H₄.C₆H₄PPh₂, [(IPr)AuCl], *p*-azido-phenylethanethiol and [AuNC-azide]⁻ was prepared according to literature procedures.^{36,42,43}

¹H, ¹³C{¹H} and ³¹P{¹H} NMR spectra were recorded on Bruker and Inova 400 MHz NMR spectrometers. The ¹H NMR spectra were referenced against residual protonated chloroform (δ 7.27 ppm, s) or dichloromethane (δ 5.32, t). Multiplicities are reported as follows: s (singlet), d (doublet), t (triplet), q (quartet), quin (quintet) dd (doublet of doublets), m (multiplet), bs (broad signal). Coupling constants are reported as *J* values in Hertz (Hz). The number of protons (n) for a given resonance has been indicated as nH and is based off of spectral integration values. The ¹³C{¹H} NMR spectra were

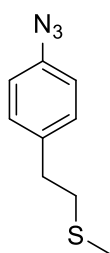
referenced against CDCl₃ (δ 77.0 ppm, t) or CD₂Cl₂ (54.0 ppm, quin). All NMR spectra are reported as δ in units of parts per million (ppm) relative to TMS at 0 ppm.

Electrospray ionization (ESI) mass spectra were obtained in negative and positive-ion mode using a Bruker microTOF II spectrometer. Set capillary was 4500 V, set end plate offset was -400 V, set nebulizer was 0.5 Bar and set dry heater was 180°C.

Solution UV-Vis absorption spectra were recorded using a Varian Cary 100 spectrometer using quartz cell (1cm path length) with a scan range of 200-800 nm. Samples were dissolved in the indicated solvents at the indicated concentrations. The background spectrum of the solvent was subtracted internally by the software. Diffuse reflectance absorption spectra were recorded using Varian Cary 100 spectrometer with a scan range of 370-800 nm. Samples were mixed with barium sulfate and Kubelka-Munk function was applied to the spectra. Attenuated total reflectance IR (ATR-IR) spectra were recorded using PerkinElmer Spectrum Two FT-IR spectrometer.

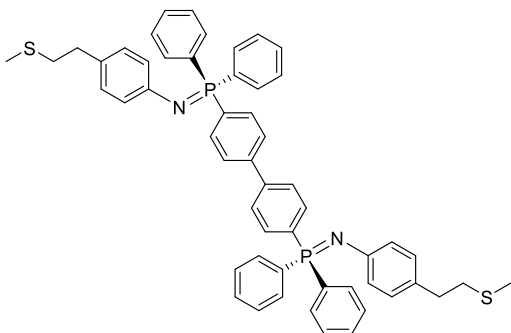
2.2.2 Preparation and Characterization of Compounds

Synthesis of p-azido-phenylethane methyl thioether (1)



To *p*-azido-phenylethanethiol³⁶ (0.366 g, 2.04 mmol) in CH₂Cl₂ (16 mL), potassium carbonate (2.81 g, 20.4 mmol) and iodomethane (1.29 mL, 20.4 mmol) were added and stirred overnight at room temperature. The volatiles were evaporated using a rotary evaporator and the crude product was purified via column chromatography, using 2:1 hexane:CH₂Cl₂ as eluent to afford **1** as a yellow oil (0.300 g, 76.1 %). ¹H NMR (CDCl₃, 400 MHz): δ 2.12 (s, 3H), 2.73 (m, 2H), 2.88 (m, 2H), 6.97 (dd, J = 6.6, 2.1 Hz, 2H), 7.20 (dd, J = 6.6, 2.1 Hz, 2H). ¹³C NMR (CDCl₃, 100 MHz): δ 15.9, 35.3, 36.0, 119.2, 130.0, 137.5, 138.3. IR (ATR-IR, cm⁻¹): 2914, 2855, 2412, 2255, 2092, 1719, 1579, 1505, 1424, 1288, 1183, 1127, 1106, 960, 958, 812, 787, 750, 640, 540. ESI-MS: calculated for C₉H₁₁N₃S [M+H⁺]: 194.0752, found 194.0755. UV-Vis (CH₂Cl₂, 5.0×10⁻⁵ M): λ_{\max} = 290 (ϵ = 2.1×10³ M⁻¹ cm⁻¹) λ_{\max} = 280 (ϵ = 3.1×10³ M⁻¹ cm⁻¹) λ_{\max} = 256 (ϵ = 1.5×10⁴ M⁻¹ cm⁻¹).

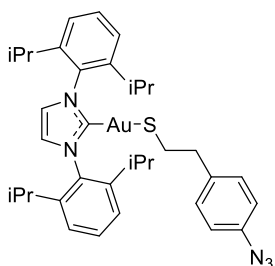
Synthesis of $\{CH_3SCH_2CH_2-p-C_6H_4-N=P(Ph)_2-C_6H_4-\}_2$ (**2**)



To *dppb*⁴² (50 mg, 0.095 mmol) in dry CH_2Cl_2 (5 mL), compound **1** (37 mg, 0.19 mmol) was added and stirred for an hour at room temperature. The volatiles were removed under vacuum and the product was washed with heptane to afford **2** in the form of a yellow film (72 mg, 89 %). ¹H NMR ($CDCl_3$, 400 MHz): δ

2.08 (s, 6H), 2.65-2.69 (m, 4H), 2.72-2.76 (m, 4H), 6.75 (d, $J=7.6$ Hz, 4H), 6.86 (d, $J=7.6$ Hz, 2H), 7.45-7.58 (m, 8H), 7.52-7.55 (m, 4H), 7.64-7.67 (m, 4H), 7.76-7.86 (m, 12 H). ¹³C NMR ($CDCl_3$, 100 MHz): δ 15.8, 35.5, 36.2, 123.4 (d, $J = 17.6$ Hz), 127.5 (d, $J = 12.1$ Hz), 128.83, 128.89 (d, $J = 12.1$ Hz), 129.5, 130.6, 131.6, 131.9 (d, $J = 3.6$ Hz), 132.8 (d, $J = 9.7$ Hz), 133.4 (d, $J = 9.7$ Hz), 143.1, 149.3. ³¹P NMR ($CDCl_3$, 162 MHz): δ 2.0. IR (ATR-IR, cm^{-1}): 3053, 3013, 2912, 1601, 1602, 1502, 1436, 1330, 1261, 1181, 1108, 1034, 1024, 1014, 999, 815, 712, 693, 525. ESI-MS: calculated for $C_{54}H_{51}N_2P_2S_2$ $[M+H^+]$: 853.2969, found 853.2963. UV-Vis (CH_2Cl_2 , 1.8×10^{-5} M): $\lambda_{max} = 268$ ($\epsilon = 3.7 \times 10^4$ $M^{-1} cm^{-1}$).

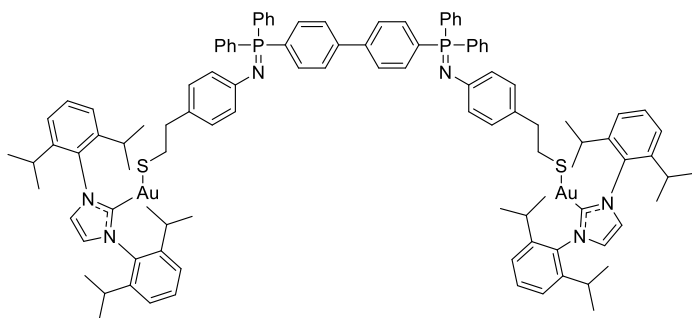
Synthesis of $[(IPr)Au(SCH_2CH_2C_6H_4N_3)]$ (**3**)



To $[(IPr)AuCl]^{43}$ (50 mg, 0.081 mmol) in 5 mL of dry THF, solution of *p*-azido-phenylethanethiol³⁶ (22 mg, 0.12 mmol) in 2.5 mL of dry THF was added. To the solution, Et_3N (21 μ L, 0.21 mmol) was added dropwise. The solution was then stirred for 16 hours at a room temperature. The volatiles were evaporated off under vacuum and the solids were extracted using CH_2Cl_2 (5 mL \times 3). The volatiles were evaporated once more and the solid was dissolved in \sim 2 mL of toluene. 10 mL of pentane was added to recrystallize the final product, which was a pale yellow powder (58 mg, 90 %). ¹H NMR ($CDCl_3$, 400 MHz): δ 1.22 (d, $J = 6.9$ Hz, 12H), 1.38 (d, $J = 6.8$ Hz, 12H), 2.29-2.34 (m, 2H), 2.57-2.67 (m, 6H), 6.85-6.91 (m, 4H), 7.15 (s, 2H), 7.26 (d, $J = 7.7$ Hz, 4H), 7.40 (t, $J = 7.9$ Hz, 2H). ¹³C NMR ($CDCl_3$, 100 MHz): δ 24.2, 24.7, 29.0, 30.0,

44.5, 118.6, 122.9, 124.2, 129.9, 130.7, 134.4, 137.2, 139.6, 145.9, 188.2. IR (ATR-IR, cm^{-1}): 2964, 2932, 2869, 2112, 1505, 1470, 1457, 1412, 1352, 1329, 1299, 1259, 1212, 1117, 1059, 948, 936, 850, 826, 803, 787, 758, 734, 702, 642, 530, 520. UV-Vis (CH_2Cl_2 , 3.0×10^{-5} M): $\lambda_{\text{max}} = 292$ ($\epsilon = 8.0 \times 10^3 \text{ M}^{-1} \text{ cm}^{-1}$), 252 ($\epsilon = 2.5 \times 10^4 \text{ M}^{-1} \text{ cm}^{-1}$). Melting point: 160-163 °C. Anal. Calcd for $\text{C}_{35}\text{H}_{44}\text{AuN}_5\text{S}$: N, 9.17; C, 55.04; H, 5.81; S, 4.20. Found: N, 8.74; C, 54.61; H, 5.13; S, 3.52

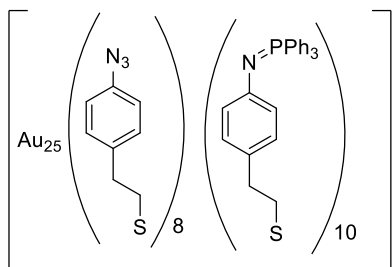
Synthesis of [(IPr)Au(SCH₂CH₂C₆H₄N)₂PPh₂C₆H₄-C₆H₄PPh₂]] (4)



To compound **3** (20.0 mg, 0.026 mmol) in dry CH_2Cl_2 (5 mL), *dppb* (6.8 mg, 0.013 mmol) was added at 0 °C and stirred for 3 days. The volatiles were evaporated to give **4** as a crude

product. ^1H NMR (CDCl_3 , 400 MHz): δ 1.20 (d, $J = 6.9$ Hz, 24H), 1.36 (d, $J = 6.9$ Hz, 24H), 2.18-2.27 (m, 4H), 2.52-2.66 (m, 6H), 6.53-6.62 (m, 4H), 6.64-6.77 (m, 2H), 7.13 (s, 4H), 7.19-7.24 (m, 7H), 7.32-7.38 (m, 6H), 7.32-7.38 (m, 6H), 7.43-7.57 (m, 14H), 7.66-7.70 (m, 4H), 7.76-7.86 (m, 10H). ^{31}P NMR (CDCl_3 , 162 MHz): δ 1.48. Spectra of the reaction in solution indicate additional peaks at δ 28.7 and 43.0, which are assigned to small amounts of $4,4'\text{-Ph}_2\text{P}(\text{O})\text{C}_6\text{H}_4\text{-C}_6\text{H}_4\text{P}(\text{O})\text{Ph}_2$ ⁴⁴ and $[4,4'\text{-Ph}_2\text{PC}_6\text{H}_4\text{-C}_6\text{H}_4\text{PPh}_2\text{-Au-IPr}]^+$ ⁴⁵, respectively. IR (ATR-IR, cm^{-1}): 2961, 2108, 1603, 1503, 1469, 1437, 1330, 1261, 1215, 1180, 1103, 1012, 947, 803, 757, 713, 696, 526.

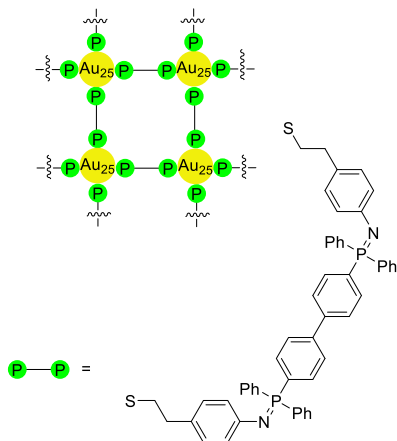
Synthesis of AuNC-triphenylphosphine Staudinger adduct (5)



Triphenylphosphine (4.4 mg, 0.017 mmol) was dissolved in 18 mL of dry THF. To AuNC-azide⁴⁶ (8.0 mg, 0.00093 mmol) in 5 mL of THF, 2 mL of triphenylphosphine solution (2 eq.) was added and the solution was stirred for 3 hours at room temperature. UV-Vis absorption spectra were obtained

after 3 hours. Subsequently, an additional 4 mL of triphenylphosphine solution (total 6 eq.) was added and stirred for an additional 3 hours at room temperature. The above step was repeated until total of 10 equivalents of triphenylphosphines were added. The volatiles were removed under vacuum and the residual solid analyzed.

Synthesis of Linked [AuNC-dppb] (6)



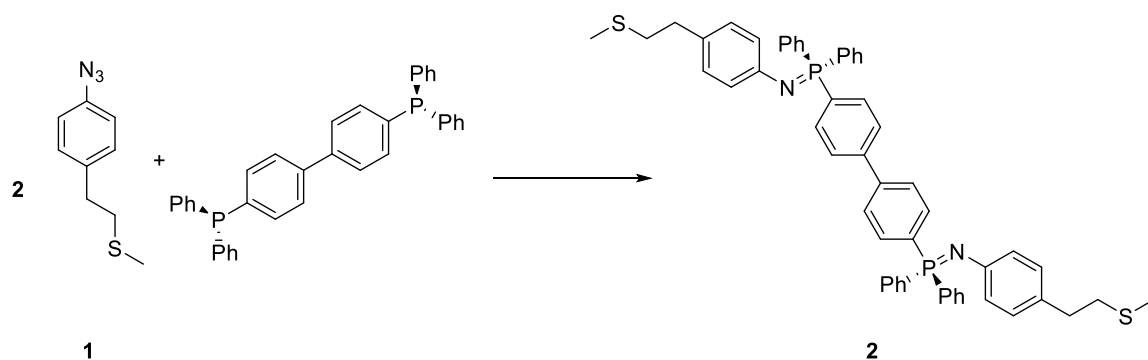
dppb (3.1 mg, 0.011 mmol) was dissolved in 9 mL of dry CH₂Cl₂. To AuNC-azide in 5 mL of THF (5.7 mg, 0.00059 mmol), 1 mL of dissolved *dppb* (1 eq. of *dppb*) was added and the solution stirred for 3 hours at room temperature. An additional 2 mL of the dissolved *dppb* (total 3 eq. of *dppb*) was added and stirred for another 3 hours at room temperature. The volatiles were removed under vacuum and the resulting solid was washed with dry ethanol. The linked gold clusters were re-dissolved

in CH₂Cl₂ and the solution was centrifuged to remove insoluble black precipitates. This was repeated until there were no precipitate. The solvent was removed to afford a reddish-brown film.

2.3 Results and Discussion

The Staudinger reaction between *dppb* and -SCH₂CH₂-*p*-C₆H₄-N₃ was first probed with the thioether CH₃SCH₂CH₂-*p*-C₆H₄-N₃ (**1**) to test the viability of the reaction and find the appropriate phosphine click partner. The thioether was itself readily prepared from the corresponding thiol³⁶ and was selected in order to eliminate the possibility of the thiol functional group reacting with iminophosphoranes.

The reaction of *dppb* with two equivalents of CH₃SCH₂CH₂-*p*-C₆H₄-N₃ under inert atmosphere at room temperature leads to the complete consumption of the azide and the formation of the di-iminophosphorane {CH₃SCH₂CH₂-*p*-C₆H₄-N=P(Ph)₂-C₆H₄-}₂ (**2**), as shown in **Scheme 2.4**.



Scheme 2.4 Reaction between two equivalents of $\text{CH}_3\text{SCH}_2\text{CH}_2\text{-}p\text{-C}_6\text{H}_4\text{-N}_3$ and *dppb*.

In the $^{31}\text{P}\{^1\text{H}\}$ NMR spectra of reactions, the original resonance at -6.1 ppm from *dppb* has been replaced with one at 2.0 ppm (**Figure 2.2a**), consistent with the formation of a iminophosphorane moiety.⁴⁷⁻⁴⁹ Equally diagnostic were the changes observed in IR spectra: the IR spectrum of the thioether **1** has a strong, sharp peak at 2107 cm^{-1} (**Figure 2.2b**) arising from the -N_3 . In contrast this peak is absent in the IR spectra of the product and clearly indicate complete consumption of the azide; the generated di-iminophosphorane displays a peak at 1330 cm^{-1} of medium intensity, consistent with a $\text{P}=\text{N}$ stretch.^{47,50,51} Additional spectroscopic characterization data confirm the formation of $\{\text{CH}_3\text{SCH}_2\text{CH}_2\text{-}p\text{-C}_6\text{H}_4\text{-N}=\text{P}(\text{Ph}_2)\text{-C}_6\text{H}_4\text{-}\}_2$.

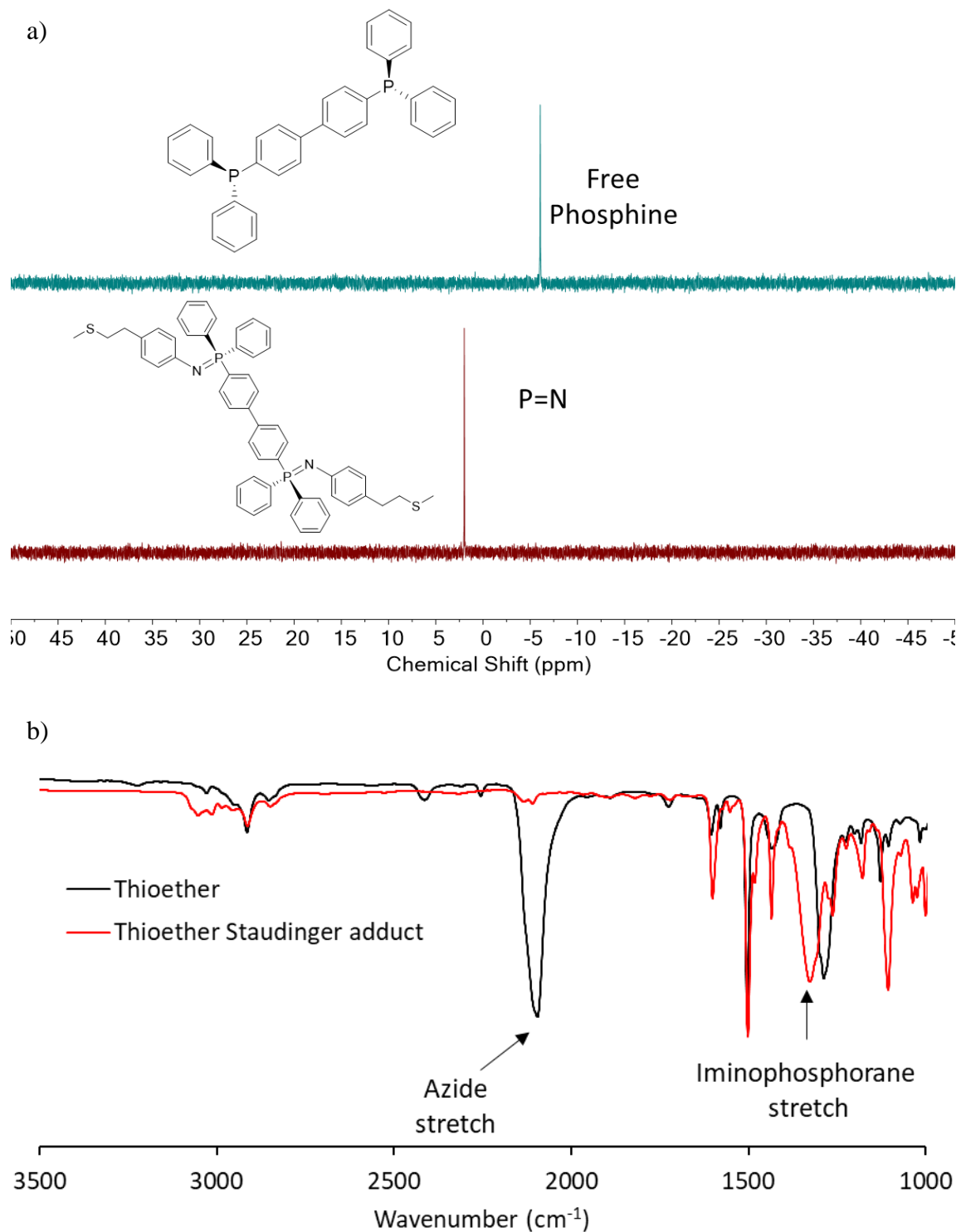


Figure 2.2 a) $^{31}\text{P}\{^1\text{H}\}$ NMR spectra of the bidentate phosphine *dppb* (green) and the thioether Staudinger adduct (**2**) (red). b) ATR-IR spectrum of the thioether (**1**) (black) and the Staudinger adduct (**2**) (red).

The model gold(I) thiolate coordination complex [(IPr)Au(SCH₂CH₂-*p*-C₆H₄-N₃)] (**3**) was also prepared as part of this study in order to examine the reactions of -ArN₃/PPh₃ in the presence of Au(I) centers. The molecular structure of **3** in the crystal, as determined from X-ray diffraction, is illustrated in **Figure 2.3** and displays the expected linear coordination of Au(I) and the accessible, pendent -N₃. The reaction of **3** with *dppb* also leads to -P=N- bond formation (**Scheme 2.5**); in the IR spectrum in **Figure 2.4a**, the intensity of the azide peak at 2107 cm⁻¹ is reduced and is replaced with an iminophosphorane (-P=N-) stretch peak at 1333 cm⁻¹. Similarly, ³¹P{¹H} NMR data indicate the formation of -P=N- but also suggest a competing process to the Staudinger reaction also occurs where the phosphine coordinates to Au(I) via displacement of the thiolate ligand. Illustrated in **Figure 2.4b** is the ³¹P{¹H} spectrum for a reaction of [(IPr)Au(SCH₂CH₂-*p*-C₆H₄-N₃)] (**3**) with *dppb* carried out at 0 °C: in addition to a broad signal centered at 1.4 ppm that is again readily assigned to -P=N-, an additional sharp resonance is observed at 40 ppm. Previous reports on the characterization of the related [(IPr)Au(PPh₃)]⁺ (δ = +40 ppm) support the assignment of this signal to *dppb* bonding directly to a gold atom, the environments for the phosphorus atoms (and thus their chemical shifts) in ligands PPh₃ and *dppb* being similar.^{45,52} ESI-MS characterization data of reaction solutions also support this assignment with a signal at m/z = 1843.6609 assigned to dimeric [(IPr)AuPPh₂(C₆H₄C₆H₄)P=N-C₆H₄C₂H₄SAu(IPr)]⁺ (calcd. m/z = 1843.7165, **Figure S2.18**). At reaction temperatures above 0°C, the intensity of the signal at +40 in the ³¹P{¹H} NMR spectra increases at the expense of the one observed at 1.4 ppm, suggesting that ligand substitution competes even more with the desired Staudinger reaction to form the iminophosphorane.

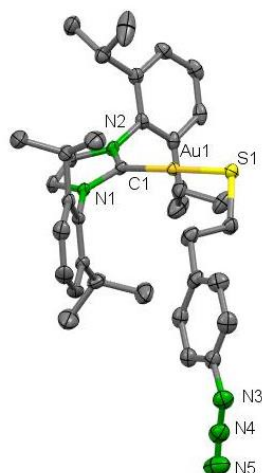
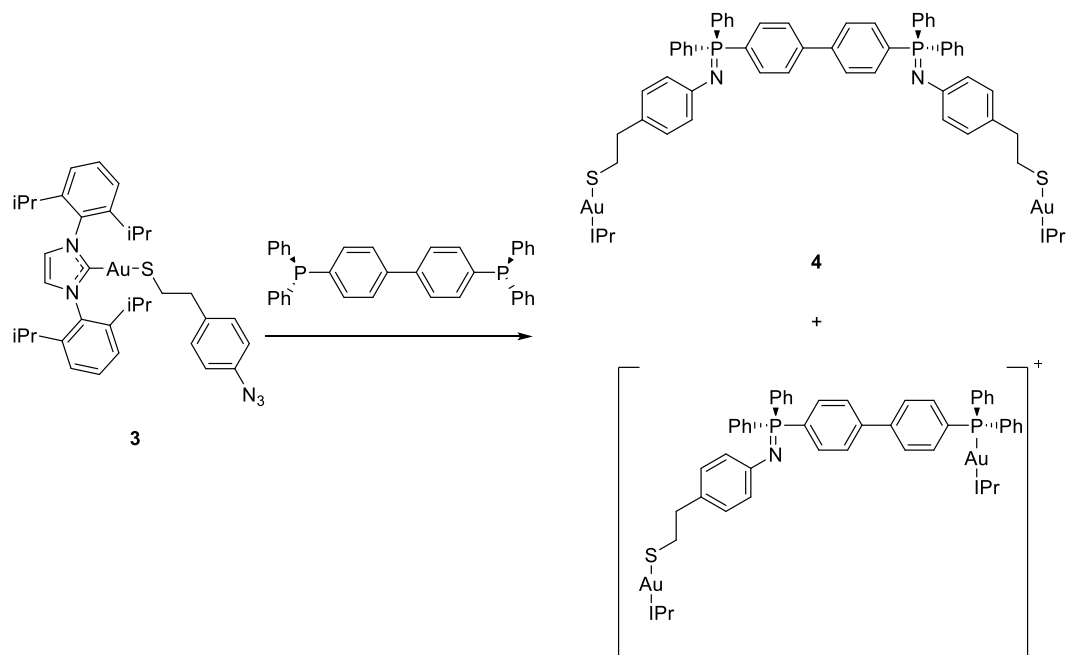


Figure 2.3 Molecular structure of the gold(I) thiolate coordination complex in the crystal. Thermal ellipsoids drawn at the 50 % probability level. Hydrogen atoms omitted for clarity. [(IPr)Au(SCH₂CH₂-p-C₆H₄-N₃)] (**3**) in the crystal. Selected angles (deg): N3-N4-N5=173.1(3), C1-Au1-S1=177.52(6), N2-C1-N1=104.2(2). Selected bond lengths (Å): C1-Au1=2.003(2) Au1-S1=2.2869(6).



Scheme 2.5 Reaction between [(IPr)Au(SCH₂CH₂-p-C₆H₄-N₃)] and *dppb* to form [(IPr)Au(SCH₂CH₂C₆H₄N)₂PPh₂C₆H₄-C₆H₄PPh₂] and side product.

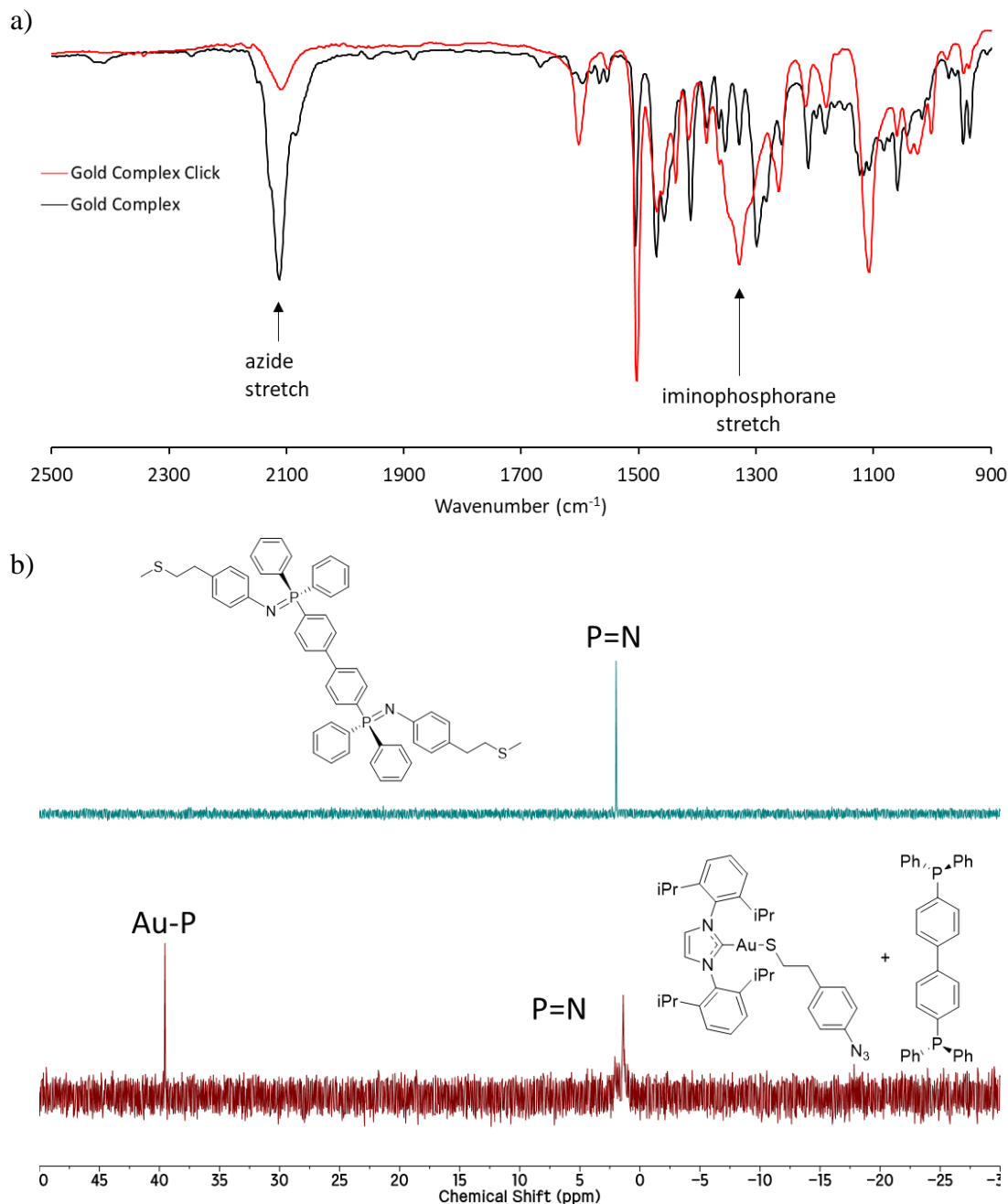
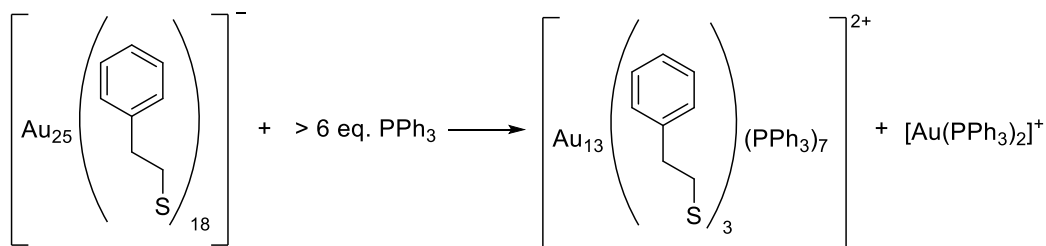


Figure 2.4 a) IR spectrum of the gold complex (3) (black) and reaction sample of gold complex (3) and *dppb* (red) b) ^{31}P { ^1H } NMR spectra of the thioether Staudinger adduct (2) (green) and the reaction sample of the gold complex (3) and *dppb* (red).

In a complementary vein, Jin and co-workers have shown previously that, somewhat counter intuitively, triphenylphosphine (PPh_3) is able to “peel” surface thiolate ligands from the cluster $[\text{Au}_{25}(\text{SCH}_2\text{CH}_2\text{Ph})_{18}]^-$ resulting in the transformation of the overall

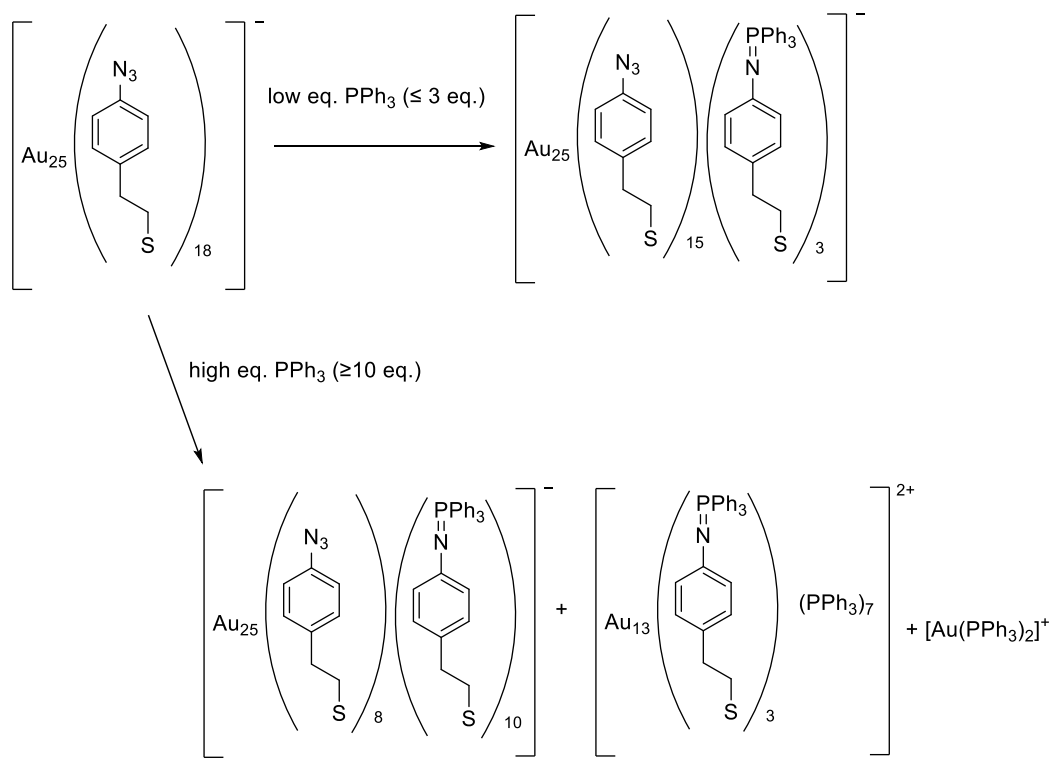
structure and the formation of mixed phosphine/thiolate Au clusters derived from the centered icosahedral core (eg. $[\text{Au}_{13}(\text{PPh}_3)_7(\text{SCH}_2\text{CH}_2\text{Ph})_3]^{2+}$) together with the by-product $[\text{Au}(\text{PPh}_3)_2]^+$, as shown in **Scheme 2.6**.⁵³ Importantly, the authors report that the degradation/reorganization reactions only occurred if the PPh_3 :cluster ratio exceeded 6:1; the reactions can be monitored via changes in the UV-Vis absorption spectra.



Scheme 2.6 Transformation of the cluster $[\text{Au}_{25}(\text{SCH}_2\text{CH}_2\text{Ph})_{18}]^-$ to $[\text{Au}_{13}(\text{PPh}_3)_7(\text{SCH}_2\text{CH}_2\text{Ph})_3]^{2+}$ via addition of PPh_3 .

Solutions of the cluster $[\text{AuNC-azide}]^-$ display characteristic absorption bands in the UV-Vis spectra at 682, 443 and 404 nm that can be used similarly to evaluate structure integrity in the presence of PPh_3 (**Figure 2.5**).³⁶ In principle, 18 surface azides on AuNC-azide are available to undergo Staudinger reactions with PPh_3 . When reacted with ≤ 14 equivalents of PPh_3 , UV-Vis absorption spectra of AuNC-azide suggested that there was no observable degradation of the cluster framework (**Figure 2.5**). However, as additional amounts of PPh_3 were added, the characteristic peak of the AuNC-azide in the UV-vis spectrum at 682 nm lost its intensity significantly and the characteristic peak at 443 nm was no longer observed. With 17 equivalents of PPh_3 added, no characteristic bands assignable to AuNC-azide are observed as the cluster has degraded, likely via a similar surface thiolate stripping process as observed by Jin *et al.*,⁵³ as shown in **Scheme 2.7**. Although the UV-Vis absorption spectra suggested no observable cluster degradation until ~ 14 equivalents of PPh_3 were added, the $^{31}\text{P}\{^1\text{H}\}$ NMR spectra of reaction solutions provide evidence that surface displacement competes with the Staudinger reaction at an earlier stage. Three equivalents of PPh_3 were added to a solution of AuNC-azide in order to see if surface displacement reaction occurs at lower equivalents. The $^{31}\text{P}\{^1\text{H}\}$ NMR spectra (**Figure 2.6a**) indicate that there was no surface displacement and

only the Staudinger reactions (iminophosphorane formation) had occurred. With reactions done at 0 °C, the UV-Vis spectrum shows that the surface rearrangement occurs with fewer equivalents used, as shown in **Figure 2.5**. When the reaction was done at room temperature, the UV-Vis spectra of the AuNC-azide showed characteristic peaks until ~14 equivalents were added. However, when the reaction was done at 0 °C, the UV-Vis spectra show that by the time 6 equivalents of PPh₃ are added, the characteristic peak at 680 nm disappears and by the time 10 equivalents of PPh₃ are added, none of the characteristic peaks of AuNC-azide are present. This shows that the surface displacement from PPh₃ is more likely to happen at lower temperature versus Staudinger reaction with N₃. ATR-IR spectra of the mixture between [AuNC-azide]⁻ and PPh₃ showed reduced intensity of the peak at 2110 cm⁻¹ and a new absorbance at 1330 cm⁻¹, both features consistent with the ³¹P {¹H} NMR spectrum and with the model reactions described above (**Figure 2.6b**). Thus, although UV-Vis spectra may only suggest minimal degradation under the reaction conditions used reaction, ³¹P {¹H} NMR data are also useful in probing reaction selectivity with PR₃.



Scheme 2.7 Possible reaction pathways between [AuNC-azide]⁻ and PPh₃

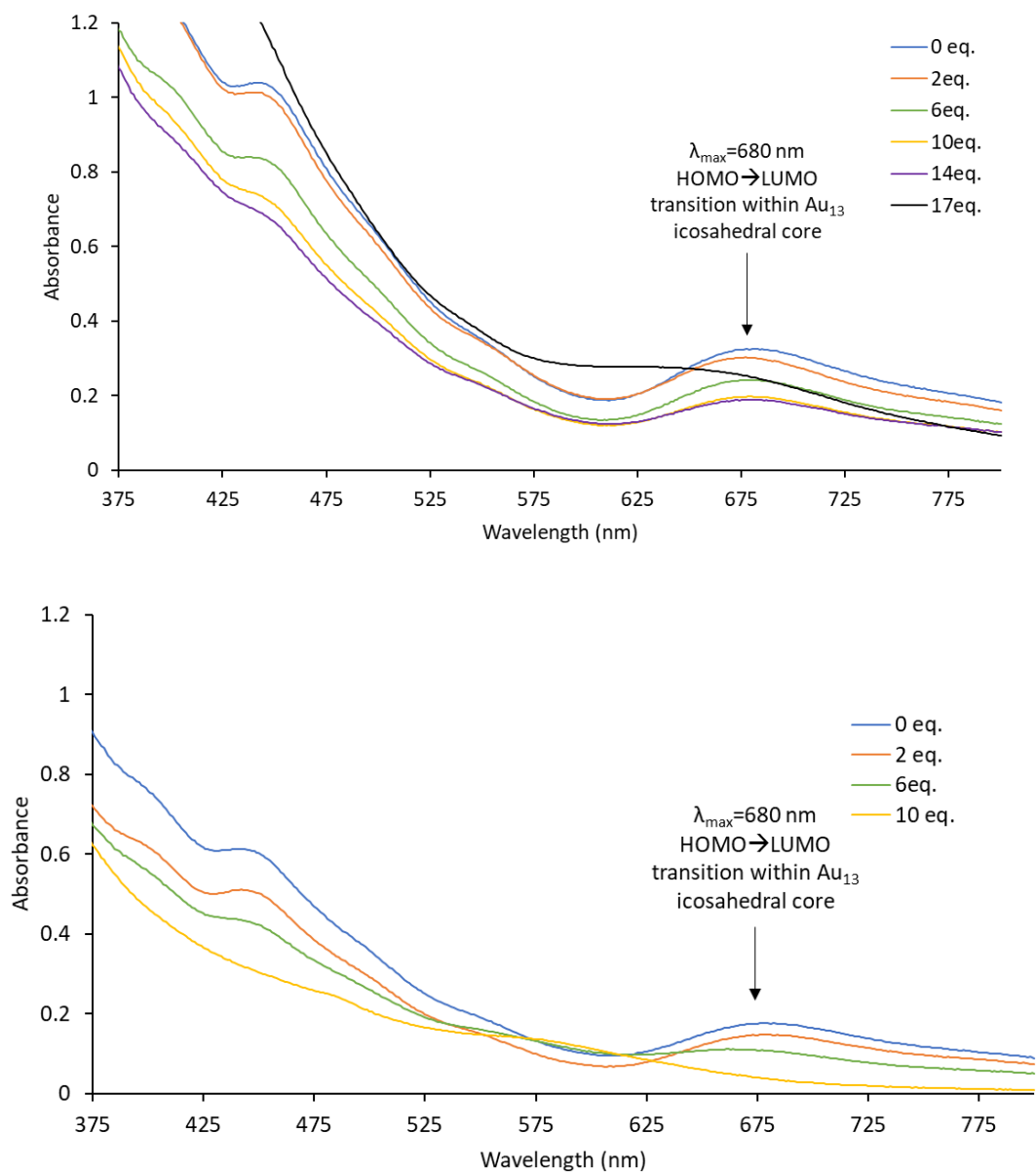


Figure 2.5 UV-Vis absorption spectra of AuNC-azide with different amounts of PPh₃ stirred at room temperature (above) and at 0°C (below).

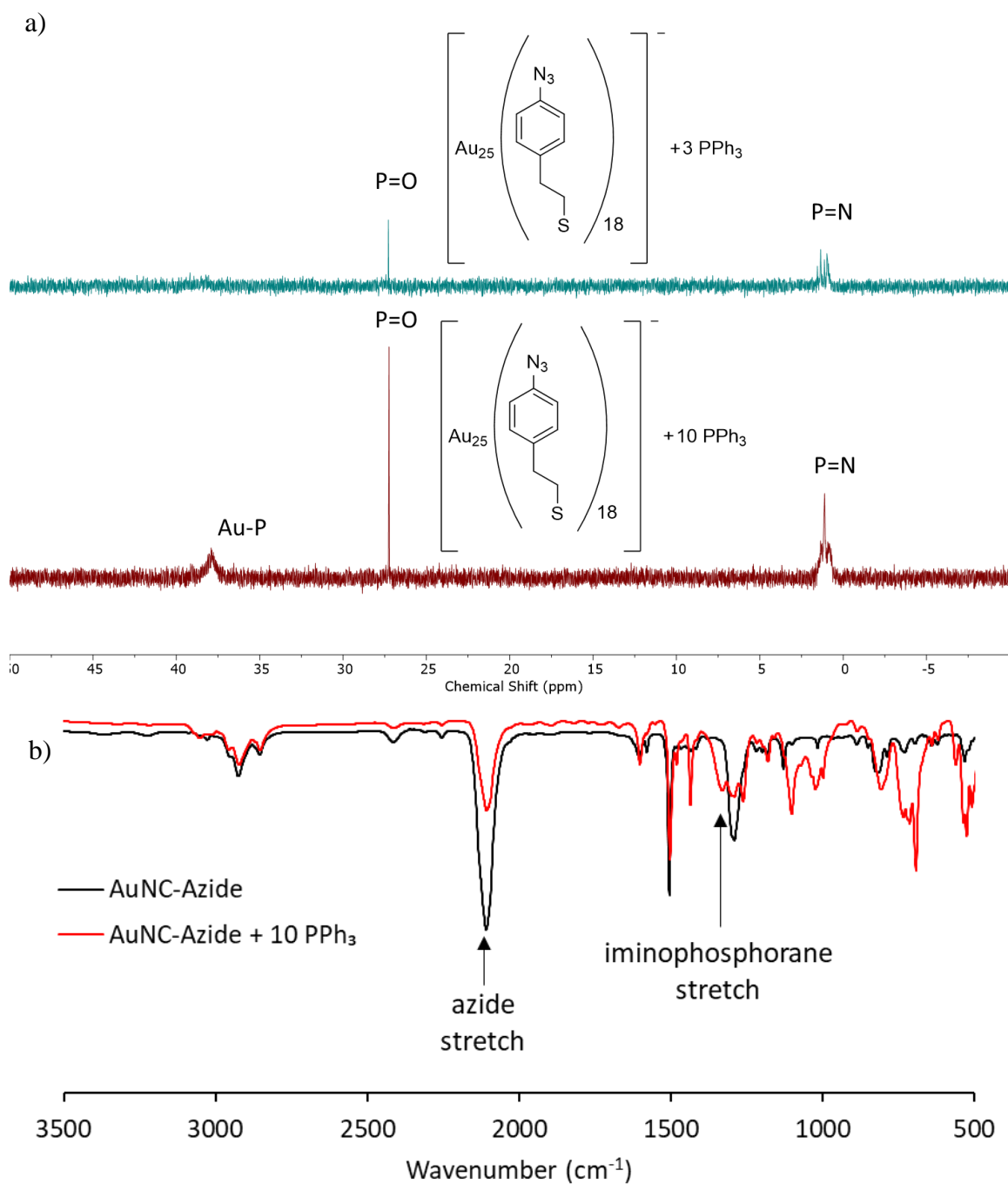
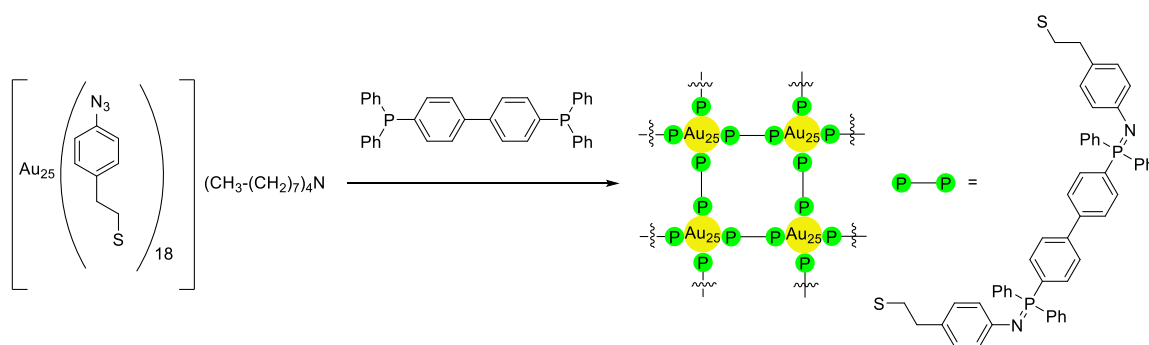


Figure 2.6 a) $^{31}\text{P}\{^1\text{H}\}$ NMR spectrum of the mixture between AuNC-azide and 3 equivalents of PPh_3 (green) and 10 equivalents of PPh_3 (red) b) ATR-IR spectrum of AuNC-azide (black) and the reaction of AuNC-azide and 10 equivalents of PPh_3 (red).

The similar electronic and geometric structures at phosphorus in PPh_3 and bidentate $\text{Ph}_2\text{PC}_6\text{H}_4\text{-C}_6\text{H}_4\text{-PPh}_2$ (*dppb*) suggested that reactions of AuNC -azide with the rigid diphosphine linker would enable coupling of Au_{25} frameworks via -P=N- covalent bond formation and intermolecular *dppb* bridges, as shown in **Scheme 2.8**. When 3 equivalents of *dppb* were added, black precipitates were observed and the amount of precipitate increased with additional amounts of *dppb* added. Reactions were probed by obtaining UV-Vis spectra of the solution.



Scheme 2.8 Formation of Au_{25} network using AuNC -azide and *dppb*.

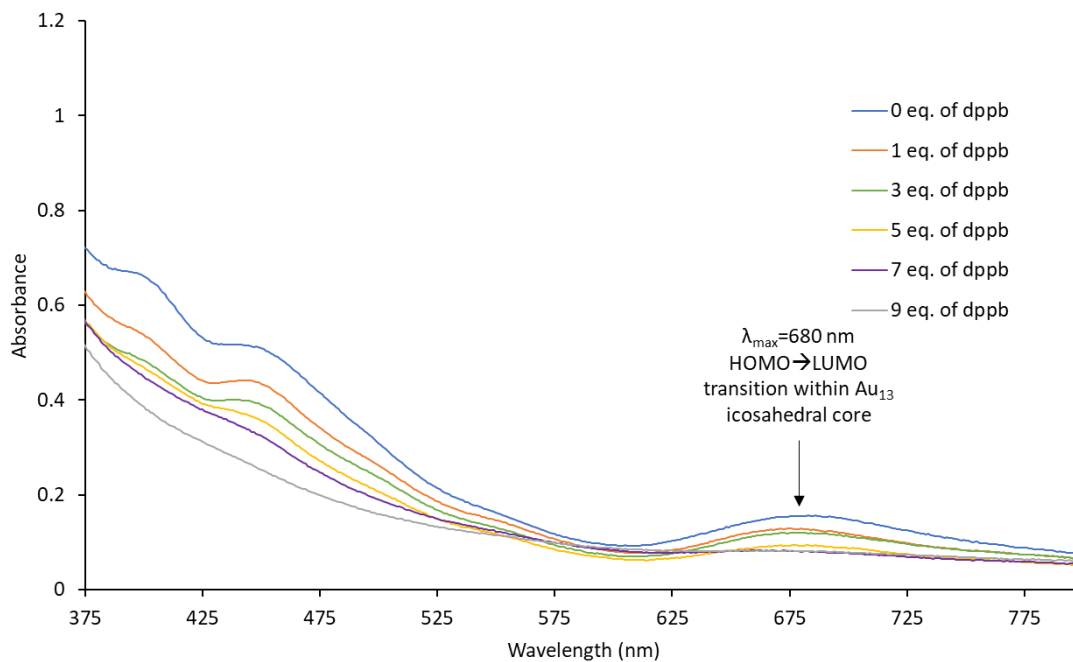


Figure 2.7 UV-Vis absorption spectra of $[\text{AuNC-azide}]$ with different amounts of *dppb*, varying from 0 to 9 equivalents.

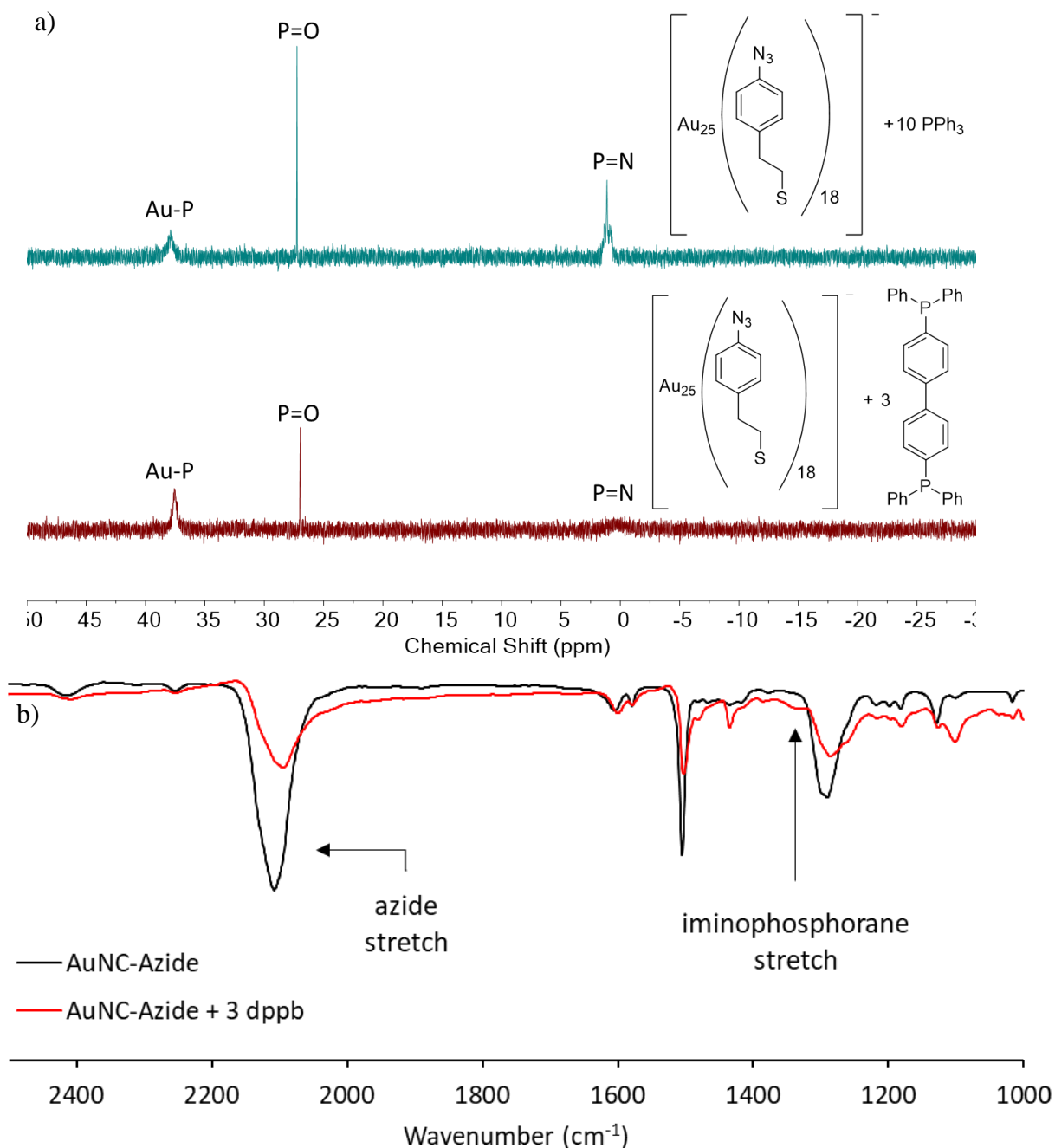


Figure 2.8 a) $^{31}\text{P}\{^1\text{H}\}$ NMR spectrum of the mixture between $[\text{AuNC-azide}]^-$ and 10 equivalents of PPh_3 (green) and the mixture between $[\text{AuNC-azide}]^-$ and 3 equivalents of dppb (red). b) ATR-IR spectra of $[\text{AuNC-azide}]^-$ (black) and the mixture between $[\text{AuNC-azide}]^-$ and 3 equivalents of dppb . (red).

With the addition of ≤ 3 equivalents of *dppb*, UV-Vis spectra of the reaction solutions display resolved absorptions at 680, 440 and 400 nm, as shown in **Figure 2.7**, consistent with those for [AuNC-azide]⁻. Despite the UV-Vis spectra showing no evidence of surface displacement at ≤ 3 equivalents, the ³¹P{¹H} NMR spectrum of the reaction mixture between [AuNC-azide]⁻ and 3 equivalents of *dppb* showed evidence of surface displacement occurring, consistent with ³¹P{¹H} NMR spectrum of the reaction mixture between 10 equivalents of PPh₃ and [AuNC-azide]⁻ cluster (**Figure 2.8a**). The ³¹P{¹H} NMR spectrum of the reaction mixture between [AuNC-azide]⁻ and 3 equivalents of *dppb* displayed a weak resonance at ~1 ppm assigned to the iminophosphorane and also contained two sharp peaks at 40 and 28 ppm which were assigned to [(*dppb*)Au]⁺ species⁴⁵ and the oxidized diphosphine,⁴⁴ respectively. With the addition of 5 equivalents of *dppb*, the intensity of the signal at 680 nm decreased significantly and the peak at 440 nm weakened as well, which suggests that the significant amount of surface displacement has started to occur. With the addition of 7 or more equivalents of *dppb*, the absorption spectra display none of the associated peaks for an intact Au₂₅ cluster framework. This loss of the characteristic [AuNC-azide]⁻ cluster occurred with fewer equivalents than was observed with PPh₃. This may have arisen due to the fact that the precipitates themselves decrease the concentration of gold clusters in solution. The weak intensity of the signal at 1 ppm in the ³¹P{¹H} NMR spectrum results from the fact that the majority of clusters (linked) precipitated out with the addition of *dppb*, resulting in low concentration of iminophosphorane species compared to when [AuNC-azide]⁻ was reacted with PPh₃. The precipitation not only decreases the concentration of the iminophosphorane-containing clusters, it would also have the effect of increasing the concentration of *dppb* relative to any remaining Au₂₅ clusters and thus enhancing displacement of surface thiolates, consistent with UV-Vis absorption spectral data. ATR-IR spectra of soluble species indicates a small iminophosphorane stretch at 1330 cm⁻¹, consistent with weak intensity of the signal at 1 ppm in the ³¹P{¹H} NMR spectrum (**Figure 2.8b**).

The diffuse reflectance UV-Vis spectrum of the precipitates formed from the reaction between [AuNC-azide]⁻ and 3 equivalents of *dppb* show absorption at 680 nm, which supports the fact that the precipitates consist of Au₂₅ clusters (**Figure 2.9**). The IR

spectrum of the precipitate from a separate experiment shows an absence of both the azide stretch at 2110 cm^{-1} and iminophosphorane stretch at 1330 cm^{-1} . However, there is a broad peak present at 1416 cm^{-1} , which is still within the range for the iminophosphorane stretch, according to the literature.⁵⁴ A broad peak is present at 3260 cm^{-1} , which implies that iminophosphorane has hydrolyzed to amine. (**Figure 2.10**) The absence of the peak at 2110 and 1330 cm^{-1} implies that while Au_{25} may be present in the precipitates according to diffuse reflectance UV-Vis spectrum, the overall reaction between *dppb* and the $[\text{AuNC-azide}]^-$ may not be as straightforward as seen in the reaction between $[\text{AuNC-azide}]^-$ and PPh_3 .

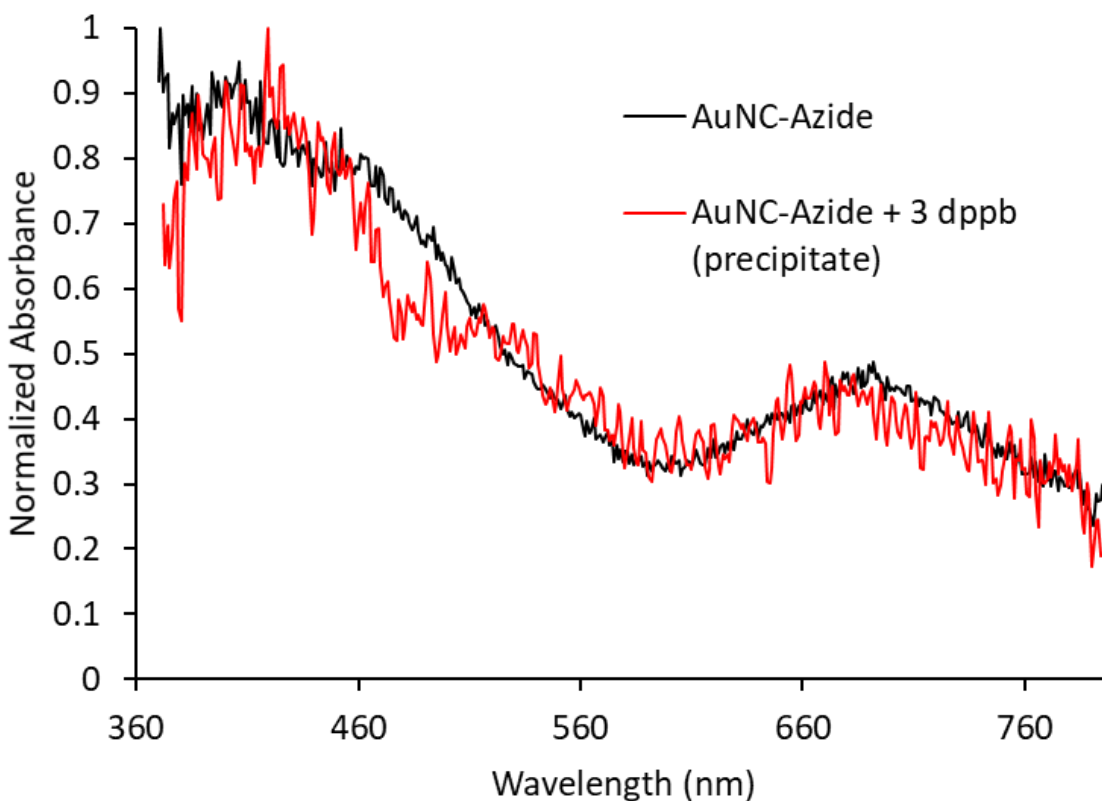


Figure 2.9 Diffuse reflectance UV-Vis absorption spectra of AuNC-azide (black) and precipitates formed between AuNC-azide and 3 equivalents of *dppb* (red).

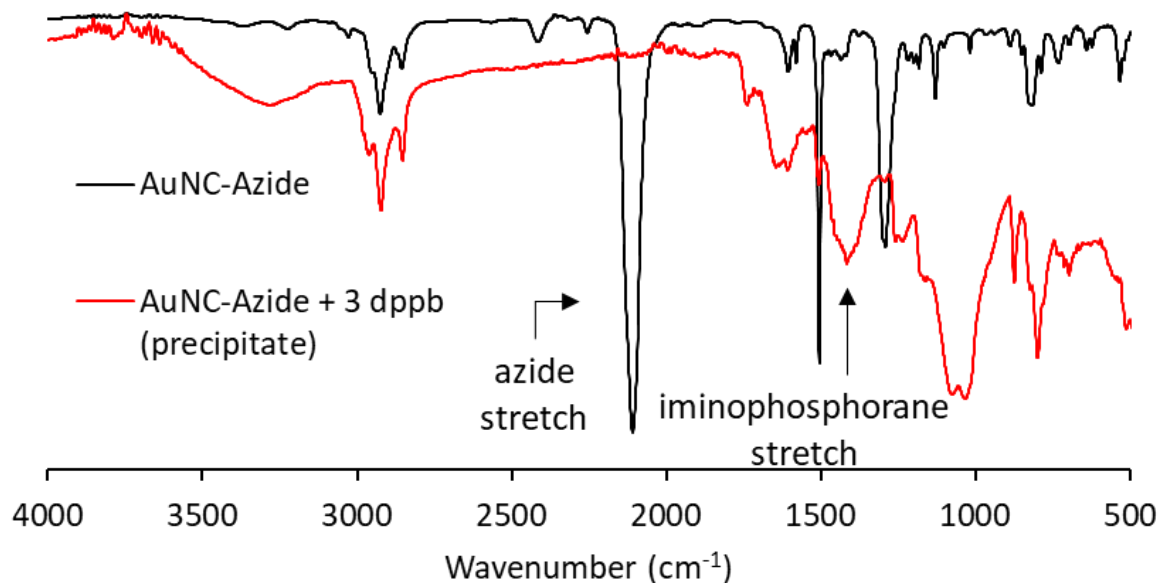


Figure 2.10 ATR-IR spectra of AuNC-azide (black) and the precipitates formed from the mixture between AuNC-azide and 3 equivalents of *dppb* (red).

The mass spectra of the reaction between $[\text{AuNC-azide}]^-$ and 1 equivalent of *dppb* also provided evidence of Staudinger reactivity. The observed m/z ratio of 8105.544 is consistent with calculated mass, where one azide containing thiolate ligand has been converted to the corresponding amine ($m/z = 8105.963$), while the observed mass of 8079.487 is consistent with the mass of Au_{25} where two ligands have been converted to amines ($m/z = 8079.973$; **Figure 2.11**). Amines on $[\text{AuNC-azide}]^-$ could only be formed after iminophosphorane from Staudinger reactions has been hydrolyzed, which strongly implies that the Staudinger reaction using *dppb* has worked successfully.

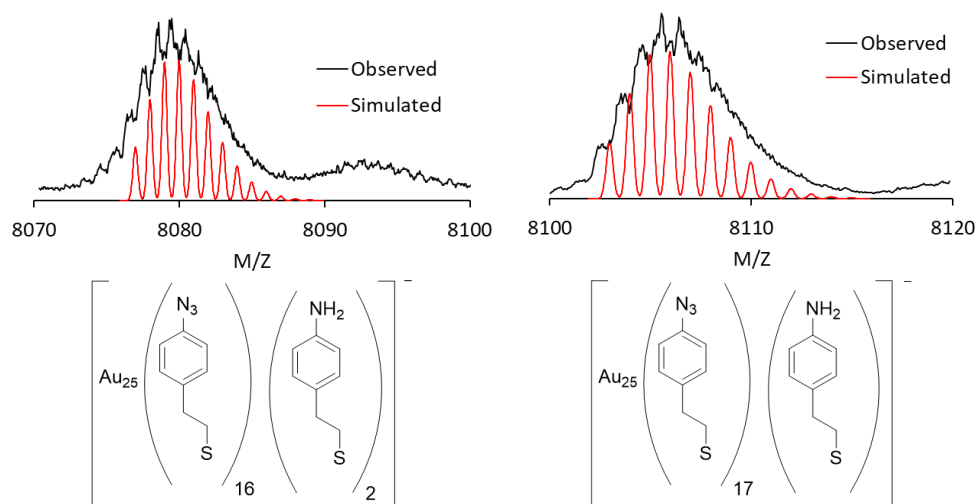


Figure 2.11 Negative ESI-MS of $[\text{Au}_{25}(\text{SCH}_2\text{CH}_2\text{C}_6\text{H}_4\text{N}_3)_{16}(\text{SCH}_2\text{CH}_2\text{C}_6\text{H}_4\text{NH}_2)_2]^-$ (left) and $[\text{Au}_{25}(\text{SCH}_2\text{CH}_2\text{C}_6\text{H}_4\text{N}_3)_{17}(\text{SCH}_2\text{CH}_2\text{C}_6\text{H}_4\text{NH}_2)]^-$ (right).

TEM images of soluble species from these 1:3 $[\text{AuNC-azide}]^-:\text{dppb}$ reactions show that two main components are present in the supernatant (**Figure 2.12**). Although difficult to resolve due to their small size, images show that there are still individual $[\text{AuNC-azide}]^-$ in the supernatant. The free Au_{25} clusters may be present because *dppb* may not have reacted uniformly with Au_{25} clusters, leading to some unreacted $[\text{AuNC-azide}]^-$. This is consistent with the fact that the reaction solution with 3 equivalents of *dppb* contains peaks for iminophosphorane (based on $^{31}\text{P}\{^1\text{H}\}$ NMR spectrum) and also black precipitates, most likely stemming from $[\text{AuNC-azide}]^-$ clusters being linked with *dppb*. The images show the Au_{25} network present in the solution. The crystal structure has shown that Au_{25} clusters have a core diameter of ~ 1.2 nm.⁵⁵ Although difficult to see, the images show dark spots, which are $[\text{AuNC-azide}]^-$. The dark spots each have a diameter around 1-1.5 nm, consistent with the literature. The distance between the two phosphorus within *dppb* is approximately 1.1 nm, while the distance between the thiolate and the nitrogen of $[\text{AuNC-azide}]^-$ is approximately 0.8 nm, according to the literature.^{36,56} Altogether, the distance between the clusters is expected to be approximately 2.7 nm. The distance between the dark spots is approximately 3 nm, which strongly indicates that $[\text{AuNC-azide}]^-$ has successfully linked with one another with the formation of iminophosphorane using *dppb*.

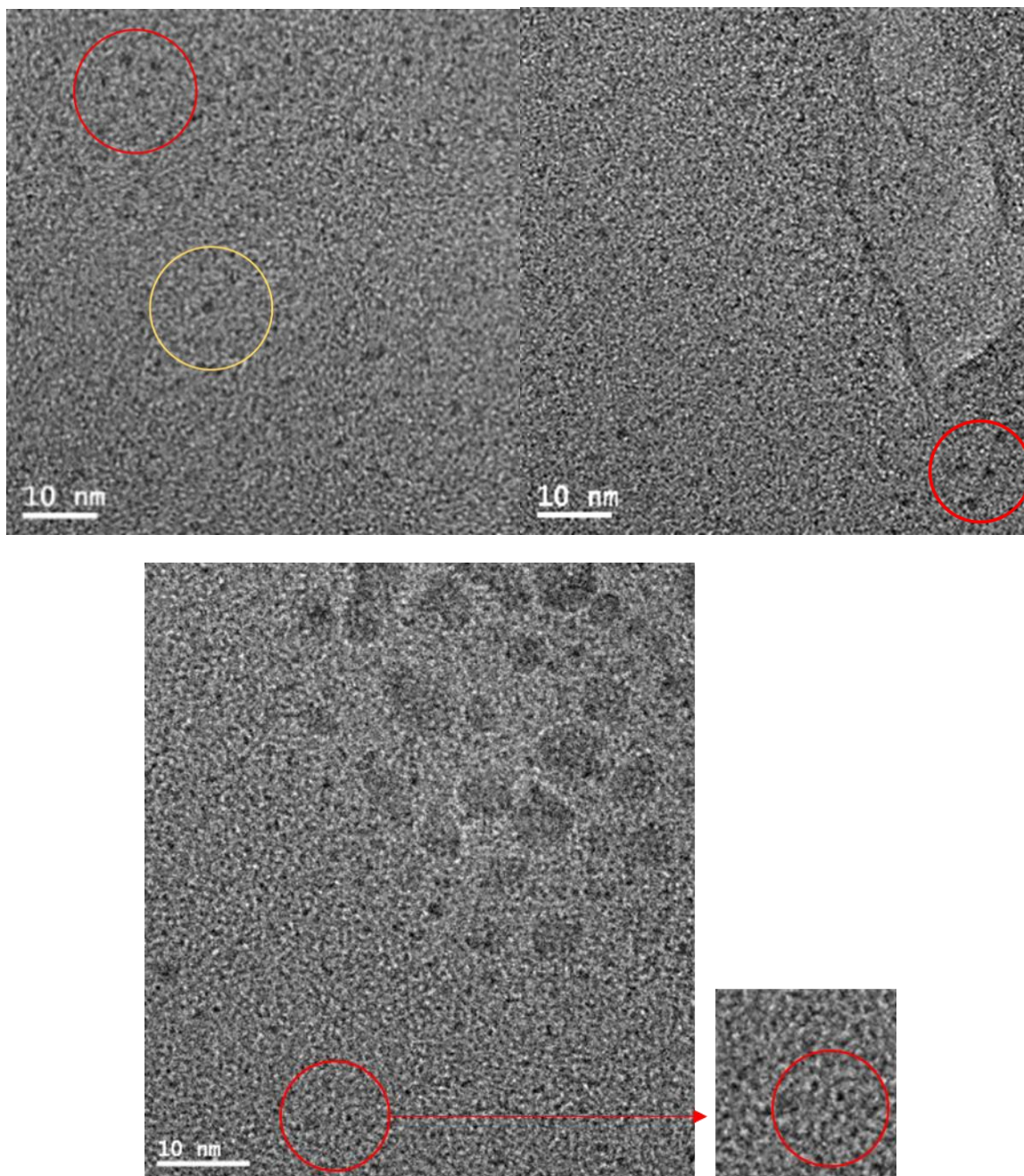


Figure 2.12 TEM image of $[\text{AuNC-azide}]^-$ with 3 equivalents of *dppb*. Top left: the 4 dark spots within the red circle have a diameter of ~ 1.2 nm, with the distance between them being ~ 3 nm. Dark spot within yellow circle also has a diameter of ~ 1.2 nm but has no additional dark spot within 3 nm. Top right: the 3 dark spots within the red circles have a diameter of ~ 1.2 nm, with the distance between them being ~ 3 nm. Bottom: the 4 dark spots within the red circles have a diameter of ~ 1.2 nm, with the distance between them being ~ 3 nm.

2.4 Conclusion

Here, we developed methods to synthesize networks of [AuNC-azide]⁻ via Staudinger reaction. Through NMR and IR spectroscopy, we found that while the Staudinger reaction does occur cleanly using the thioether compound, when compounds containing gold are used for Staudinger reaction, the displacement of the thiolates for phosphine also competes. With [AuNC-azide]⁻ clusters, while the Staudinger reaction does occur with lower equivalents of phosphines, the Au₂₅ slowly degrades with higher equivalents of phosphines added. The synthesis of networks of [AuNC-azide]⁻ was done with lower equivalents of *dppb* and the formation of iminophosphorane and the network was confirmed via NMR and IR spectra and TEM images. With higher equivalents of *dppb*, black precipitates formed, which consists of Au₂₅ but was not able to confirm the presence of iminophosphorane.

2.5 Reference

- (1) Jin, R.; Zeng, C.; Zhou, M.; Chen, Y. Atomically Precise Colloidal Metal Nanoclusters and Nanoparticles: Fundamentals and Opportunities. *Chem. Rev.* **2016**, *116*, 10346–10413.
- (2) Jin, R. Atomically Precise Metal Nanoclusters: Stable Sizes and Optical Properties. *Nanoscale* **2015**, *7*, 1549–1565.
- (3) Qian, H.; Zhu, M.; Wu, Z.; Jin, R. Quantum Sized Gold Nanoclusters with Atomic Precision. *Acc. Chem. Res.* **2012**, *45*, 1470–1479.
- (4) Kang, X.; Chong, H.; Zhu, M. Au₂₅(SR)₁₈: The Captain of the Great Nanocluster Ship. *Nanoscale* **2018**, *10*, 10758–10834.
- (5) Yao, Q.; Wu, Z.; Liu, Z.; Lin, Y.; Yuan, X.; Xie, J. Molecular Reactivity of Thiolate-Protected Noble Metal Nanoclusters: Synthesis, Self-Assembly, and

- Applications. *Chem. Sci.* **2021**, *12*, 99–127.
- (6) Lei, Z.; Li, J. J.; Wan, X. K.; Zhang, W. H.; Wang, Q. M. Isolation and Total Structure Determination of an All-Alkynyl-Protected Gold Nanocluster Au₁₄₄. *Angew. Chem. Int. Ed.* **2018**, *57*, 8639–8643.
- (7) Han, X. S.; Luan, X.; Su, H. F.; Li, J. J.; Yuan, S. F.; Lei, Z.; Pei, Y.; Wang, Q. M. Structure Determination of Alkynyl-Protected Gold Nanocluster Au₂₂(TBuC≡C)₁₈ and Its Thermochromic Luminescence. *Angew. Chem. Int. Ed.* **2020**, *59*, 2309–2312.
- (8) Wang, J. Q.; Shi, S.; He, R. L.; Yuan, S. F.; Yang, G. Y.; Liang, G. J.; Wang, Q. M. Total Structure Determination of the Largest Alkynyl-Protected Fcc Gold Nanocluster Au₁₁₀ and the Study on Its Ultrafast Excited-State Dynamics. *J. Am. Chem. Soc.* **2020**, *142*, 18086–18092.
- (9) Konishi, K.; Iwasaki, M.; Shichibu, Y. Phosphine-Ligated Gold Clusters with Core+ Exo Geometries: Unique Properties and Interactions at the Ligand-Cluster Interface. *Acc. Chem. Res.* **2018**, *51*, 3125–3133.
- (10) Wan, X.-K.; Yuan, S.-F.; Lin, Z.-W.; Wang, Q.-M. A Chiral Gold Nanocluster Au₂₀ Protected by Tetradentate Phosphine Ligands. *Angew. Chem. Int. Ed.* **2014**, *53*, 2923–2926.
- (11) Zhang, S. S.; Senanayake, R. D.; Zhao, Q. Q.; Su, H. F.; Aikens, C. M.; Wang, X. P.; Tung, C. H.; Sun, D.; Zheng, L. S. [Au₁₈(Dppm)₆Cl₄]⁴⁺: A Phosphine-Protected Gold Nanocluster with Rich Charge States. *Dalton Trans.* **2019**, *48*, 3635–3640.
- (12) Mckenzie, L. C.; Zaikova, T. O.; Hutchison, J. E. Structurally Similar Triphenylphosphine-Stabilized Undecagolds, Au₁₁(PPh₃)₇Cl₃ and [Au₁₁(PPh₃)₈Cl₂]Cl, Exhibit Distinct Ligand Exchange Pathways with Glutathione. *J. Am. Chem. Soc.* **2014**, *136*, 13426–13435.
- (13) Jin, S.; Du, W.; Wang, S.; Kang, X.; Chen, M.; Hu, D.; Chen, S.; Zou, X.; Sun, G.;

- Zhu, M. Thiol-Induced Synthesis of Phosphine-Protected Gold Nanoclusters with Atomic Precision and Controlling the Structure by Ligand/Metal Engineering. *Inorg. Chem.* **2017**, *56*, 11151–11159.
- (14) Narouz, M. R.; Takano, S.; Lummis, P. A.; Levchenko, T. I.; Nazemi, A.; Kaappa, S.; Malola, S.; Yousefalizadeh, G.; Calhoun, L. A.; Stamplecoskie, K. G.; Häkkinen, H.; Tsukuda, T.; Crudden, C. M. Robust, Highly Luminescent Au₁₃ Superatoms Protected by N-Heterocyclic Carbenes. *J. Am. Chem. Soc.* **2019**, *141*, 14997–15002.
- (15) Shen, H.; Xu, Z.; Hazer, M. S. A.; Wu, Q.; Peng, J.; Qin, R.; Malola, S.; Teo, B. K.; Häkkinen, H.; Zheng, N. Surface Coordination of Multiple Ligands Endows N-Heterocyclic Carbene-Stabilized Gold Nanoclusters with High Robustness and Surface Reactivity. *Angew. Chem. Int. Ed.* **2021**, *60*, 3752–3758.
- (16) Shen, H.; Deng, G.; Kaappa, S.; Tan, T.; Han, Y.; Malola, S.; Lin, S.; Teo, B. K.; Hannu, H.; Zheng, N. Highly Robust but Surface-Active: An N-Heterocyclic Carbene-Stabilized Au₂₅ Nanocluster. *Angew. Chem. Int. Ed.* **2019**, *58*, 17731–17735.
- (17) Narouz, M. R.; Osten, K. M.; Unsworth, P. J.; Man, R. W. Y.; Salorinne, K.; Takano, S.; Tomihara, R.; Kaappa, S.; Malola, S.; Dinh, C. T.; Padmos, J. D.; Ayoo, K.; Garrett, P. J.; Nambo, M.; Horton, J. H.; Sargent, E. H.; Häkkinen, H.; Tsukuda, T.; Crudden, C. M. N-Heterocyclic Carbene-Functionalized Magic-Number Gold Nanoclusters. *Nat. Chem.* **2019**, *11*, 419–425.
- (18) Cirri, A.; Morales Hernández, H.; Kmiotek, C.; Johnson, C. J. Systematically Tuning the Electronic Structure of Gold Nanoclusters through Ligand Derivatization. *Angew. Chem. Int. Ed.* **2019**, *58*, 13818–13822.
- (19) Zhu, M.; Lanni, E.; Garg, N.; Bier, M. E.; Jin, R. Kinetically Controlled, High-Yield Synthesis of Au₂₅ Clusters. *J. Am. Chem. Soc.* **2008**, *130*, 1138–1139.
- (20) Donkers, R. L.; Lee, D.; Murray, R. W. Synthesis and Isolation of the Molecule-

like Cluster $\text{Au}_{38}(\text{PhCH}_2\text{CH}_2\text{S})_{24}$. *Langmuir* **2004**, *20*, 1945–1952.

- (21) Akola, J.; Walter, M.; Whetten, R. L.; Hakkinen, H.; Gronbeck, H. On the Structure of Thiolate-Protected Au_{25} . *J. Am. Chem. Soc.* **2008**, *130*, 3756–3757.
- (22) Heaven, M. W.; Dass, A.; White, P. S.; Holt, K. M.; Murray, R. W. Crystal Structure of the Gold Nanoparticle $[\text{N}(\text{C}_8\text{H}_{17})_4][\text{Au}_{25}(\text{SCH}_2\text{CH}_2\text{Ph})_{18}]$. *J. Am. Chem. Soc.* **2008**, *130*, 3754–3755.
- (23) Zhu, M.; Aikens, C. M.; Hollander, F. J.; Schatz, G. C.; Jin, R. Correlating the Crystal Structure of A Thiol-Protected Au_{25} Cluster and Optical Properties. *J. Am. Chem. Soc.* **2008**, *130*, 5883–5885.
- (24) Antonello, S.; Perera, N. V.; Ruzzi, M.; Gascón, J. A.; Maran, F. Interplay of Charge State, Lability, and Magnetism in the Molecule-like $\text{Au}_{25}(\text{SR})_{18}$ Cluster. *J. Am. Chem. Soc.* **2013**, *135*, 15585–15594.
- (25) Zhu, M.; Aikens, C. M.; Hendrich, M. P.; Gupta, R.; Qian, H.; Schatz, G. C.; Jin, R. Reversible Switching of Magnetism in Thiolate-Protected Au_{25} Superatoms. *J. Am. Chem. Soc.* **2009**, *131*, 2490–2492.
- (26) Nasaruddin, R. R.; Yao, Q.; Chen, T.; Hülsey, M. J.; Yan, N.; Xie, J. Hydride-Induced Ligand Dynamic and Structural Transformation of Gold Nanoclusters during a Catalytic Reaction. *Nanoscale* **2018**, *10*, 23113–23121.
- (27) Wan, X.-K.; Wang, J.-Q.; Nan, Z.-A.; Wang, Q.-M. Ligand Effects in Catalysis by Atomically Precise Gold Nanoclusters. *Sci. Adv.* **2017**, *3*, 1–6.
- (28) Zheng, K.; Setyawati, M. I.; Leong, D. T.; Xie, J. Antimicrobial Gold Nanoclusters. *ACS Nano* **2017**, *11*, 6904–6910.
- (29) Yang, H.; Cai, R.; Zhang, Y.; Chen, Y.; Gu, B. Gold Nanoclusters as an Antibacterial Alternative against *Clostridium Difficile*. *Int. J. Nanomedicine* **2020**, *15*, 6401–6408.

- (30) Zhang, Y.; Wu, M.; Dai, W.; Chen, M.; Guo, Z.; Wang, X.; Tan, D.; Shi, K.; Xue, L.; Liu, S.; Lei, Y. High Drug-Loading Gold Nanoclusters for Responsive Glucose Control in Type 1 Diabetes. *J. Nanobiotechnology* **2019**, *17*, 1–11.
- (31) Raut, S. L.; Shumilov, D.; Chib, R.; Rich, R.; Gryczynski, Z.; Gryczynski, I. Two Photon Induced Luminescence of BSA Protected Gold Clusters. *Chem. Phys. Lett.* **2013**, *561–562*, 74–76.
- (32) Cantelli, A.; Battistelli, G.; Guidetti, G.; Manzi, J.; Di Giosia, M.; Montalti, M. Luminescent Gold Nanoclusters as Biocompatible Probes for Optical Imaging and Theranostics. *Dye. Pigm.* **2016**, *135*, 64–79.
- (33) Hostetler, M. J.; Templeton, A. C.; Murray, R. W. Dynamics of Place-Exchange Reactions on Monolayer-Protected Gold Cluster Molecules. *Langmuir* **1999**, *15*, 3782–3789.
- (34) Dass, A.; Stevenson, A.; Dubay, G. R.; Tracy, J. B.; Murray, R. W. Nanoparticle MALDI-TOF Mass Spectrometry without Fragmentation: $\text{Au}_{25}(\text{SCH}_2\text{CH}_2\text{Ph})_{18}$ and Mixed Monolayer $\text{Au}_{25}(\text{SCH}_2\text{CH}_2\text{Ph})_{18-x}(\text{L})_x$. *J. Am. Chem. Soc.* **2008**, *130*, 5940–5946.
- (35) Kang, X.; Ren, M.; Zhu, M.; Zhang, K. Azide-Functionalized Nanoclusters via a Ligand-Induced Rearrangement. *Chem. Mater.* **2020**, *32*, 6736–6743.
- (36) Gunawardene, P. N.; Corrigan, J. F.; Workentin, M. S. Golden Opportunity: A Clickable Azide-Functionalized $[\text{Au}_{25}(\text{SR})_{18}]$ – Nanocluster Platform for Interfacial Surface Modifications. *J. Am. Chem. Soc.* **2019**, *141*, 11781–11785.
- (37) Kolb, H. C.; Finn, M. G.; Sharpless, K. B. Click Chemistry: Diverse Chemical Function from a Few Good Reactions. *Angew. Chem. Int. Ed.* **2001**, *40*, 2004–2021.
- (38) Zambrano, G.; Chino, M.; Renzi, E.; Di Girolamo, R.; Maglio, O.; Pavone, V.; Lombardi, A.; Nastri, F. Clickable Artificial Heme-Peroxidases for the

Development of Functional Nanomaterials. *Biotechnol. Appl. Biochem.* **2020**, *67*, 549–562.

- (39) Gobbo, P.; Novoa, S.; Biesinger, M. C.; Workentin, M. S. Interfacial Strain-Promoted Alkyne-Azide Cycloaddition (I-SPAAC) for the Synthesis of Nanomaterial Hybrids. *Chem. Commun.* **2013**, *49*, 3982–3984.
- (40) Gololobov, Y. G.; Kasukhin, L. F. Recent Advances in the Staudinger Reaction. *Tetrahedron* **1992**, *48*, 1353–1406.
- (41) Huang, H. Y.; Cai, K. Bin; Talite, M. J.; Chou, W. C.; Chen, P. W.; Yuan, C. T. Coordination-Induced Emission Enhancement in Gold-Nanoclusters with Solid-State Quantum Yields up to 40% for Eco-Friendly, Low-Reabsorption Nano-Phosphors. *Sci. Rep.* **2019**, *9*, 1–11.
- (42) Stol, M.; Snelders, D. J. M.; Kooijman, H.; Spek, A. L.; Van Klink, G. P. M.; Van Koten, G. A New, Easily Recyclable Arylating Agent Based on a Diphosphino-Digold(i) Complex. *Dalton. Trans.* **2007**, No. 24, 2589–2593.
- (43) Collado, A.; Gómez-Suárez, A.; Martin, A. R.; Slawin, A. M. Z.; Nolan, S. P. Straightforward Synthesis of [Au(NHC)X] (NHC = N-Heterocyclic Carbene, X = Cl, Br, I) Complexes. *Chem. Commun.* **2013**, *49*, 5541–5543.
- (44) Zhang, X.; Liu, H.; Hu, X.; Tang, G.; Zhu, J.; Zhao, Y. Ni(II)/Zn Catalyzed Reductive Coupling of Aryl Halides with Diphenylphosphine Oxide in Water. *Org. Lett.* **2011**, *13*, 3478–3481.
- (45) Gaillard, S.; Nun, P.; Slawin, A. M. Z.; Nolan, S. P. Expedient Synthesis of [Au(NHC)(L)]⁺ (NHC = N-Heterocyclic Carbene; L = Phosphine or NHC) Complexes. *Organometallics* **2010**, *29*, 5402–5408.
- (46) Leffler, J. E.; Temple, R. D. The Staudinger Reaction between Triarylphosphines and Azides. A Study of the Mechanism. *J. Am. Chem. Soc.* **1967**, *89*, 5235–5246.
- (47) Yavari, I.; Adib, M.; Hojabri, L. Vinyltriphenylphosphonium Salt Mediated

- Serendipitous Synthesis of Aryliminophosphoranes. *Tetrahedron* **2002**, *58*, 7213–7219.
- (48) Briggs, E. M.; Brown, G. W.; Cairns, P. M.; Jiricny, J.; Meidine, M. F. 31P Chemical Shifts in N-aryliminotriphenylphosphoranes. *Org. Magn. Reson.* **1980**, *13*, 306–307.
- (49) Albright, T. A.; Freeman, W. J.; Schweizer, E. E. Nuclear Magnetic Resonance Studies. 6. Properties of Phosphorus-Nitrogen Ylides. *J. Org. Chem.* **1976**, *41*, 2716–2720.
- (50) Kabachnik, M. I.; Lobanov, D. I.; Matveeva, A. G.; Kovsheva, O. E.; Terekhova, M. I.; Petrov, E. S.; Petrovskii, P. V.; Matrosov, E. I. Synthesis and CH-Acidity of N,N-Disubstituted Aminotriphenylphosphonium Salts. *Bull. Acad. Sci. USSR, Div. Chem. Sci.* **1991**, *40*, 1417–1422.
- (51) Laszlo, P.; Polla, E. Facile Conversion of Hydrazines to Iminophosphoranes. *Tetrahedron Lett.* **1984**, *25*, 4651–4654.
- (52) Polgar, A. M.; Weigend, F.; Zhang, A.; Stillman, M. J.; Corrigan, J. F. A N-Heterocyclic Carbene-Stabilized Coinage Metal-Chalcogenide Framework with Tunable Optical Properties. *J. Am. Chem. Soc.* **2017**, *139*, 14045–14048.
- (53) Li, M. B.; Tian, S. K.; Wu, Z.; Jin, R. Peeling the Core-Shell Au₂₅ Nanocluster by Reverse Ligand-Exchange. *Chem. Mater.* **2016**, *28*, 1022–1025.
- (54) Socrates, G. *Infrared Characteristic Group Frequencies: Tables and Charts*, 2nd ed.; Wiley, 1995.
- (55) Wu, Z.; Suhan, J.; Jin, R. One-Pot Synthesis of Atomically Monodisperse, Thiol-Functionalized Au₂₅ Nanoclusters. *J. Mater. Chem.* **2009**, *19*, 622–626.
- (56) Chuchuryukin, A. V.; Huang, R.; van Faassen, E. E.; van Klink, G. P. M.; Lutz, M.; Chadwick, J. C.; Spek, A. L.; van Koten, G. Mono N,C,N-Pincer Complexes of Titanium, Vanadium and Niobium. Synthesis, Structure and Catalytic Activity

in Olefin Polymerisation. *Dalton. Trans.* **2011**, *40*, 8887–8895.

Chapter 3

3 Conclusion and Outlook

3.1 Summary and conclusion

In this thesis, the post-assembly surface modification of [AuNC-azide]⁻ has been demonstrated via the Staudinger reaction. The Staudinger reaction with *p*-azidophenylethyl thioether formed iminophosphorane and yielded minimal impurities, as confirmed by ³¹P {¹H} NMR and IR spectra. In the Staudinger reaction with the [(IPr)Au(SCH₂CH₂C₆H₄N₃)] and *dppb*, ³¹P{¹H} NMR, IR and mass spectra have shown that the formation of iminophosphorane competed with the phosphine coordinating to Au(I) via the displacement of the thiolate ligand. It was found that by lowering the temperature of the reaction, the formation of iminophosphorane improves via reduction of the rate of ligand displacement.

The Staudinger reaction with [AuNC-azide]⁻ and PPh₃ has shown that with lower ratio of PPh₃, the phosphines undergo Staudinger reactions with the surface azides to form iminophosphoranes. However, with higher ratio of phosphines, the reaction starts to favor the ligand displacement of [AuNC-azide]⁻, which lead to surface rearrangement of the cluster. Although the UV-Vis spectrum with 10 equivalents of PPh₃ show that there is minimal ligand displacement, ³¹P{¹H} NMR spectra indicate that the ligand displacement may start with even fewer equivalents. When the reaction was done at a lower temperature, the ligand displacement of the [AuNC-azide]⁻ started at lower ratio PPh₃: [AuNC-azide]⁻, according to the UV-Vis spectra.

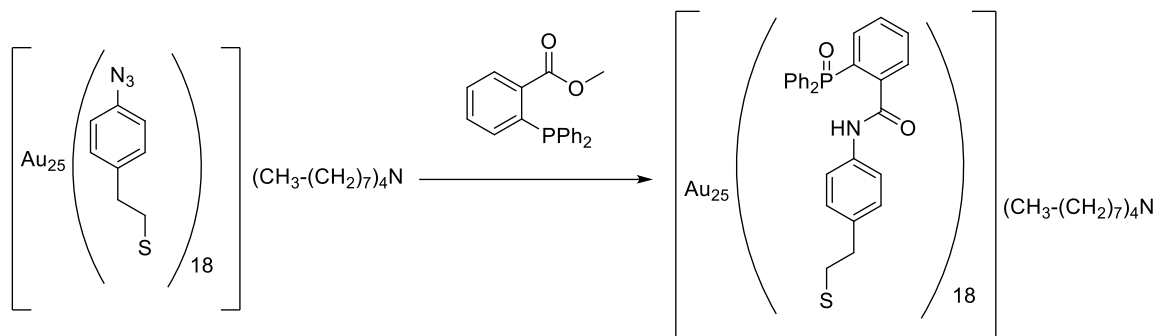
The Staudinger reaction with [AuNC-azide]⁻ and *dppb* has shown that the assemblies of [AuNC-azide]⁻ could be made with lower concentration of *dppb*. Compared to the Staudinger reaction with PPh₃ and [AuNC-azide]⁻, the ligand displacement starts at lower ratio of phosphines. The formation of the black precipitates from the reaction lead to lower concentration of [AuNC-azide]⁻ in the reaction solution, leading to excess amounts of *dppb* compared to [AuNC-azide]⁻. The excess equivalents of *dppb* compared to [AuNC-azide]⁻ enhance the ligand displacement of surface thiolates. The presence of

[AuNC-azide]⁻ in the precipitate was confirmed via diffuse-reflectance UV-Vis absorption spectroscopy. However, the IR spectrum of the precipitate did not show any iminophosphorane or azide stretches. This implies that while there may be Au₂₅ present in the precipitate, the overall reaction between the cluster and *dppb* are not as straightforward as the reaction between [AuNC-azide]⁻ and triphenylphosphine. The assemblies of [AuNC-azide]⁻ via formation of iminophosphorane in the solution was confirmed via ³¹P{¹H} NMR, IR spectra and TEM images.

3.2 Future Work

Although the post-assembly surface modification of [AuNC-azide]⁻ was demonstrated via Staudinger reaction with *dppb*, the photophysical properties, such as PL-QY of the cluster assemblies still needs to be investigated. Once the photophysical properties of the assemblies have been measured, the change in photophysical and chemical properties could be investigated with different diphosphines. For example, longer diphosphine linkers could be used to see if there are any improvements in PL-QY, compared to *dppb*. Also, it is possible that the stability of the cluster could be observed with longer diphosphine linkers. By using longer linkers, the clusters within the assemblies would be further apart, leading to less steric hinderance between the clusters within the assembly, which could potentially increase the formation of iminophosphorane, which in turn increases the linking between the clusters and decrease the ligand displacement. Different types of phosphines could also be employed to observe cluster stability. For example, by using less bulky phosphines such as trimethylphosphine, it could potentially lead to the formation of iminophosphorane with less steric hinderance and more accessible azide on the cluster, which would increase the equivalents of phosphines undergoing Staudinger reaction and decrease the possibility of ligand displacement. The formation of the cluster networks could also be done using linker with different reactive partner, such as strained alkynes. It has been shown by Workentin, Corrigan and Zhang's groups that the click reaction via SPAAC gives no ligand displacement, so the use of bis-strained alkyne linkers could potentially form assemblies of [AuNC-azide]⁻ without any ligand displacement.^{1,2}

Further surface modification of $[\text{AuNC-azide}]^-$ could be achieved by incorporating functional substrates to the phosphines, which can potentially add functionality to the nanocluster via the Staudinger reaction. Also, different types of click reactions, such as Staudinger-Bertozzi ligation, could be employed to show different methods of post-assembly surface modification on gold nanocluster, as done on gold nanoparticle (**Scheme 3.1**).³



Scheme 3.1 General scheme of Staudinger-Bertozzi ligation on $[\text{AuNC-azide}]^-$

3.3 Reference

- (1) Gunawardene, P. N.; Corrigan, J. F.; Workentin, M. S. Golden Opportunity: A Clickable Azide-Functionalized $[\text{Au}_{25}(\text{SR})_{18}]^-$ Nanocluster Platform for Interfacial Surface Modifications. *J. Am. Chem. Soc.* **2019**, *141*, 11781–11785.
- (2) Kang, X.; Ren, M.; Zhu, M.; Zhang, K. Azide-Functionalized Nanoclusters via a Ligand-Induced Rearrangement. *Chem. Mater.* **2020**, *32*, 6736–6743.
- (3) Gobbo, P.; Luo, W.; Cho, S. J.; Wang, X.; Biesinger, M. C.; Hudson, R. H. E.; Workentin, M. S. Small Gold Nanoparticles for Interfacial Staudinger–Bertozzi Ligation. *Org. Biomol. Chem.* **2015**, *13*, 4605–4612.

Appendices

Appendix 1 Permission to Reuse Copy Right Material

Permission to reproduce **Figure 1.3** – [Section 1.4, Reference 45]



Azide-Functionalized Nanoclusters via a Ligand-Induced Rearrangement



Author: Xi Kang, Mengqi Ren, Manzhou Zhu, et al

Publication: Chemistry of Materials

Publisher: American Chemical Society

Date: Aug 1, 2020

Copyright © 2020, American Chemical Society

PERMISSION/LICENSE IS GRANTED FOR YOUR ORDER AT NO CHARGE

This type of permission/license, instead of the standard Terms and Conditions, is sent to you because no fee is being charged for your order. Please note the following:

- Permission is granted for your request in both print and electronic formats, and translations.
- If figures and/or tables were requested, they may be adapted or used in part.
- Please print this page for your records and send a copy of it to your publisher/graduate school.
- Appropriate credit for the requested material should be given as follows: "Reprinted (adapted) with permission from {COMPLETE REFERENCE CITATION}. Copyright {YEAR} American Chemical Society." Insert appropriate information in place of the capitalized words.
- One-time permission is granted only for the use specified in your RightsLink request. No additional uses are granted (such as derivative works or other editions). For any uses, please submit a new request.

If credit is given to another source for the material you requested from RightsLink, permission must be obtained from that source.

BACK

CLOSE WINDOW

Permission to reproduce **Figure 2.1** – [Section 2.1, Reference 36]



Solution proposed to your case.

Short Description: Permission for one of the article

Priority: 3 - Moderate

If you feel your case is not completely resolved, please select the button below and select "Reject Solution" from the portal.

Leave a comment as to what is still causing the issue to your case.

[Reopen Case](#)

Comments:

12-10-2021 04:52:15 PM EST - Drew Jenkins Additional comments

Hello Dr. Lim,

Your permission requested is granted and there is no fee for this reuse.

In your planned reuse, you must cite the ACS article as the source, add this direct link:

<https://pubs.acs.org/doi/10.1021/jacs.9b05182> and include a notice to readers that further permission related to the material excerpted should be directed to the ACS.

Please do not hesitate to contact me if you need any further assistance.

Drew Jenkins

ACS Publications Support

Customer Services & Information

Website: <https://acs.service-now.com/acs>

Email: support@services.acs.org

Phone: [800-227-9919](tel:800-227-9919) | [202-872-\(HELP\) 4357](tel:202-872-4357)

Appendix 2 Supporting information for Chapter 2

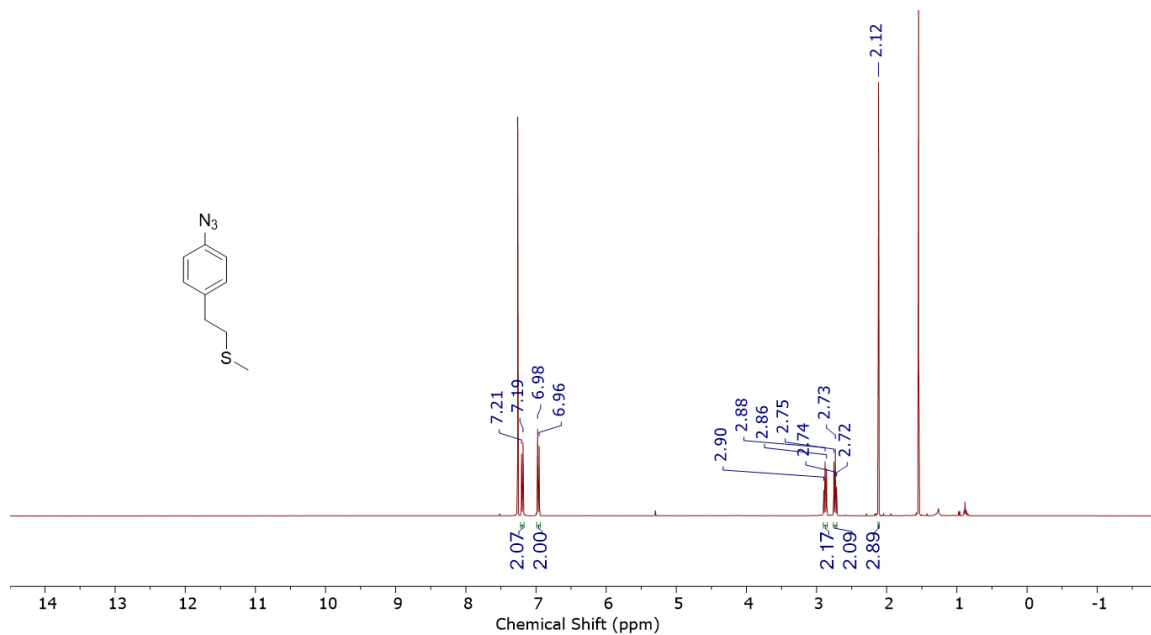


Figure S2.1 ^1H NMR spectrum of compound *p*-azido-phenylethyl methyl thioether in CDCl_3 . The spectrum was referenced against residual CHCl_3 .

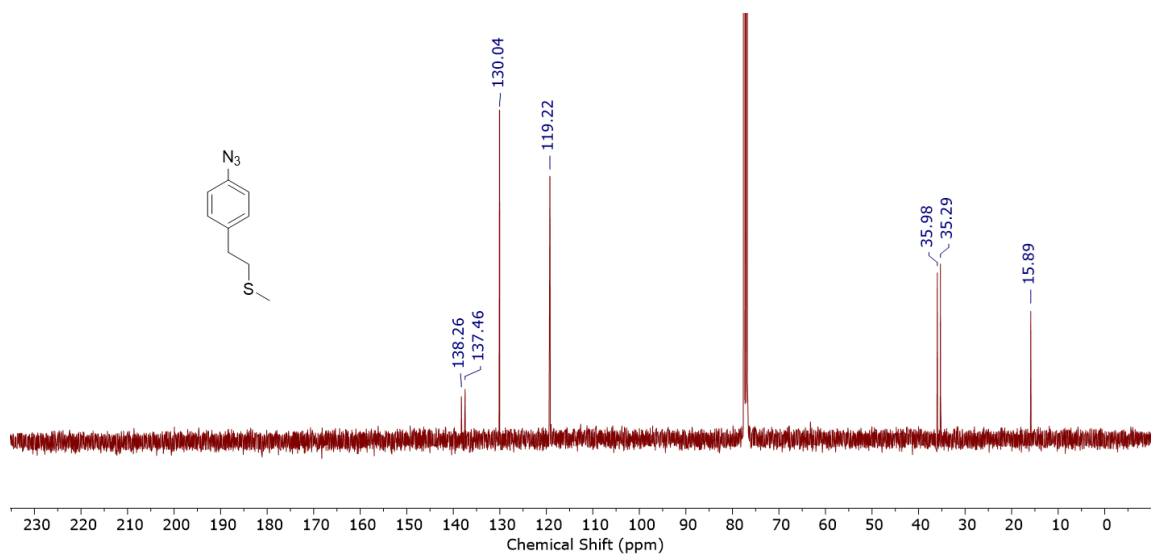


Figure S2.2 $^{13}\text{C}\{^1\text{H}\}$ NMR spectrum of compound *p*-azido-phenylethyl methyl thioether in CDCl_3 . The spectrum was referenced against CDCl_3 .

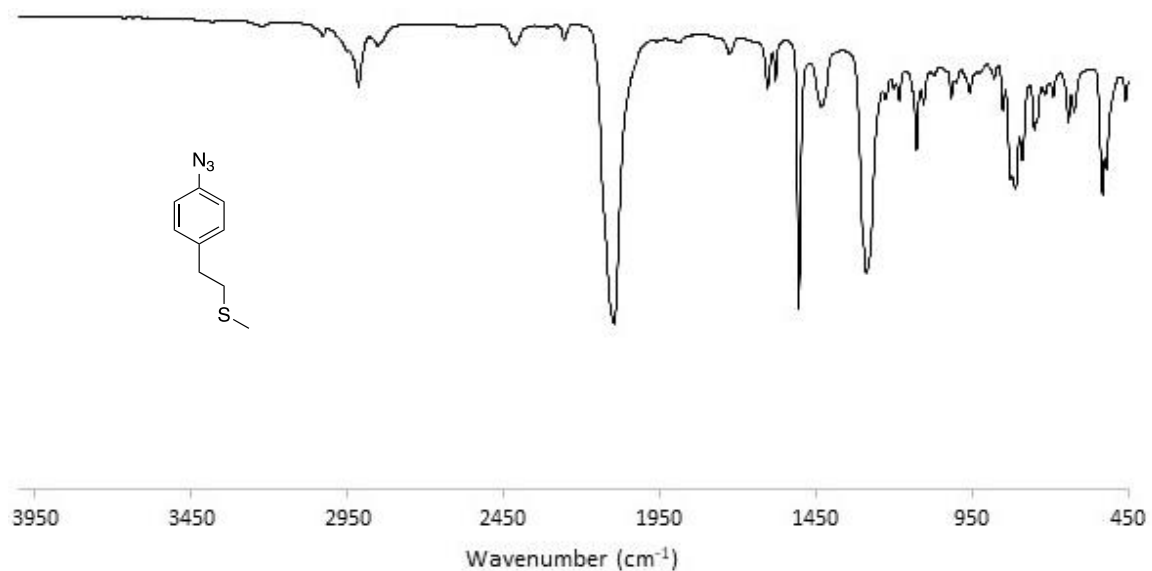


Figure S2.3 ATR-IR spectrum of compound *p*-azido-phenylethyl methyl thioether.

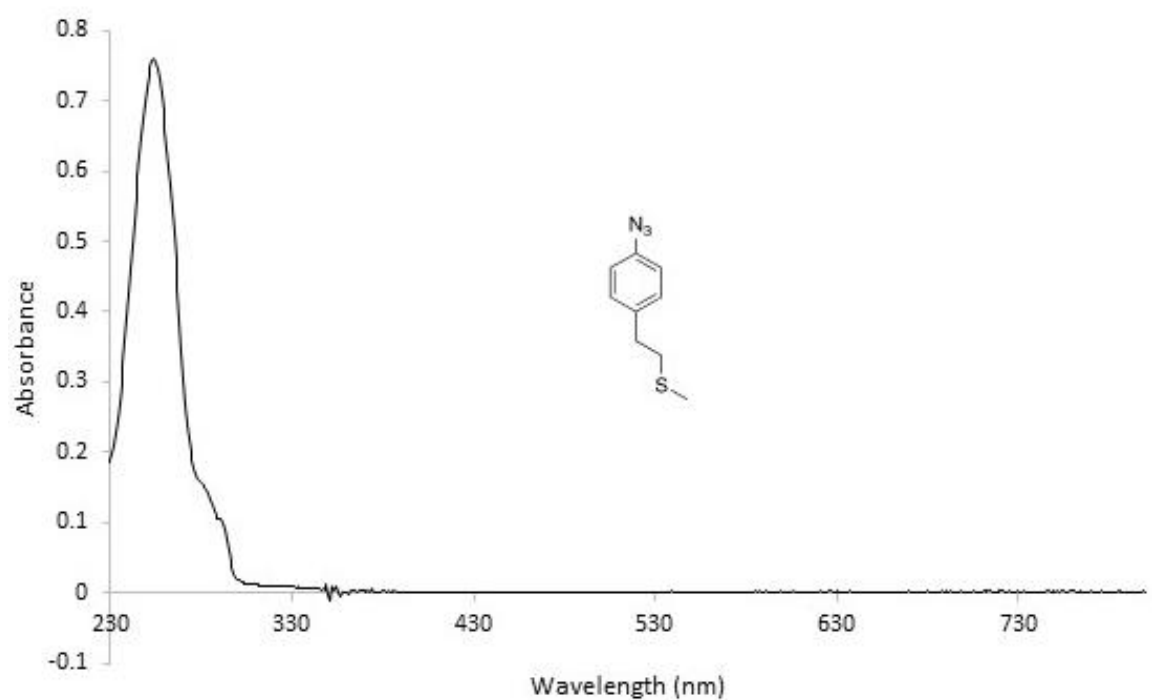


Figure S2.4 UV-Vis absorption spectrum of 5×10^{-5} M solution *p*-azido-phenylethyl methyl thioether in CH₂Cl₂ at 23 °C.

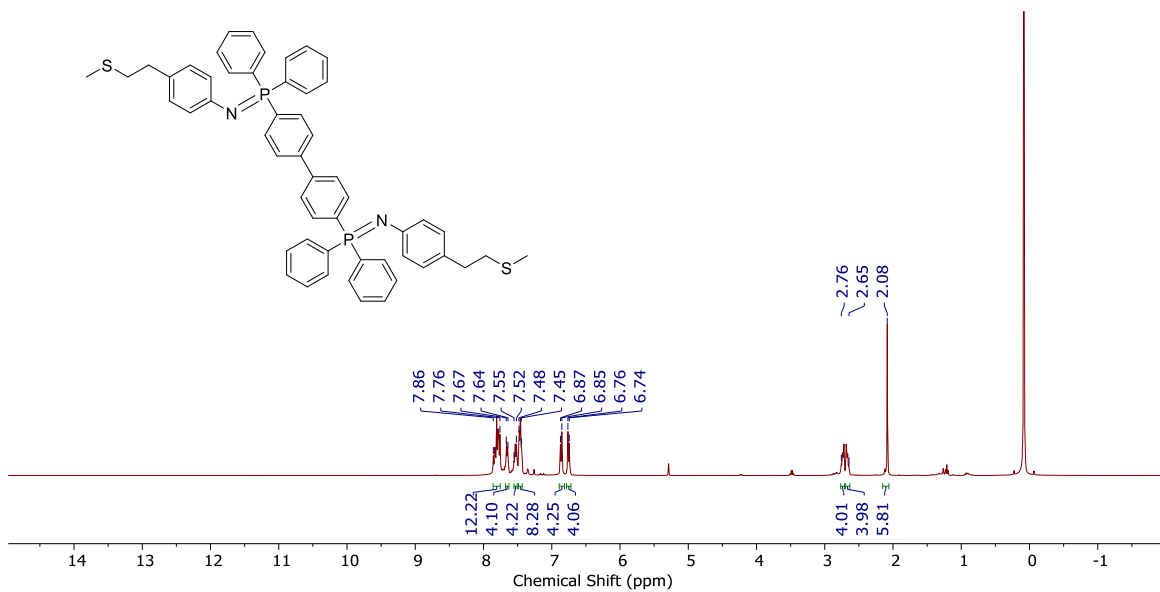


Figure S2.5 ¹H NMR spectrum of {CH₃SCH₂CH₂-*p*-C₆H₄-N=P(Ph₂)-C₆H₄-}₂ in CDCl₃. The spectrum was referenced against residual CHCl₃.

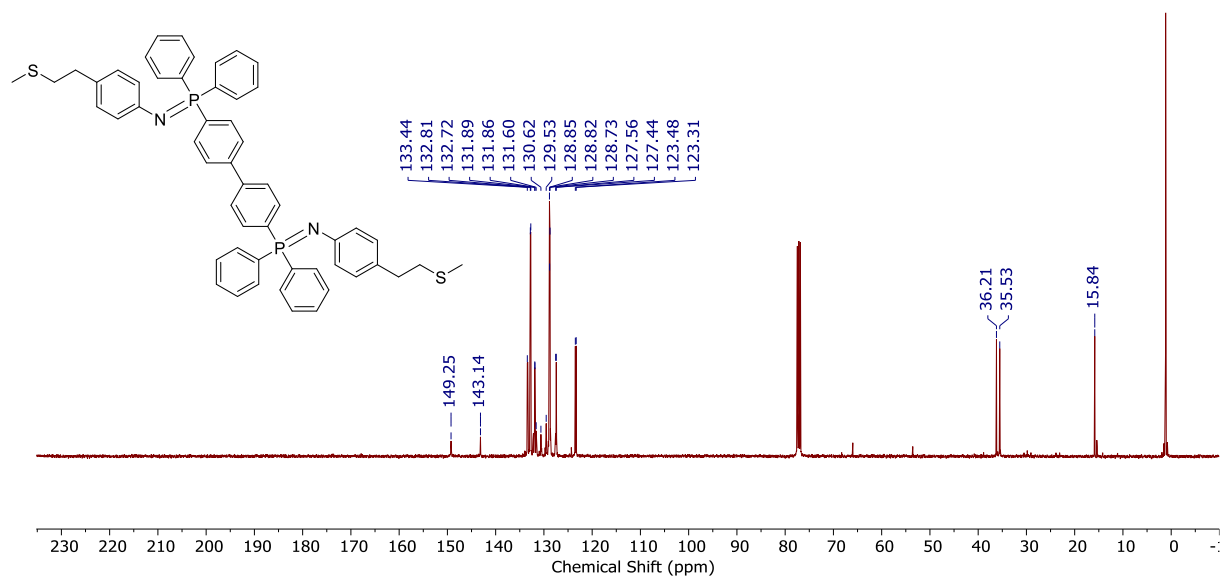


Figure S2.6 ¹³C{¹H} NMR spectrum of {CH₃SCH₂CH₂-*p*-C₆H₄-N=P(Ph₂)-C₆H₄-}₂ in CDCl₃. The spectrum was referenced against CDCl₃.

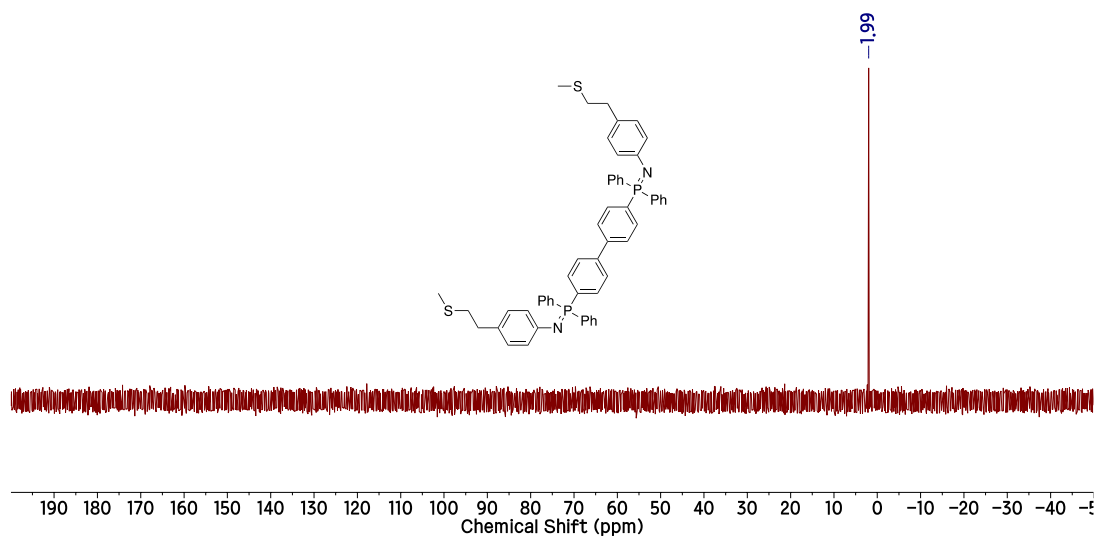


Figure S2.7 $^{31}\text{P}\{^1\text{H}\}$ NMR spectrum of $\{\text{CH}_3\text{SCH}_2\text{CH}_2\text{-}p\text{-C}_6\text{H}_4\text{-N=P(Ph)}_2\text{-C}_6\text{H}_4\}_2$ in CDCl_3 .

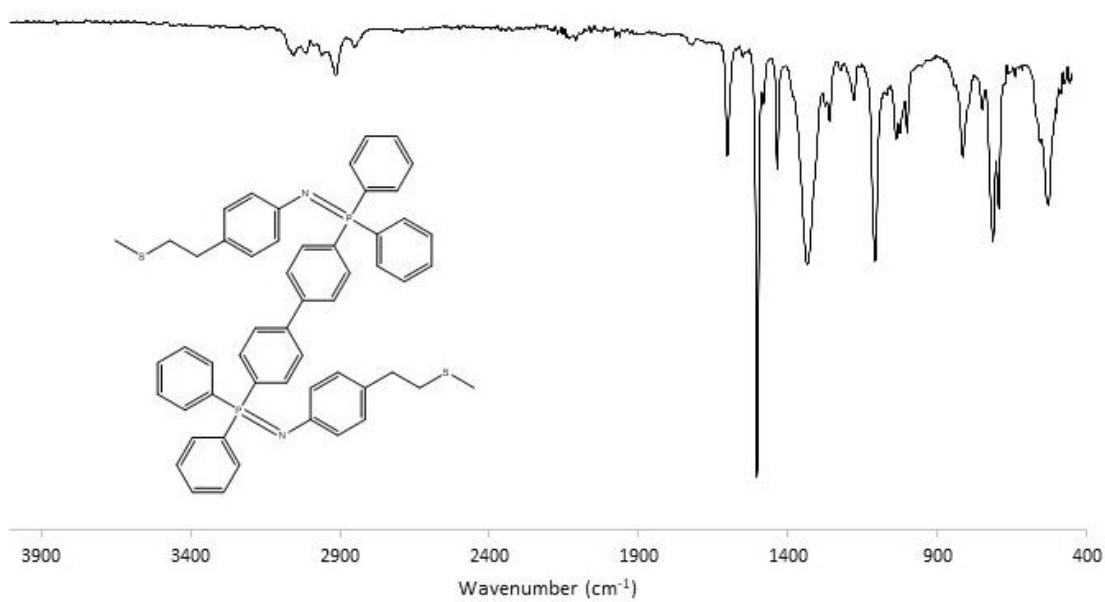


Figure S2.8 ATR-IR absorption spectrum of $\{\text{CH}_3\text{SCH}_2\text{CH}_2\text{-}p\text{-C}_6\text{H}_4\text{-N=P(Ph)}_2\text{-C}_6\text{H}_4\}_2$.

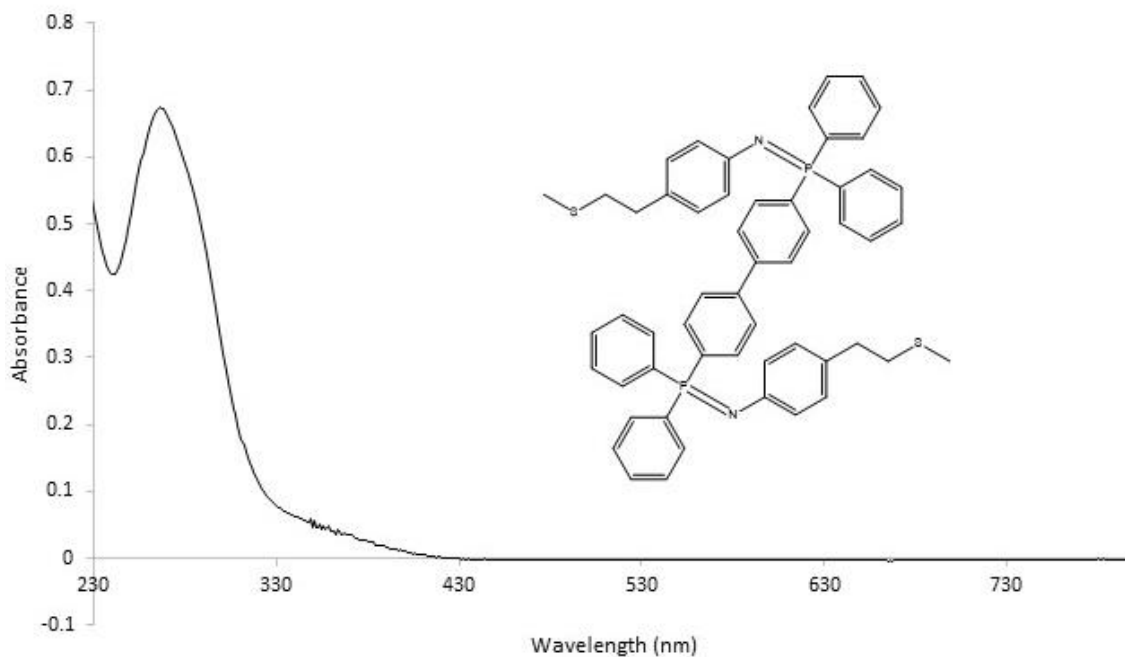


Figure S2.9 UV-Vis absorption spectrum of 1.8×10^{-5} M solution of $\{\text{CH}_3\text{SCH}_2\text{CH}_2\text{-}p\text{-C}_6\text{H}_4\text{-N}=\text{P}(\text{Ph})_2\text{-C}_6\text{H}_4\text{-}\}_2$ in CH_2Cl_2 at 23°C .

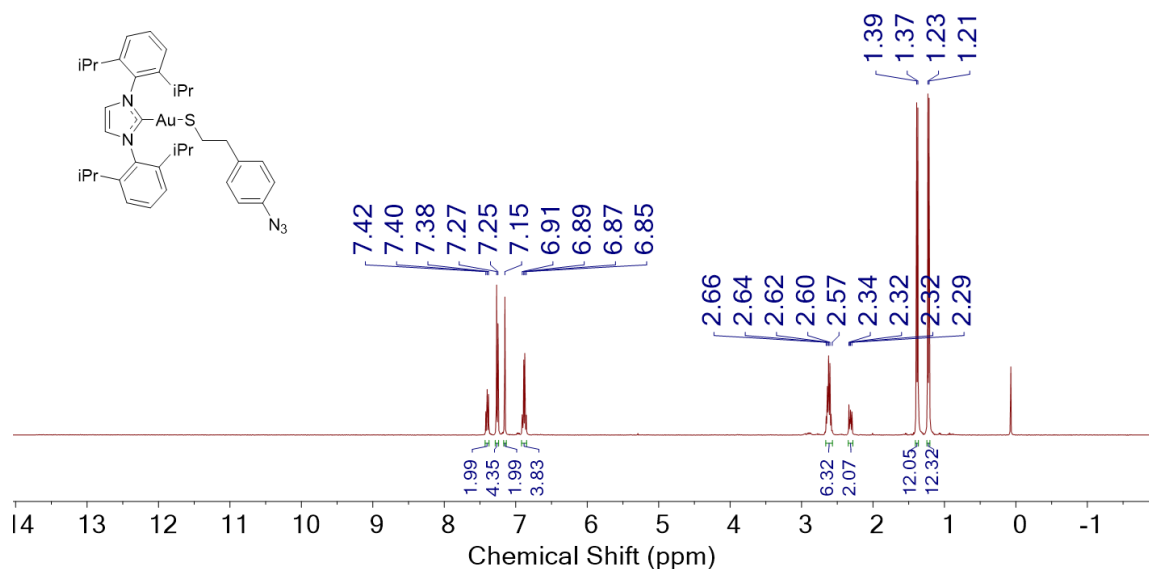


Figure S2.10 ^1H NMR spectrum of $[(\text{IPr})\text{Au}(\text{SCH}_2\text{CH}_2\text{C}_6\text{H}_4\text{N}_3)]$ in CDCl_3 . The spectrum was referenced against residual CHCl_3 .

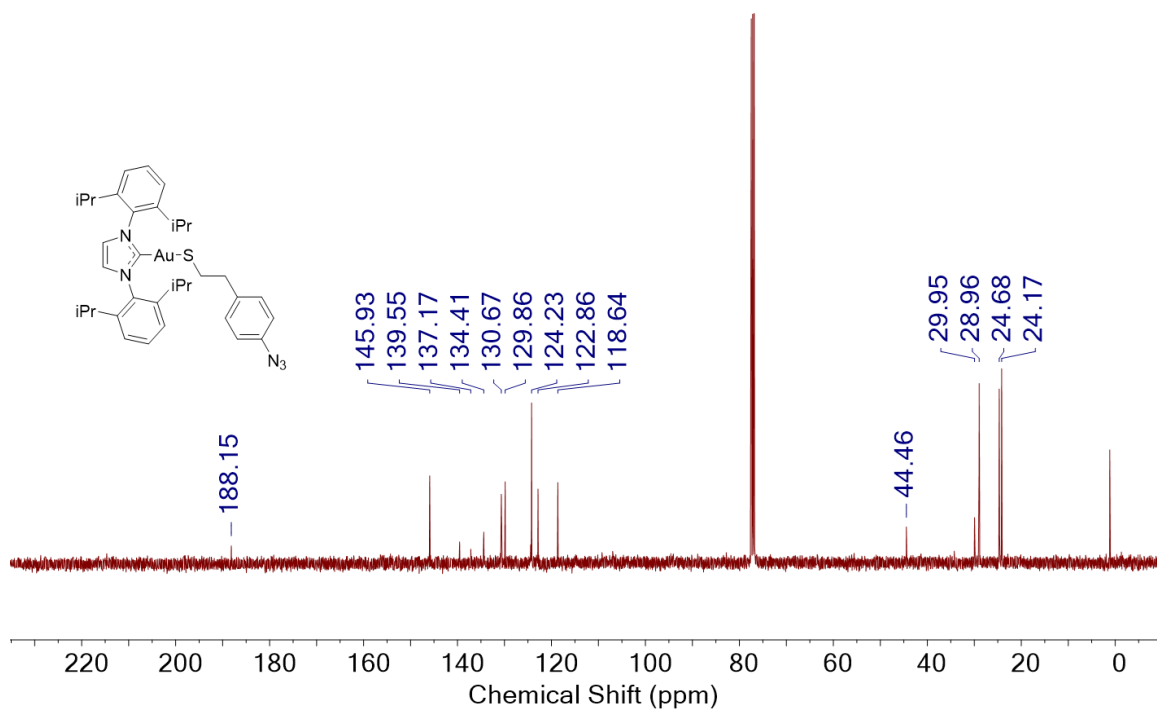


Figure S2.11 $^{13}\text{C}\{^1\text{H}\}$ NMR spectrum of $[(\text{IPr})\text{Au}(\text{SCH}_2\text{CH}_2\text{C}_6\text{H}_4\text{N}_3)]$ in CDCl_3 . The spectrum was referenced against CDCl_3 .

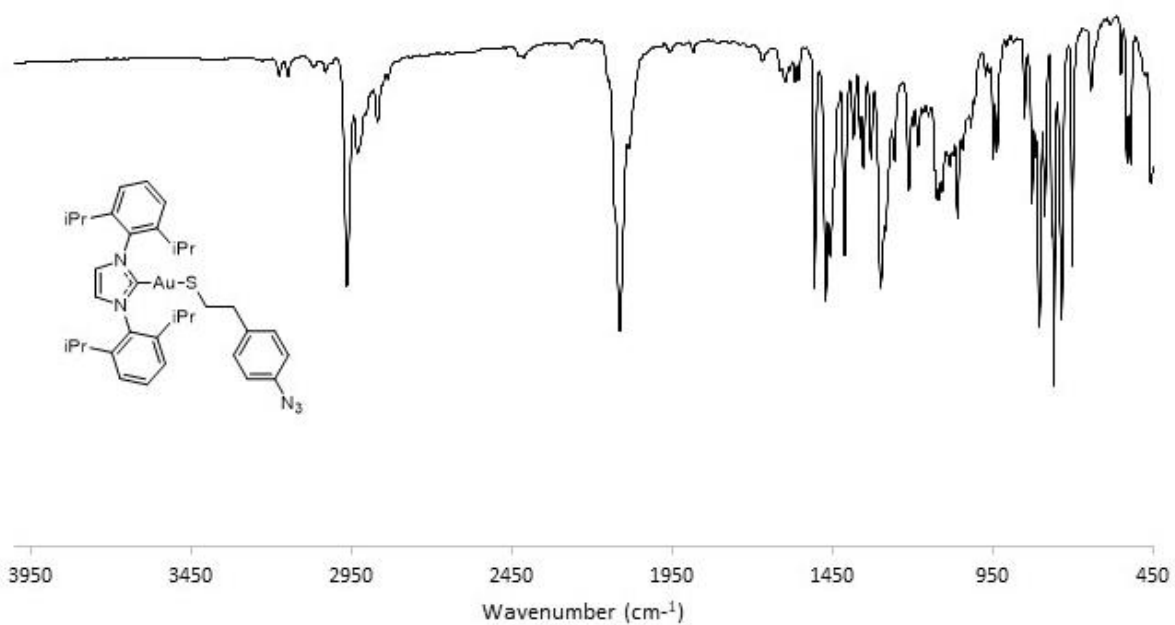


Figure S2.12 ATR-IR absorption spectrum of $[(\text{IPr})\text{Au}(\text{SCH}_2\text{CH}_2\text{C}_6\text{H}_4\text{N}_3)]$.

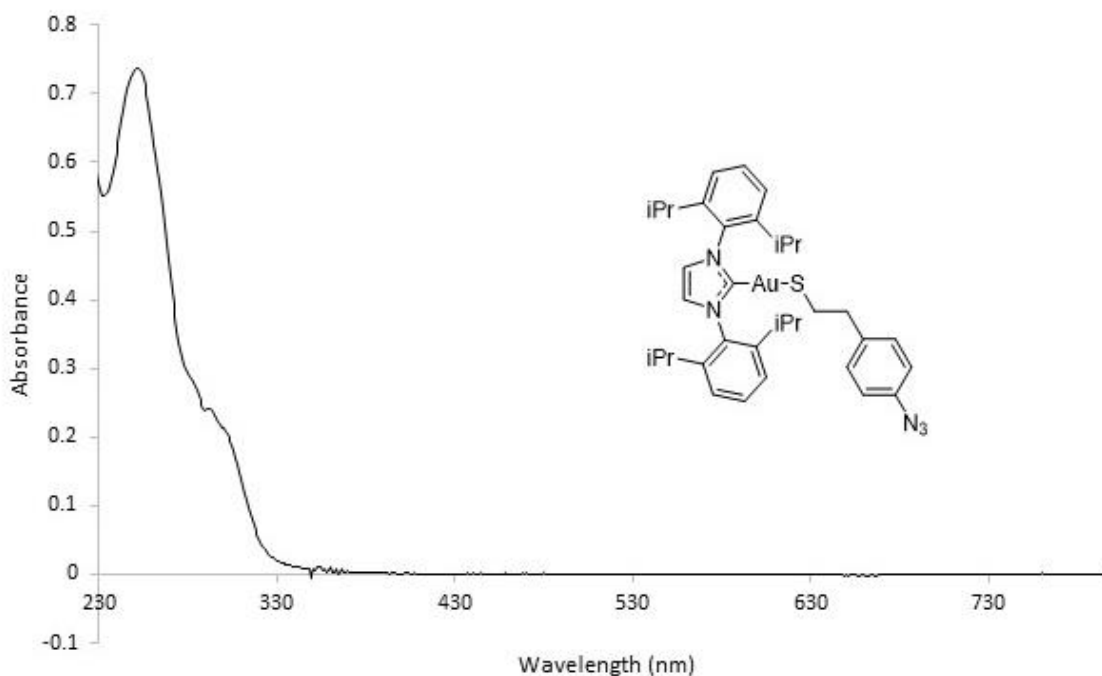


Figure S2.13 UV-Vis absorption spectrum of 3×10^{-5} M solution of $[(\text{IPr})\text{Au}(\text{SCH}_2\text{CH}_2\text{C}_6\text{H}_4\text{N}_3)]$ in CH_2Cl_2 at 23°C .

Table S2.1 Summary of Crystal Data for $[(\text{IPr})\text{Au}(\text{SCH}_2\text{CH}_2\text{C}_6\text{H}_4\text{N}_3)]$

Formula	$\text{C}_{35}\text{H}_{44}\text{AuN}_5\text{S}$
Formula Weight (<i>g/mol</i>)	763.78
Crystal Dimensions (<i>mm</i>)	$0.159 \times 0.121 \times 0.040$
Crystal Color and Habit	yellow Plate
Crystal System	monoclinic
Space Group	$P 2_1/n$
Temperature, K	110
<i>a</i> , Å	14.6626(10)
<i>b</i> , Å	16.4581(14)
<i>c</i> , Å	15.7623(13)
α , °	90
β , °	115.644(3)
γ , °	90
<i>V</i> , Å ³	3429.1(5)
Number of reflections to determine final unit cell	9922
Min and Max 2θ for cell determination, °	4.94, 53.54
<i>Z</i>	4
<i>F</i> (000)	1536
ρ (<i>g/cm</i>)	1.479
λ , Å, (MoK α)	0.71073

μ , (cm^{-1})	4.381
Diffractometer Type	Bruker Kappa Axis Apex2
Scan Type(s)	phi and omega scans
Max 2θ for data collection, $^{\circ}$	65.132
Measured fraction of data	0.999
Number of reflections measured	94617
Unique reflections measured	12454
R_{merge}	0.0563
Number of reflections included in refinement	12454
Cut off Threshold Expression	$I > 2\sigma(I)$
Structure refined using	full matrix least-squares using F^2
Weighting Scheme	$w=1/[\sigma^2(F_o^2)+(0.0143P)^2+2.4784P]$ where $P=(F_o^2+2F_c^2)/3$
Number of parameters in least-squares	387
R_1	0.0260
wR_2	0.0484
R_1 (all data)	0.0408
wR_2 (all data)	0.0529
GOF	1.023
Maximum shift/error	0.005
Min & Max peak heights on final ΔF Map ($e^{-}/\text{\AA}$)	-0.770, 1.204

Where:

$$R_1 = \frac{\sum (|F_o| - |F_c|)}{\sum F_o}$$

$$wR_2 = \left[\frac{\sum w (F_o^2 - F_c^2)^2}{\sum w F_o^4} \right]^{1/2}$$

$$GOF = \left[\frac{\sum w (F_o^2 - F_c^2)^2}{(\text{No. of reflns.} - \text{No. of params.})} \right]^{1/2}$$

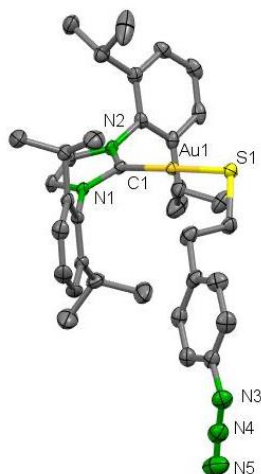


Figure S2.14 Molecular structure of $[(IPr)Au(SCH_2CH_2C_6H_4N_3)]$ in the crystal.

Hydrogen atoms are omitted for clarity and thermal ellipsoids are drawn at the 50% level of probability.

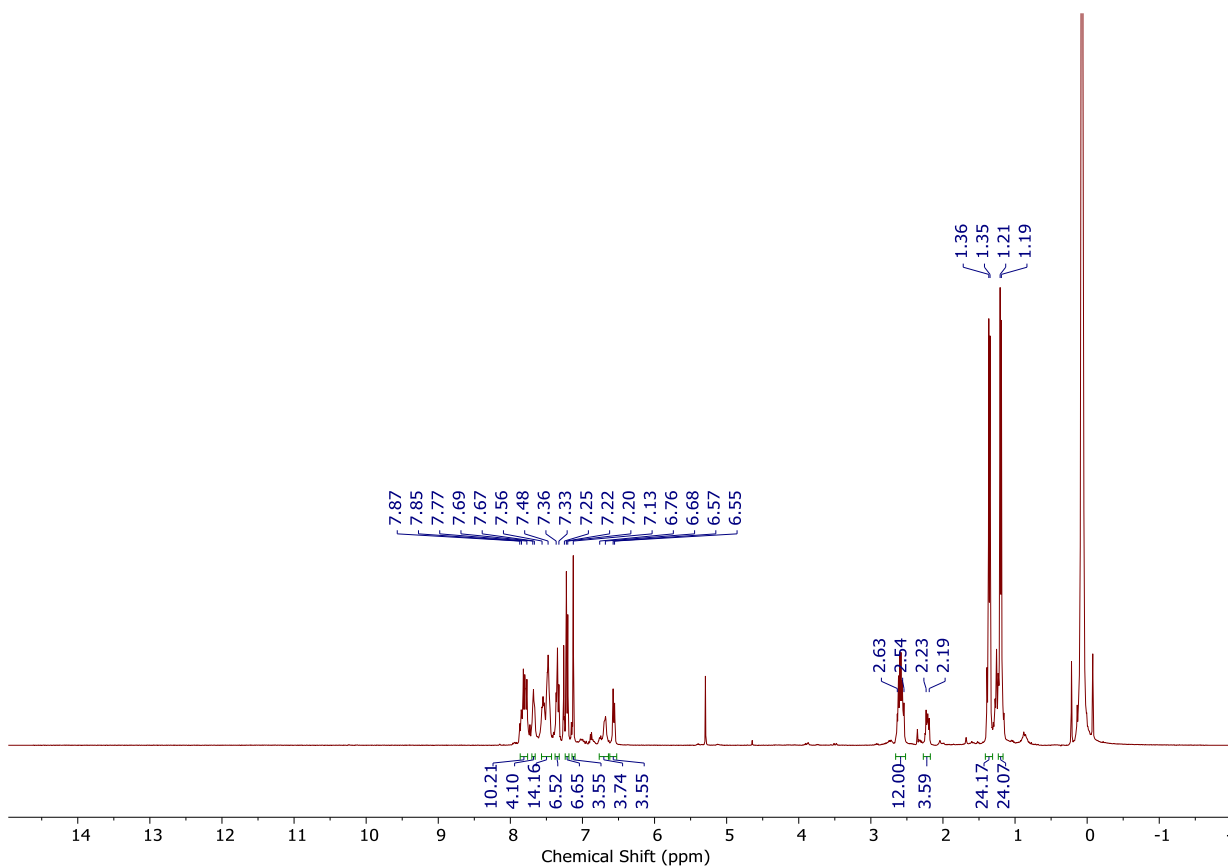


Figure S2.15 ^1H NMR spectrum of a reaction mixture of *dppb* with $[(\text{IPr})\text{Au}(\text{SCH}_2\text{CH}_2\text{C}_6\text{H}_4\text{N}_3)]$ in CDCl_3 . The spectrum was referenced against residual CHCl_3 .

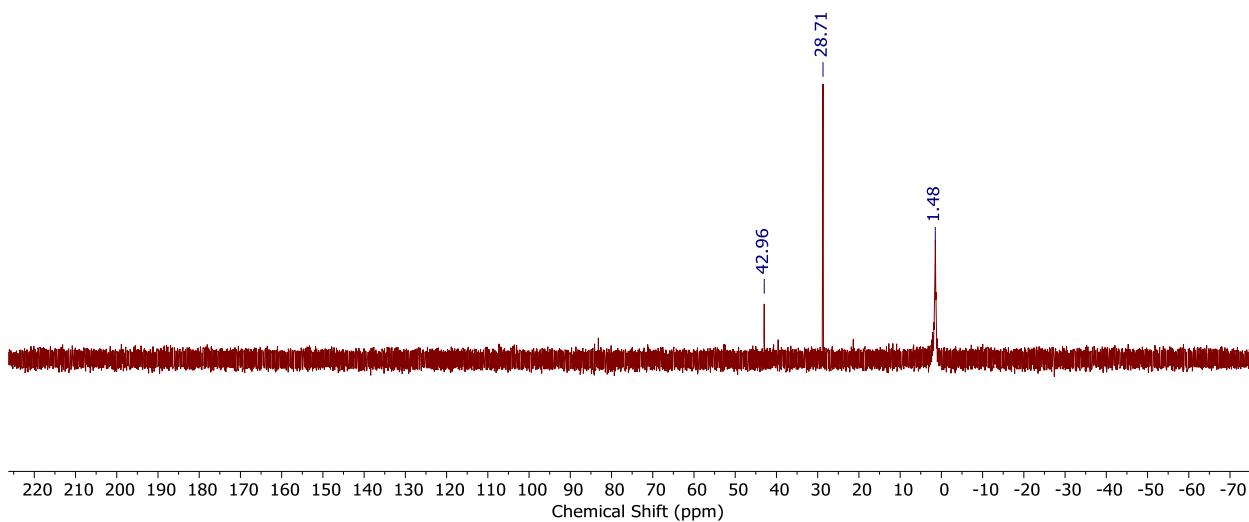


Figure S2.16 $^{31}\text{P}\{^1\text{H}\}$ NMR spectrum of a reaction mixture of *dppb* with $[(\text{IPr})\text{Au}(\text{SCH}_2\text{CH}_2\text{C}_6\text{H}_4\text{N}_3)]$ in CDCl_3 .

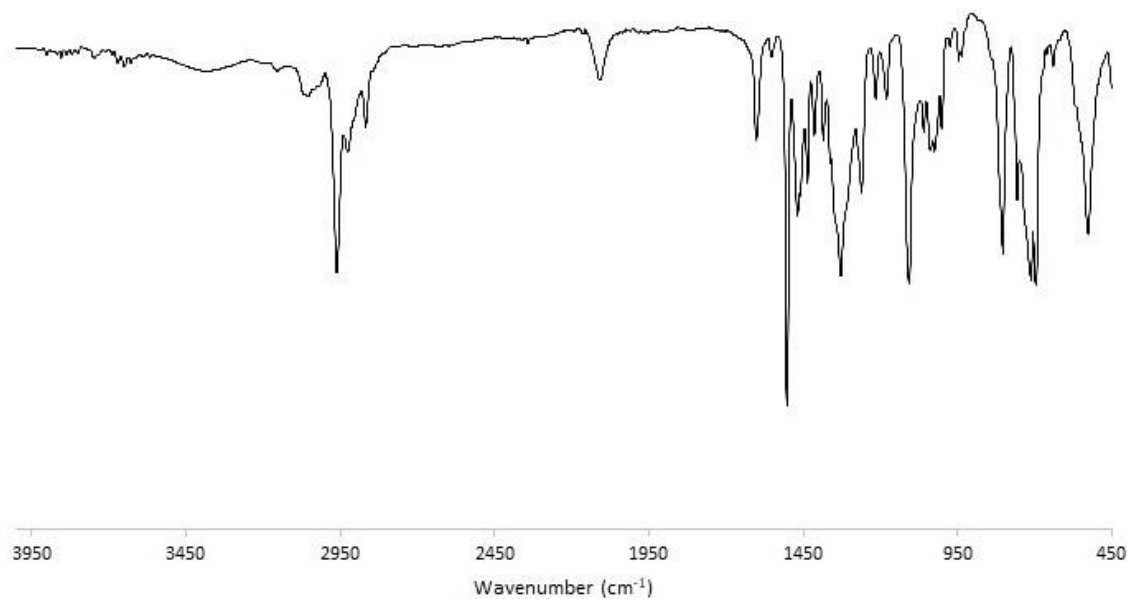


Figure S2.17 ATR-IR spectrum of a reaction mixture of *dppb* with $[(\text{IPr})\text{Au}(\text{SCH}_2\text{CH}_2\text{C}_6\text{H}_4\text{N}_3)]$.

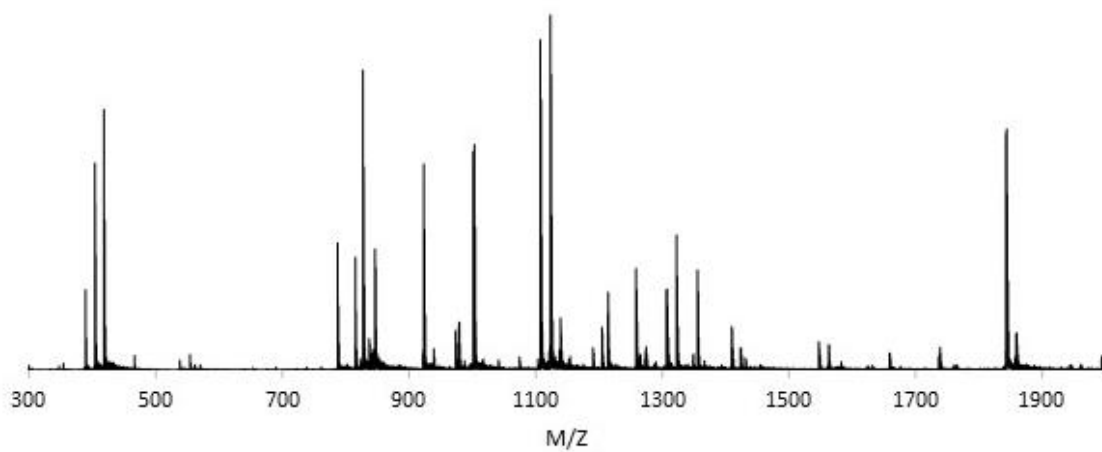


Figure S2.18 Negative ion mode ESI Mass spectrum of the mixture of *dppb* with $[(\text{IPr})\text{Au}(\text{SCH}_2\text{CH}_2\text{C}_6\text{H}_4\text{N}_3)]$.

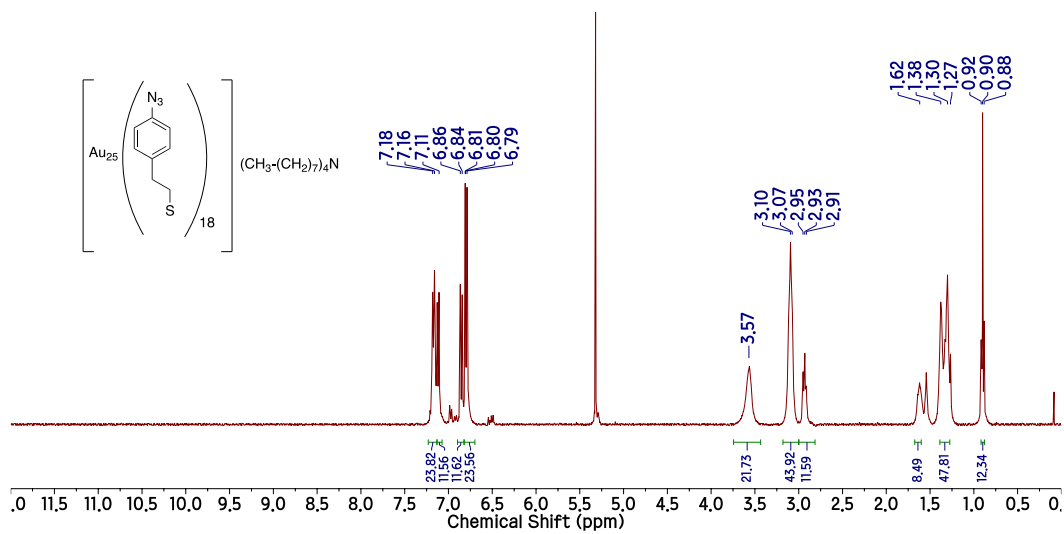


Figure S2.19 ^1H NMR spectrum of $[\text{AuNC-azide}]^-$ in CD_2Cl_2 . The spectrum was referenced against residual CHDCl_2 .

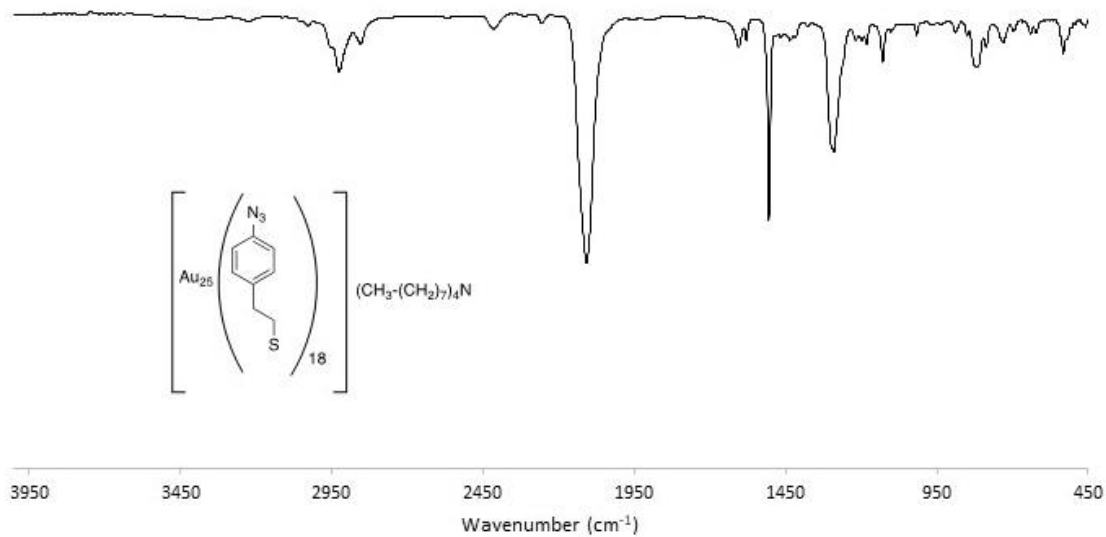


Figure S2.20 ATR-IR spectrum of $[\text{AuNC-azide}]^-$.

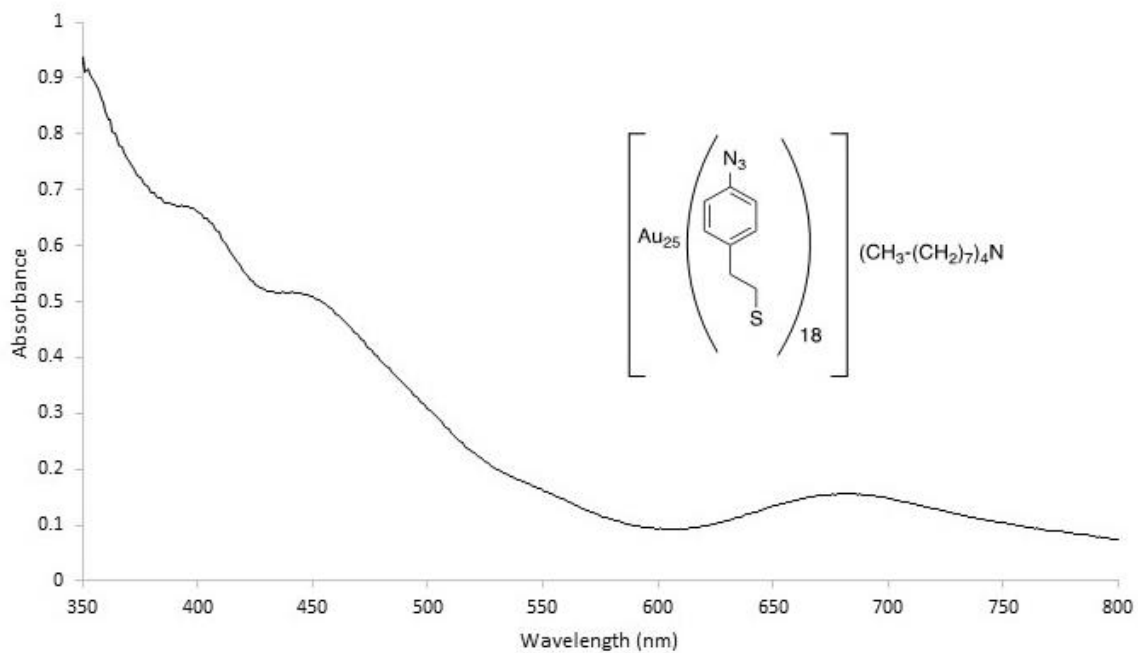


Figure S2.21 UV-Vis absorption spectrum of 1.7×10^{-5} solution of $[\text{AuNC-azide}]^-$ in CH_2Cl_2 at 23°C .

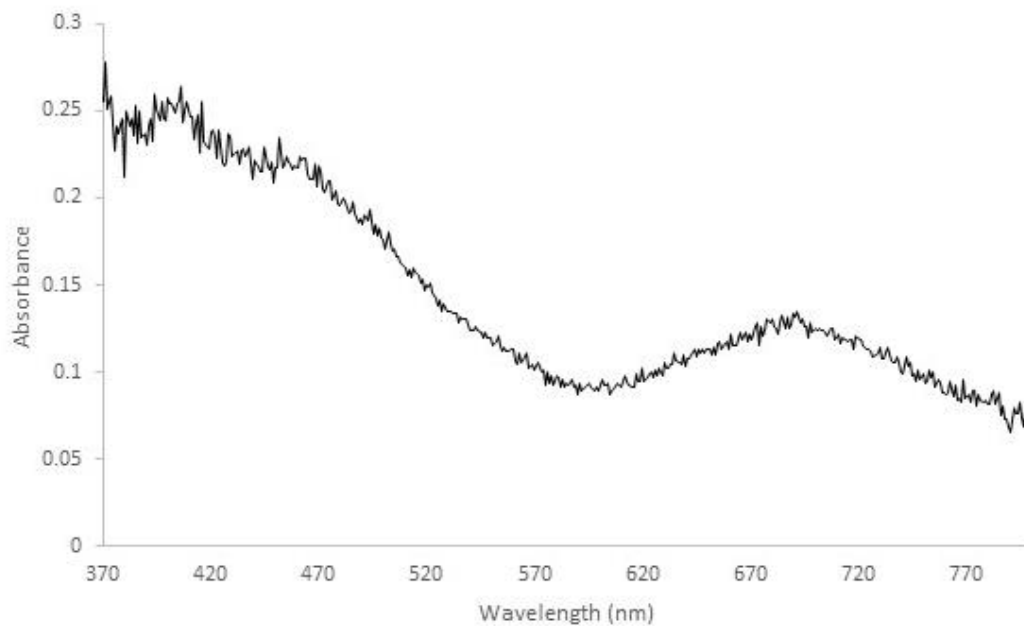


Figure S2.22 Diffuse reflectance UV-Vis absorption spectrum of the solid $[\text{AuNC-azide}]^-$.

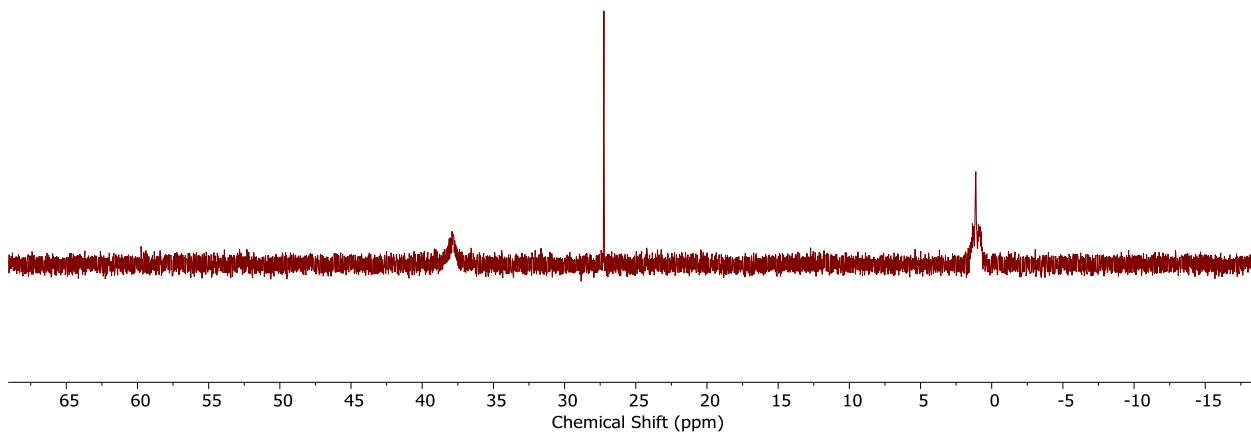


Figure S2.23 $^{31}\text{P}\{^1\text{H}\}$ NMR spectrum of a reaction mixture of $[\text{AuNC-azide}]^-$ with 10 equivalents of triphenylphosphine in CD_2Cl_2 .

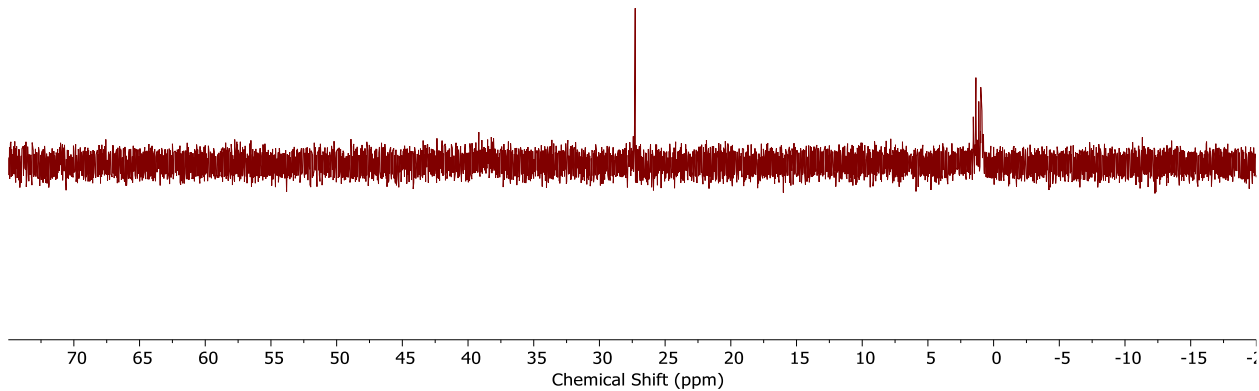


Figure S2.24 $^{31}\text{P}\{^1\text{H}\}$ NMR spectrum of a reaction mixture of $[\text{AuNC-azide}]^-$ with 3 equivalents of triphenylphosphine in CD_2Cl_2 .

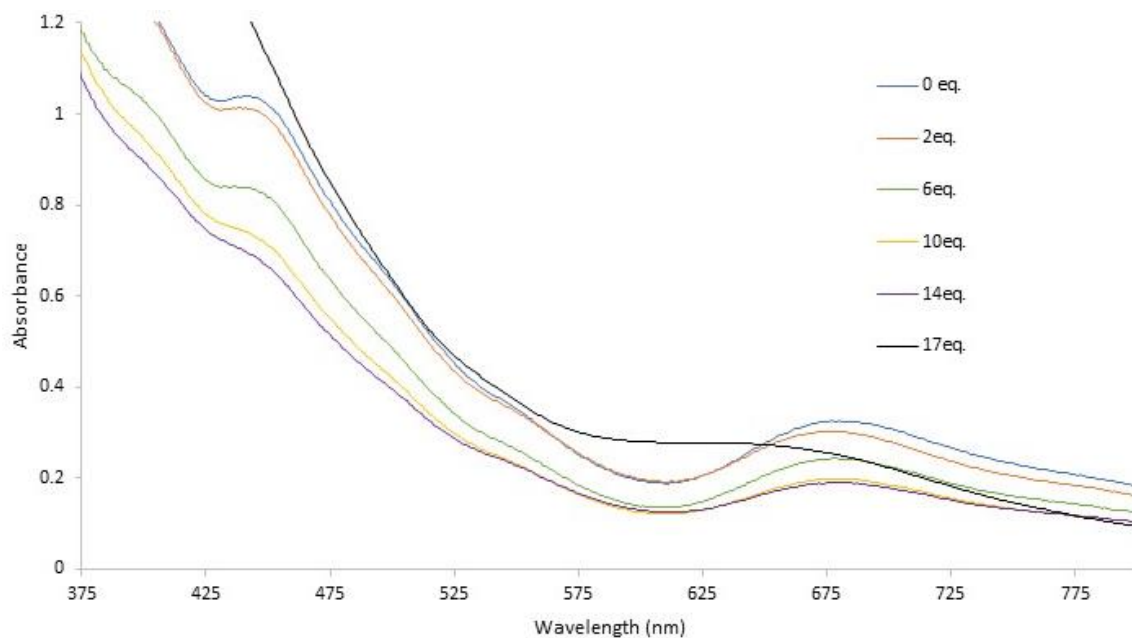


Figure S2.25 UV-Vis absorption spectra of 3.4×10^{-5} solution of $[\text{AuNC-azide}]^-$ mixed with triphenylphosphine and stirred at room temperature in CH_2Cl_2 at 23°C .

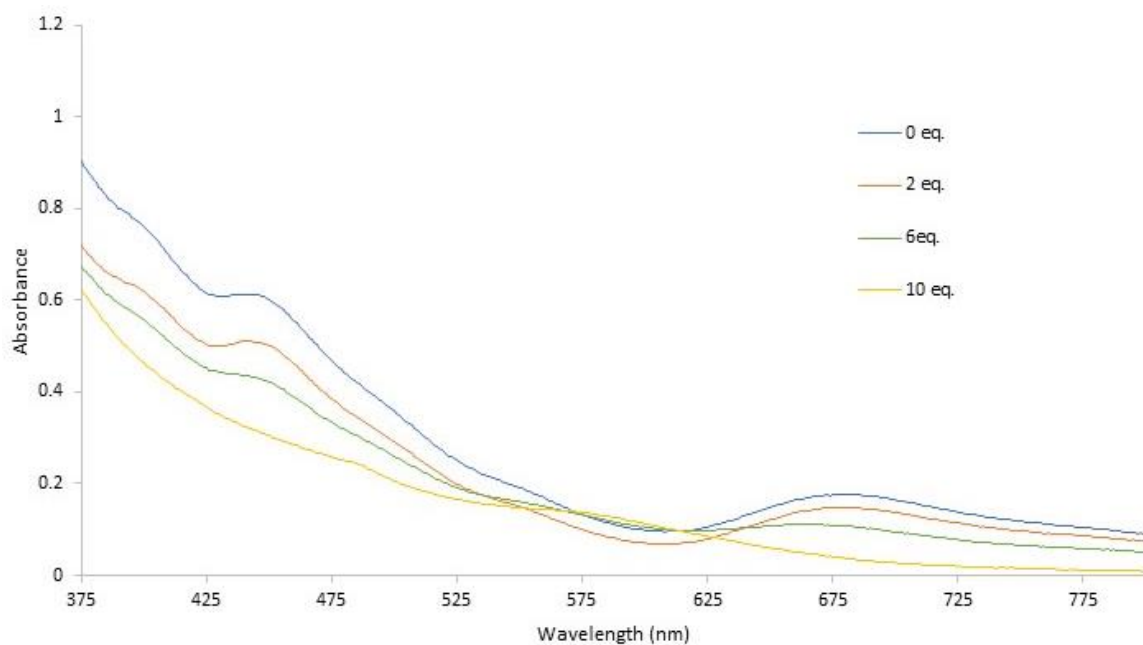


Figure S2.26 UV-Vis absorption spectra of 2.0×10^{-5} solution of $[\text{AuNC-azide}]^-$ mixed with triphenylphosphine and stirred at 0°C . The spectra were measured in CH_2Cl_2 at 23°C .

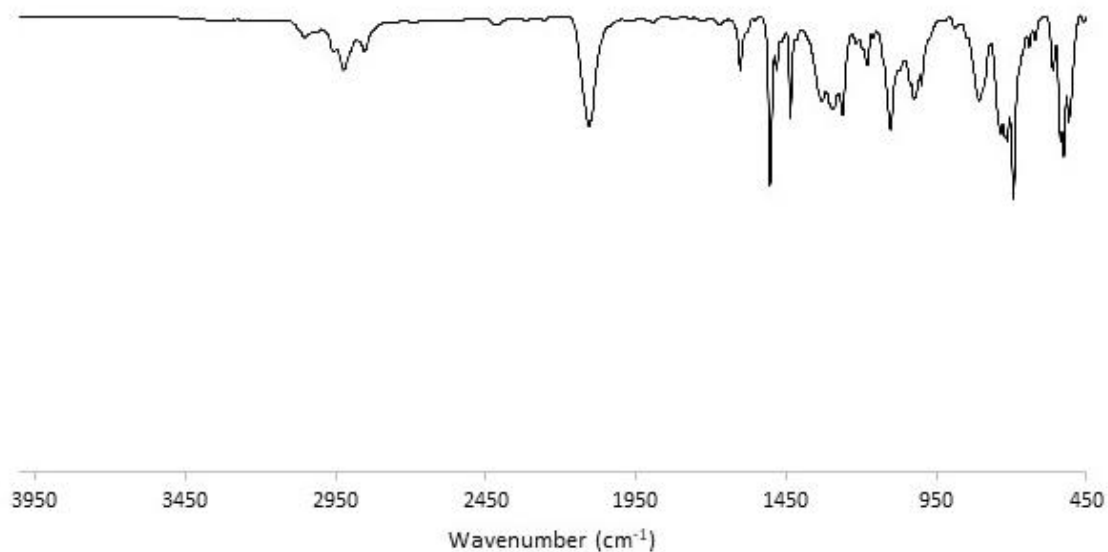


Figure S2.27 ATR-IR spectrum of the reaction mixture of $[\text{AuNC-azide}]^-$ with 10 equivalents of triphenylphosphine.

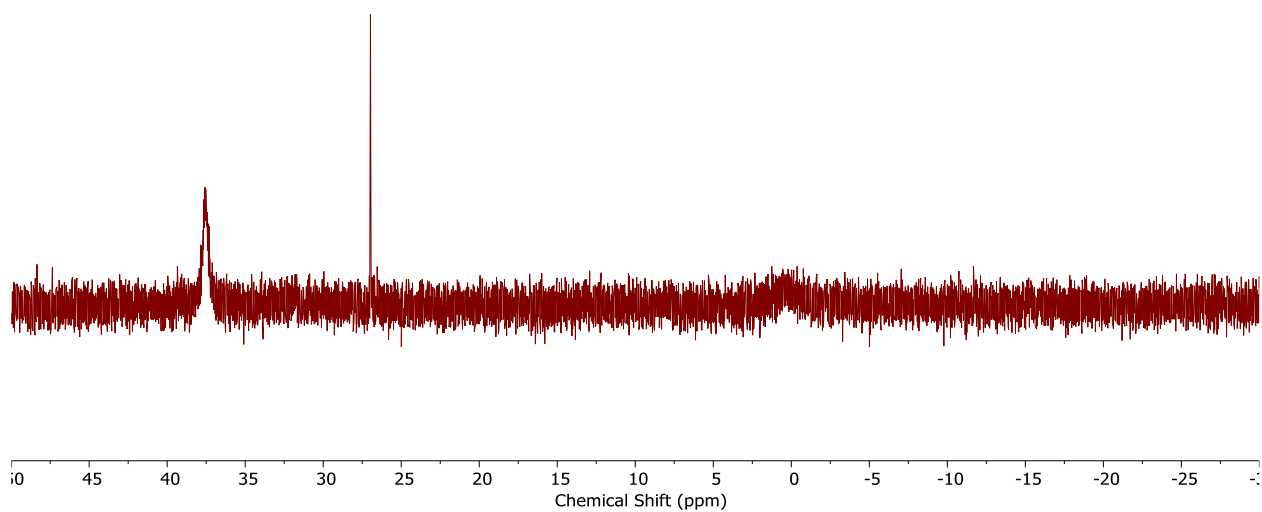


Figure S2.28 $^{31}\text{P}\{^1\text{H}\}$ NMR spectrum of a reaction mixture of $[\text{AuNC-azide}]^-$ with 3 equivalents of *dppb* in CD_2Cl_2 .

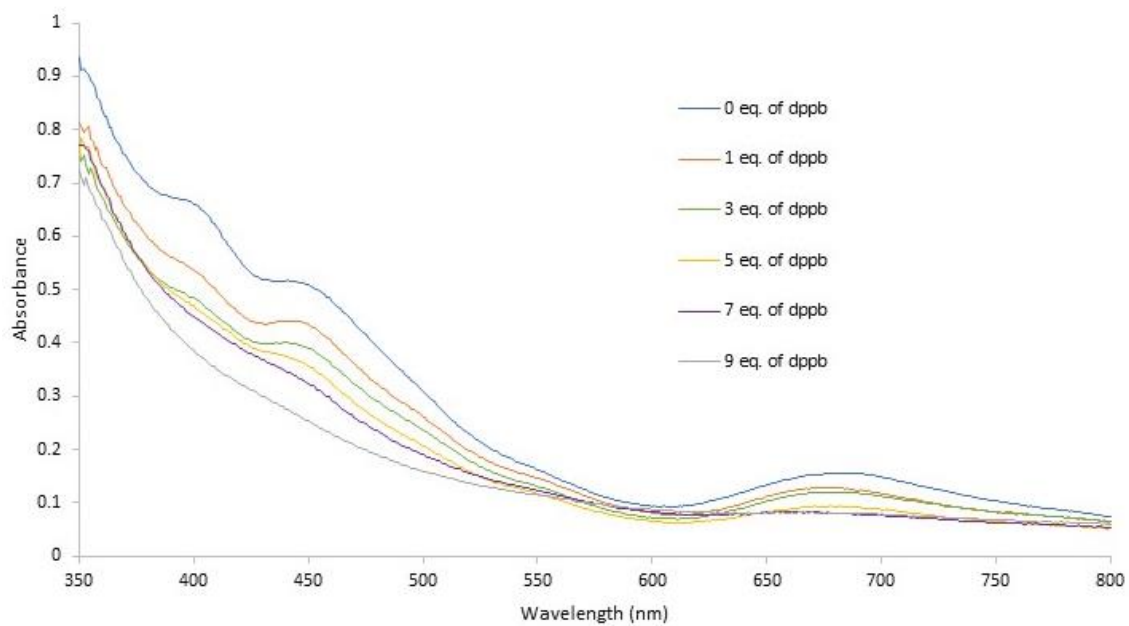


Figure S2.29 UV-Vis absorption spectrum of the reaction mixture between $[\text{AuNC-azide}]^-$ and different equivalents of *dppb* added in CH_2Cl_2 at 23 °C.

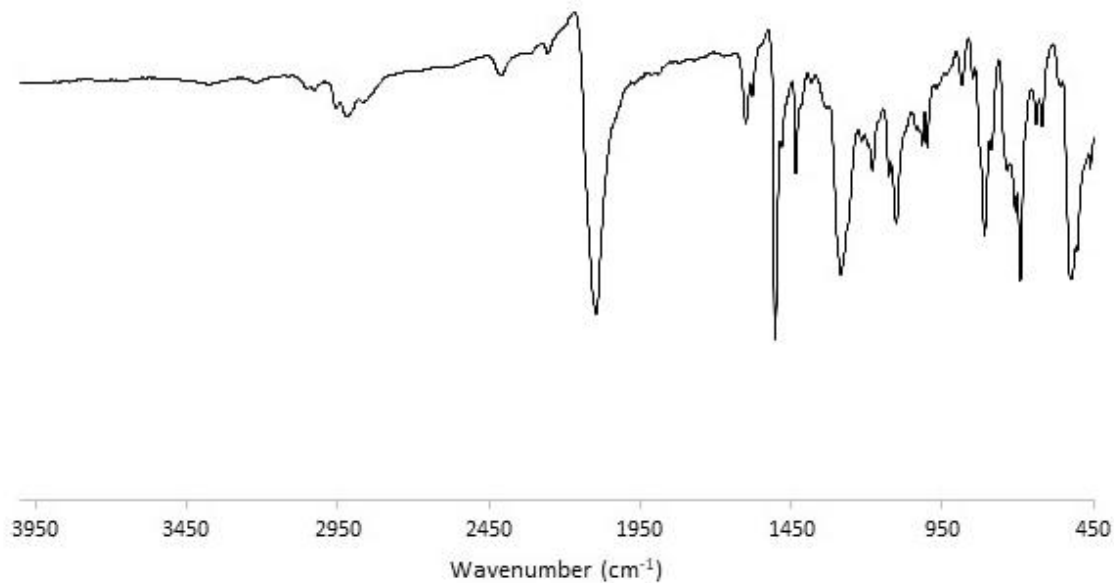


Figure S2.30 ATR-IR spectrum of the reaction mixture of $[\text{AuNC-azide}]^-$ with 3 equivalents of *dppb*.

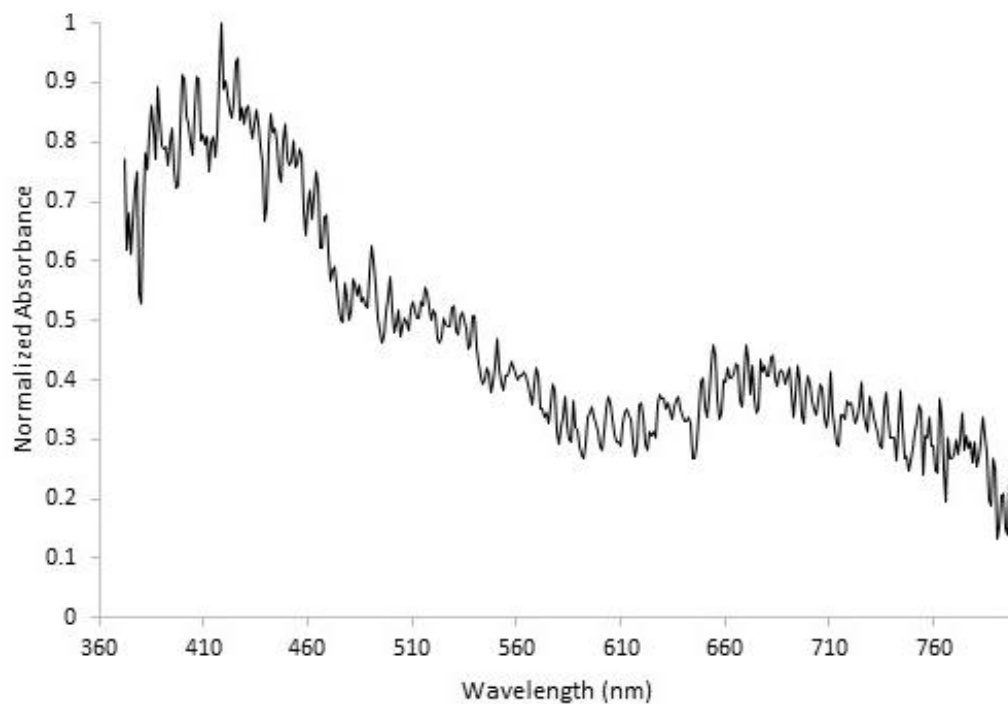


Figure S2.31 Diffuse reflectance UV-Vis absorption spectrum of the precipitate formed from reaction mixture between $[\text{AuNC-azide}]^-$ and 3 equivalents of *dppb*.

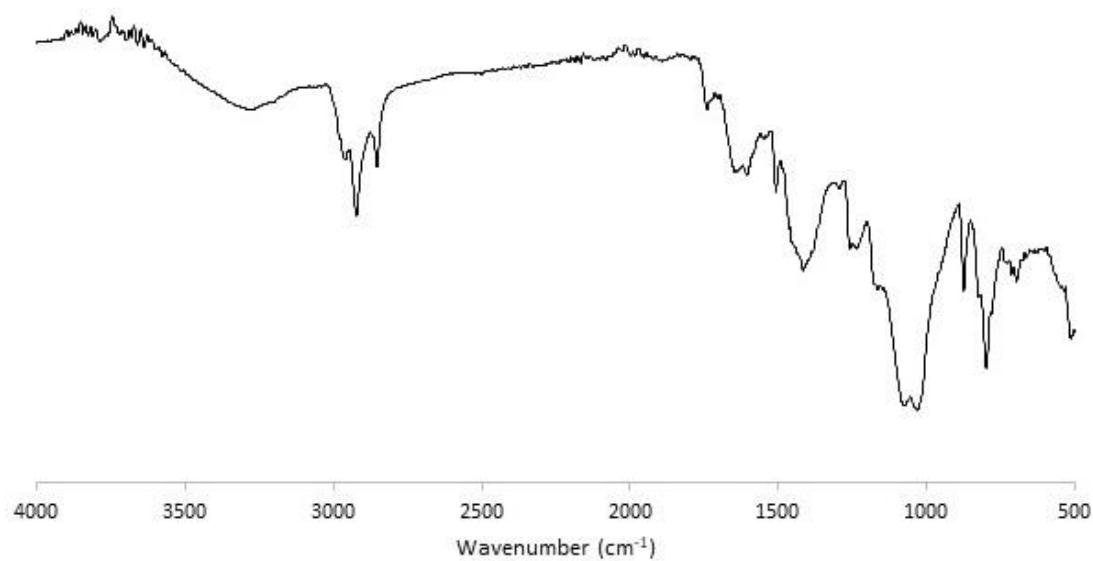


Figure S2.32 ATR-IR spectrum of the precipitate formed from reaction mixture between $[\text{AuNC-azide}]^-$ and 3 equivalents of *dppb*.

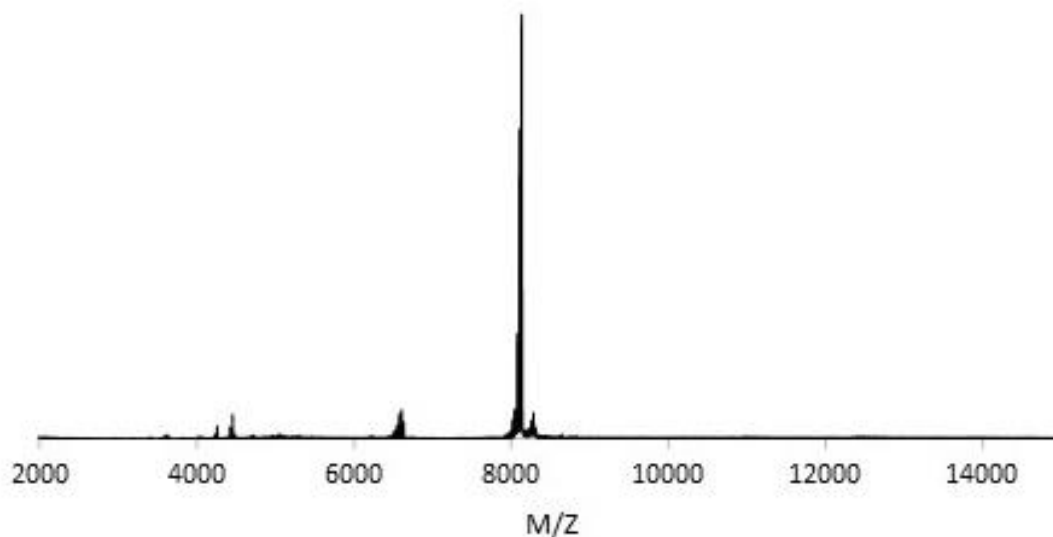


Figure S2.33 Negative ion mode ESI Mass spectrum of the reaction mixture between $[\text{AuNC-azide}]^-$ and 3 equivalents of *dppb*.

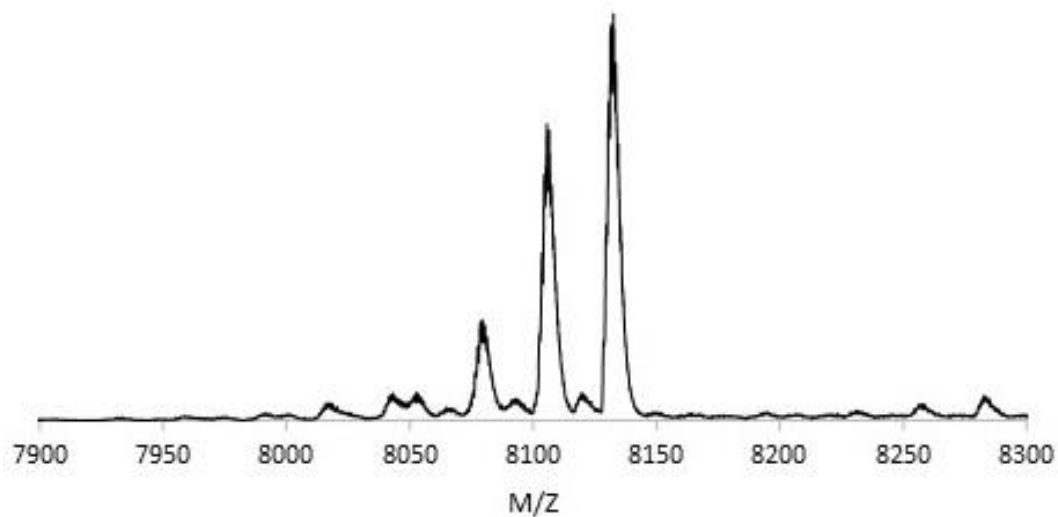


Figure S2.34 Negative ion mode ESI mass spectrum of the reaction mixture between $[\text{AuNC-azide}]^-$ and 3 equivalents of *dppb*, zoomed in between 7900 and 8300 to show $[\text{Au}_{25}(\text{SCH}_2\text{CH}_2\text{C}_6\text{H}_4\text{N}_3)_{18}]^-$, $[\text{Au}_{25}(\text{SCH}_2\text{CH}_2\text{C}_6\text{H}_4\text{N}_3)_{17}(\text{SCH}_2\text{CH}_2\text{C}_6\text{H}_4\text{NH}_2)]^-$ (calculated: 8105.963, observed: 8105.544) and $[\text{Au}_{25}(\text{SCH}_2\text{CH}_2\text{C}_6\text{H}_4\text{N}_3)_{16}(\text{SCH}_2\text{CH}_2\text{C}_6\text{H}_4\text{NH}_2)_2]^-$ (calculated: 8079.487, observed: 8079.973).

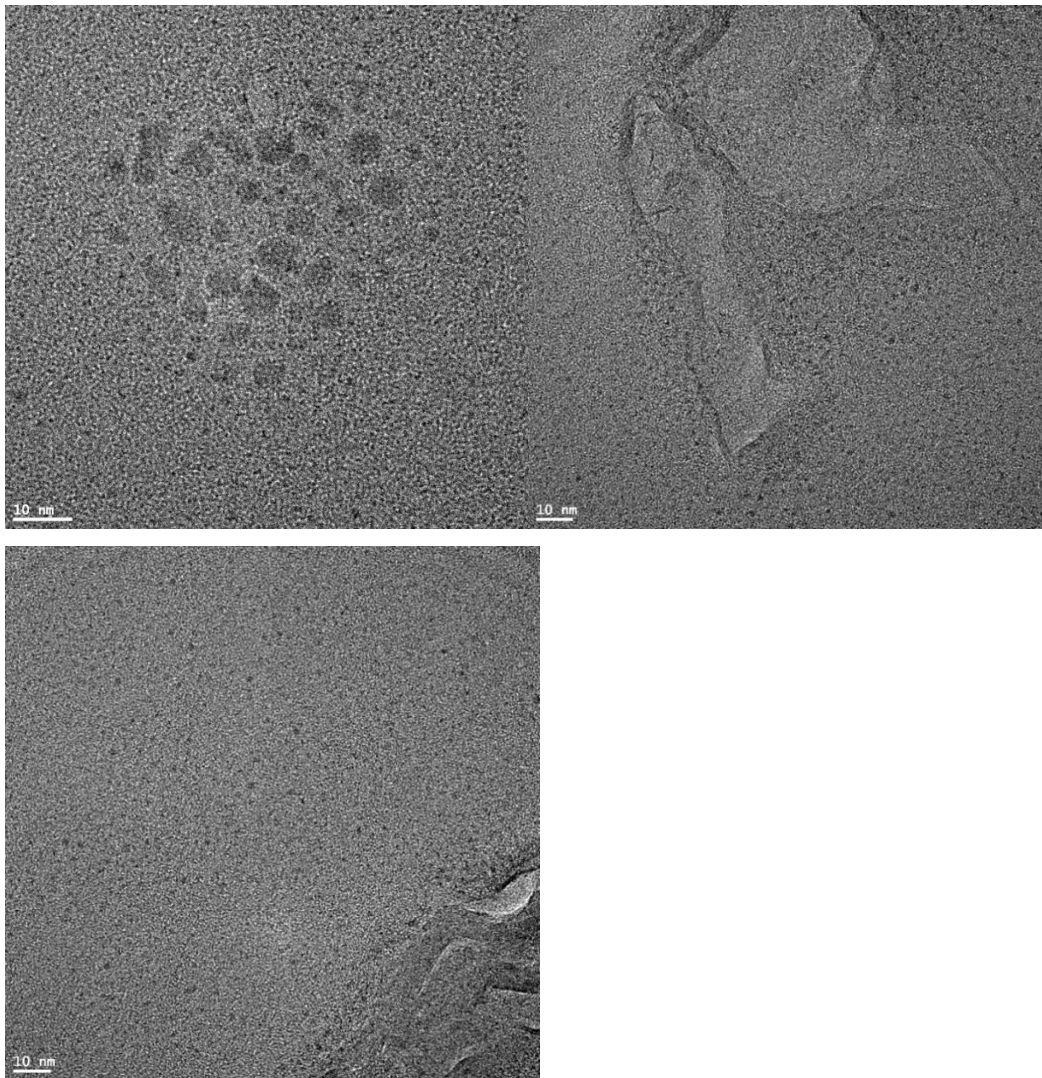


Figure S2.35 TEM images of the $[\text{AuNC-azide}]^-$ with 3 equivalents of *dppb*.

Curriculum Vitae

Andy Lim

Education

The University of Western Ontario

London, ON

M Sc candidate, Department of Chemistry, Sept. 2019 - present

Thesis: Staudinger Reactions on Azide Functionalized Au₂₅ Nanoclusters as a Route to Linked Frameworks

The University of Western Ontario

London, ON

B Sc Honours Chemistry and Major Medical Science, Sept. 2012 - May 2019

Thesis: Investigating Triazolinedione (TAD) Transclick Chemistry on Gold Nanoparticles

Teaching Assistantships

The University of Western Ontario London, ON

Chem 3373F Organic Chemistry III

Fall 2019, 2020

Chem 2223B Organic Chemistry of Biological Molecules

Winter 2021

Scholarships and Awards

Ontario Graduate Scholarship

2019-2020

Summary of Course Work

9823R-Heterocycles

88

9653S-Polymers: Synthesis to Function

83

79

9504T-Advanced NMR Spectroscopy	90
9555T Organic Photochemistry	90